Fabrication of Mesoscale Polymer Structures by Self-Organization

(自己組織化によるメゾスケール高分子構造の作製)

by

Hiroshi Yabu

June, 2004

Doctoral Thesis

Fabrication of Mesoscale Polymer Structures by Self-Organization

Hiroshi Yabu

Division of Chemistry, Graduate School of Science,
Hokkaido University

Table of Contents

Chapter 1

Introduction

1.1. Background

Top down approaches of micro-fabrication technologies. Micro-fabrication technologies are cores of producing high performance semiconductors, and other electrical, optical and biological applications. They need different size scale of patterns. In electronics field, the atom or molecular level minimization is the final goal. According to Moore's law [1-1], the gate length of field effect transistor (FET) doubly minimized a half year (Recently, it reached the process of 90nm). This minimization was mainly achieved by recent developments of photolithography. The photolithography is a representative method of present micro-fabrication technologies. This method enable to fabricate as one likes structures in tens nanometer scale. This method is consisted of main six procedures (Figure 1-1);

(1) Preparing "master" structure.

(2) Coating photo-resist onto silicon oxide surface.

(3) Irradiation of light (especially deep ultra violet light) onto the photo-resist through the master.

(4) Elusion of degraded photo-resist.

(5) Etching silicon oxide layer.

(6) Removing whole photo-resists.

When small dust particles attach silicon wafer in one process, the processors have fatal damage. All procedures should be performed under low contamination conditions. Therefore, high cost environmental controlling is needed. However, the whole steps to prepare 1 patterned silicon wafer include more than 100 detail procedures. Some contamination is still inevitable. To reduce these elaborate procedures, nano-imprint lithography [1-2], LIGA process [1-3] and other emboss methods have been developed.

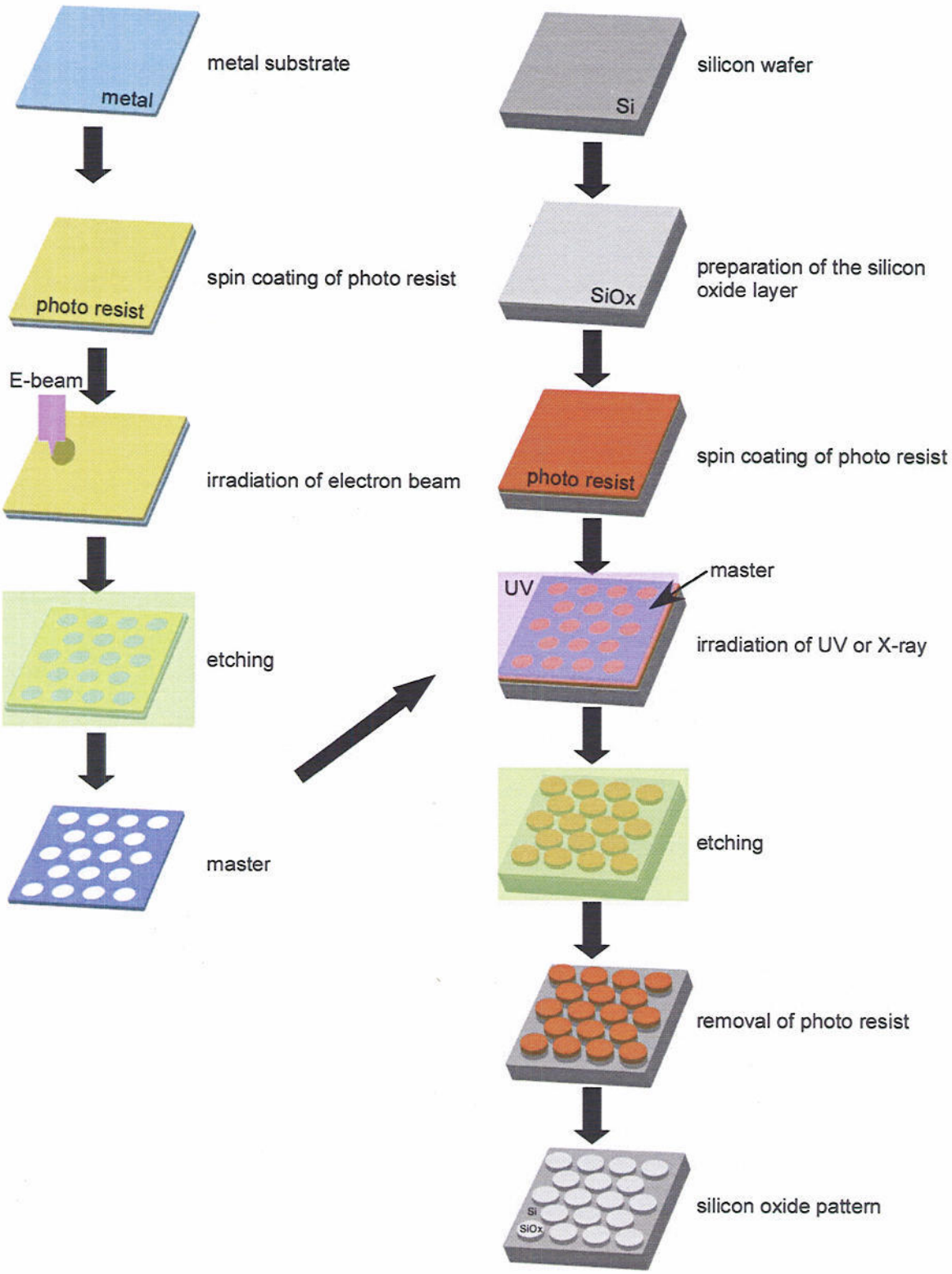

Figure 1-1. Fabrication process of micro-structures by photo-lithography.

These methods include alternatives of one or more steps in photolithography. The pattern transfer method is mainly changed from light irradiation to solid molds (nano-imprint lithography, LIGA process, etc.). Though some steps are reduced comparing with photolithography, they had still same problems such as, high cost, producing large amount of wastes, time-consuming, and produced from limited materials. These methods are classified as "top-down approaches", which mean the micro-fabrication methods by miniaturizing bulk materials. The top-down approach is the method of cutting the 3 dimensional structures into the low dimensional line or dot structures.

Furthermore, the required structure is not only ranging under 100nm scale. In photonics field, the structure ranging the length of light wave, which is in the submicron scale, is needed [1-4]. Moreover, the micron scale periodicities are required in the fields of biotechnology [1-5]. These size scale is classified "meso-scale", which is the intermediate state between the nanoscale and the macroscale. To produce microstructures in these scales, the photolithography is not desirable option.

Bottom up approaches of micro-fabrication technologies. Another approaches building up small components into large size architectures have been attempted. Such building up micro-fabrication methods are called "bottom up approaches". The bottoms up approaches are simple and non-expensive method because they need no or few energy consumption. Furthermore, hierarchic superstructures can be formed by building up the small components.

To produce nano-meter scale structure, molecular self-assembly is energetically studied. The self-assembly of molecules is the main theme of supramolecular chemistry [1-6]. Week and non-covalent interaction between molecules are used for produce molecular assemblies in the nano-meter scale. The representative example of the molecular self-assembly is the structure of lipids, which forms liposome, tube, lamellae, and hexagonal lattice in the case of changing the conditions [1-7]. To functionalize and fabricate the thin

lipid layer, lipid monolayers and Langmuir-blodgett films [1-8] using the liquid-gas interface was invented. By using the solid-gas interface, the self-assembled monolayer is prepared by using thiol-gold interaction [1-9]. These molecular scale self-assembly succeeded in produce small and thin structures up to 10nm. In the range from 10nm to 100nm, micro-phase separation of block-copolymers forms periodic microstructures [1-10~1-11]. The block-copolymers have two or more separated segments in their polymer chains. The interaction between inter segments is repulsion, the segments are phase separated. This micro-phase separation forms several kinds of micro-structures (i.e. lamellae, hexagonal, gyroid etc.) in the range of tens nm depending on their segment fractions. In larger scale, the bulk surface properties affect the structure formation. By using capillary force, colloidal particles spontaneously form 2 or 3 dimensional colloidal crystals [1-12~1-22]. The two particles in the presence of thin liquid film, the contact line of the particles deformed by capillary force. This deformation induces attraction force between two particles. As the result, the particles assembled in the surface of liquid. This interaction used actively, fabrication of colloidal crystals can be performed (i.e. advection accumulation, sedimentation etc.). The colloidal crystals had also periodic micro-structures in the range of submicron to micron scale.

Combination of lithographic techniques and self-assemblies. Whitesides et. al. proposed that the combination of top down lithographic technique and self-assemblies. They developed "Soft-lithography", which was the technique of produce silicon rubber molds and transfer the microstructures onto another substrate by them [1-23~1-24]. It is noteworthy that they use thiol groups as transferring inks (Figure 1-2). The thiol groups (usually alkane thiols) are adsorbed on the patterned silicon rubber surface, the ink thiol groups transferred onto gold substrate. After etching of gold layer, the gold pattern is generated. This is one of the soft-lithographic method named "micro contact printing (μCP). Some related methods are

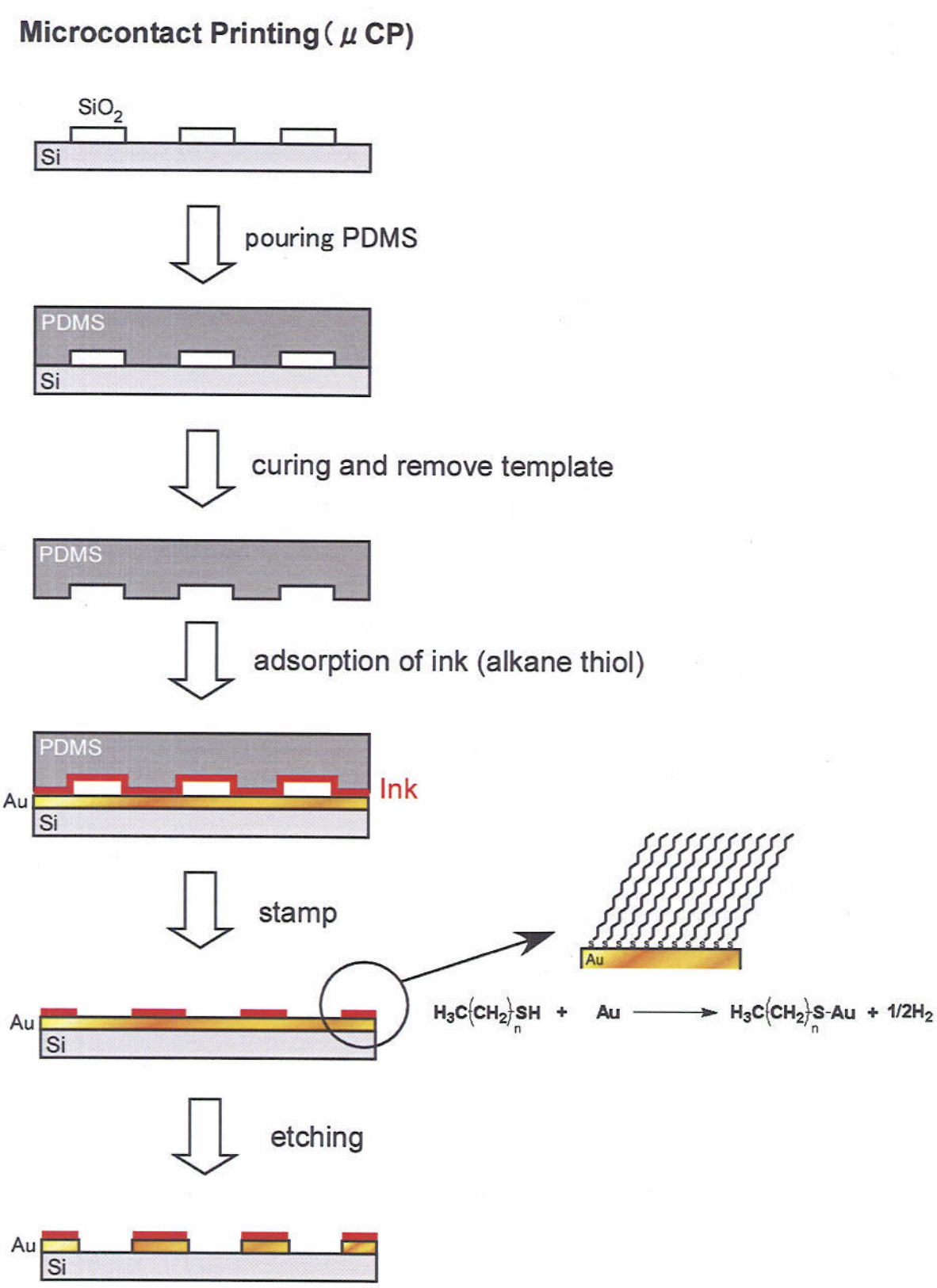

Figure 1-2. Schematic illustration of μCP.

exist such as micro transfer molding (μTM), replica molding (REM) and micro molding in capillary (MIMIC). They can utilized not only for patterning cross-linkable polymers but also for colloidal particles, and other functional materials. These methods are representative examples of combination of lithographic techniques and self-assemblies.

They also developed the method of fabricating the structures ranging micrometer to millimeter named "Mesoscale Self-assembly" [1-25]. The fuctinalized particles (hexagonal or more complicated structures), which have hydrophobic part and hydrophilic parts, are prepared by using photolithography [1-26] or soft-lithography [1-27]. When they placed interface of hydrophobic and hydrophilic media, they form 2 or 3 dimensional assemblies reflect their surface properties. These works are worthy because they extends the capabilities of self-assembly of precisely controlled properties of materials from molecular level to mesoscale.

Micro-fabrication method based on self-organization. The self-assembly method have many advantages to develop mesoscale architectures. However, they are using the interaction originated from the properties of themselves. Therefore they have poor choice of materials.

It is reported that regular patterns can be observed in the system of far from equilibrium. One representative example is Bénard convection cell [1-28]. When silicone oil heated from bottom surface, the heat passes through the oil and dissipated from the upper surface. When the heating temperature was low, the input heat and dissipative heat is constant. On the other hand, the temperature was elevated, the input heat excess the heat dissipation from the upper surface. The heat energy converted to the driving force of convectional flow. Such structure formation is named "Dissipative Structures" coined by Prigogine and the process of structure formation is called "Self-organization", especially in physics field [1-29]. These structure formations are completely physical phenomena, they can be utilized for any scale and any materials. However, there is no example about fabrication process using the

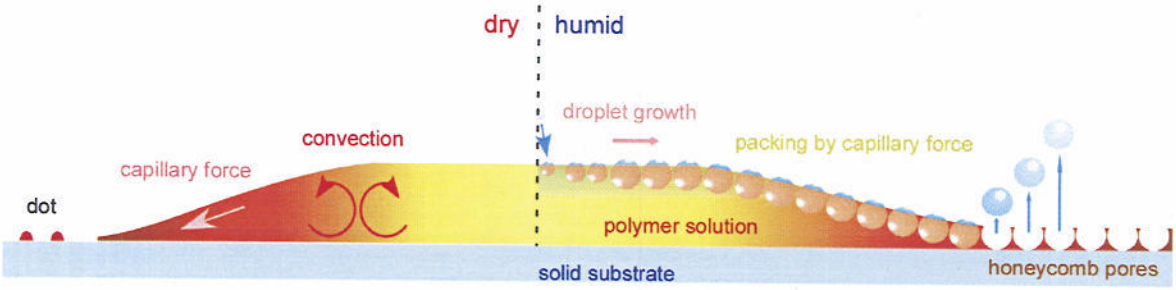

Figure 1-3. Schematic illustration of pattern formation by casting polymer solution (side view).

dissipative structures for long time because of their experimental and theoretical complexities. Recently, Kumacheva et. al reported formation of periodic microstructures induced by the convections [1-30]. In this case, the convectional flow was used as templates of cross-linkable polymer. Furthermore, Karthaus et. al. reported ordered micro-dot structures can be fabricated by dewetting of casting dilute polymer solution on solid substrate [1-31] (Figure 1-3, left). This order was originated from the localized concentration of polymer molecules induced by dissipative structure in evaporating solution [1-32]. When the solvent evaporates from the solution, the heat energy is dissipated and the suitable condition for form dissipative structures is formed. By changing the casting conditions, another patterns including stripes and other patterns also formed. Moreover, in the case of applying humid air, François et. al. found that the honeycomb-patterned micro-porous films can be fabricated by using spontaneously assembled condensed water droplets on block-copolymer solution as templates [1-33] (Figure 1-3, right). Karthaus et. al. reveals that this phenomenon is general for polymeric materials [1-34]. The strategy of these methods is transferring the patterns generated from dissipative structures onto another materials (especially onto polymers).

These self-organization methods need not to use any formally prepared templates or guides. If these structures are controllable and functionalized, they can be novel types of bottom up fabrication method.

1.2. Objective

According to the former mentioned backgrounds, this research aims establishment of the method of preparing mesoscale structures by self-organization in polymer solution with solvent evaporation.

This doctoral thesis consisted of four major topics. In chapter 2, a novel preparation method of nano- and micro-particles from organic materials is discussed as a first issue. Nano-particles from versatile functional materials as building blocks of meso scale architectures were prepared by "self-organized precipitation" method. The particle formation mechanism, controlling particle sizes and their functions are discussed. In chapter 3, fabrications of nano- and micro-structures based on the honeycomb-patterned films are shown. The honeycomb-patterned films from functional materials will be shown. And their properties are discussed. Several micro-structures including micron sized lens, spheres, rings and other structures are fabricated by the secondary elaboration of the honeycomb-patterned films. The novel fabrication method to prepare the films continuously is also shown. The micro-patterns based on dewetting phenomena are presented in chapter 4. To control the micro-structures, novel fabrication method is developed. The controlling factor and formation mechanisms will be discussed. In chapter 5, the hybrid structures consisted from nano-particles and other self-organized patterns are shown. Finally, the all stories are summarized in chapter 6

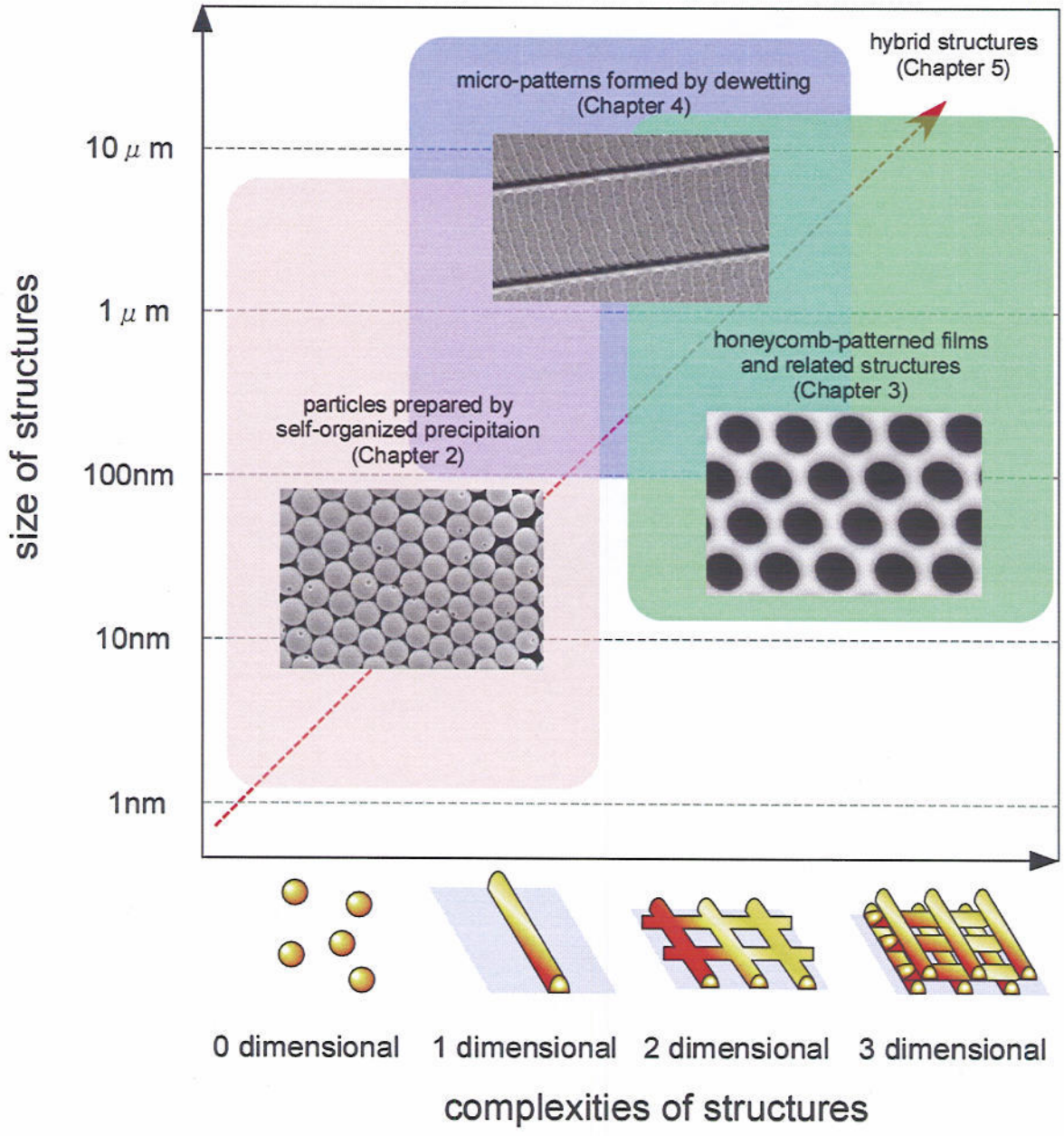

Figure 1-4. Strategy of this research

Reference

[1-1] (a) G. E. Moore, Electronics, **38**(8) (1965), (b) P. P. Gelsinge, P. A. Gargini, G. H. Parlcer, A. Y. C. Yu, IEEE Spectrum, **89**, 43 (1989)

[1-2] , T. A. tervoort. K. Bastiaansen, P. Smith, *Nature*, **407**, 613 (2000)

[1-3] S. Voigt, S. Kufner, A. Kufner, I. Frese, *IEEE Photonics Tech. lett.*, **14**(10), 1484- 1486 (2002)

[1-4] S. Noda, A. Chutinan, M. Imada, *Nature*, **407**, 608 (2000)

[1-5] C. S. Chen, M. Mrksich, S. Huang, G. M. Whitesides, D. E. Ingber, *Science*, **276**, 1425 (1997)

[1-6] J. M. Lean, "Supramolecular Chemisty", VCH, GmbH (1995)

[1-7] J. N. Israelachvili, "Intermolecular and Surface Forces", Academic Press, London (1992)

[1-8] M. C. Petty, "Langmuir-Blodgett films", Cambridge University Press, (1996)

[1-9] G. M. Whitesides, P. E. Laibinis, *Langmuir*, **6**, 87 (1990)

[1-10] (a) K. Shin, K. Amanda Leach, J. T. Goldbach, D. H. Kim, J. Y. Jho, M. Tuominen, C. J. Hawker, T. P. Russell, *Nano Lett.*, **2**(9), 933-936 (2002), (b) M. B. Urdache, M. T. Tuominen, J. T. Goldbach, T. P. Russell, *Appl. Phys. Lett.*, **81**(18), 3479-3481 (2002) (c) T. Thrun-Albrecht, J. DeRouchey, T. P. Russell, R. Kolb, *Macromolecules*, **35**, 8106-8110 (2002)

[1-11] T. Kowalewski, N. V. Tsarevsky, K. Matyjaszewski, *J. Am. Chem. Soc.*, **124**, 10632-10633 (2002)

[1-12] (a) A. van Blaaderen, R. Ruel, P. Wiltzius, *Nature*, **385**, 321-324 (1997), (b) K. P. Velikov, C. G. Christova, R. P. A. Dullens, A. van Blaaderen, *Science*, **296**, 106-109 (2002)

[1-13] (a) Y. Xia, B. Gates, Y. Yin, Y. Lu, *Adv. Mater.*, **12**(10), 693-713 (2000), (b) B. Gates, Y. Xia, *Appl. Phys. Lett.*, **78**(21), 3178-3180 (2001), (c) Y. Yin, Z.-Y. Li, Y. Xia, *Langmuir*,**19**(3), 622- 631 (2003), (d) H. Fudouzi, Y. Xia, *Adv. Mater.*, **15**(11), 892-896 (2003), (f) Y. Xia, Y. Yin, Y. Lu, J. McLellan, *Adv. Func. Mater.*, **13**(12), 907-918 (2003)

[1-14] H. Cong, W. Cao, *Langmuir*, **19**(20), 8177-8181 (2003)

[1-15] A. Rugge, W. T. Ford, S. H. Tolbert, *Langmuir*, **19**(19), 7852-7861 (2003)H. Cong, W. Cao, *Langmuir*, **19**(20), 8177-8181 (2003)

[1-16] L. Cadmartiri, A. Sutti, G. Calestani, *Langmuir*, **19**(19), 7944-7947 (2003)A. Rugge, W. T. Ford, S. H. Tolbert, *Langmuir*, **19**(19), 7852-7861 (2003)

[1-18] S. H. Im, Y. T. Lim, D. J. Suh, O. O. Park, *Adv. Mater.*, **14**(19), 1367-1369 (2002)L. Cadmartiri, A. Sutti, G. Calestani, *Langmuir*, **19**(19), 7944-7947 (2003)

[1-19] (a) L. M. Goldberg, J. Wagner, J. Stumpe, B.-R. Paulke, E. Görnitz, *Langmuir*, **18**(8), 3319-3323 S. H. Im, Y. T. Lim, D. J. Suh, O. O. Park, *Adv. Mater.*, **14**(19), 1367-1369 (2002)

[1-20] (2002), (b) L. M. Goldberg, B.-D. Jung, J. Wagner, J. Stumpe, B.-R. Paulke, E. Görnitz, *Langmuir*, (a) L. M. Goldberg, J. Wagner, J. Stumpe, B.-R. Paulke, E. Görnitz, *Langmuir*, **18**(8), 3319-3323 **19**(1), 205-207 (2003)(2002), (b) L. M. Goldberg, B.-D. Jung, J. Wagner, J. Stumpe, B.-R. Paulke, E. Görnitz, *Langmuir*, F. Caruso, H. Möhwald, *Langmuir*, **15**(23), 8276-8281 (1999)**19**(1), 205-207 (2003)

[1-21] (a) Z.-Z. Gu, S. Kubo, W. Qian, Y. Einaga, D. A. Tryk, A. Fujishima, O. Sato, *Langmuir*, **17**(22), F. Caruso, H. Möhwald, *Langmuir*, **15**(23), 8276-8281 (1999)

[1-22] 6751-6753 (2001), (b) Z.-Z. Gu, R. Horie, S. Kubo, Y. Yamada, A. Fujishima, O. Sato, *Angew. Chem.*

(a) Z.-Z. Gu, S. Kubo, W. Qian, Y. Einaga, D. A. Tryk, A. Fujishima, O. Sato, *Langmuir*, **17**(22), *Int. Ed.*, **41**(7), 1153-1156 (2002)6751-6753 (2001), (b) Z.-Z. Gu, R. Horie, S. Kubo, Y. Yamada, A. Fujishima, O. Sato, *Angew. Chem.* (a) A. Kumar, G. M. Whitesides, *Appl. Phys. Lett.*, **63**, 2002-2004, (1993), (b)A. Kumar, H. A. *Int. Ed.*, **41**(7), 1153-1156 (2002)

[1-23] Biebuyck, G. M. Whitesides, *Langmuir*, **10**, 1498 (1994) (a) A. Kumar, G. M. Whitesides, *Appl. Phys. Lett.*, **63**, 2002-2004, (1993), (b)A. Kumar, H. A. a) Y. Xia, G. M. Whitesides, *Angew. Chem. Int. Ed.*, **37**, 550-575, (1998), (b) Y. Xia, G. M. Whitesides, Biebuyck, G. M. Whitesides, *Langmuir*, **10**, 1498 (1994)

[1-24] (a) Y. Xia, G. M. Whitesides, *Angew. Chem. Int. Ed.*, **37**, 550-575, (1998), (b) Y. Xia, G. M. Whitesides, *Annu. Rev. Mater. Sci.*, **28**, 153-184 (1998)

[1-25] G. M. Whitesides, M. Boncheva, PNAS, 99(8), 4769 (2002)

[1-26] (a) B. A. Grzybowski, N. Bowden, F. Arias, H. Yang, G. M. Whitesides, *J. Phys. Chem. B*, **105**, 404 (2001), (b) T. D. Clark, R. Ferrigno, J. Tien, K. E. Paul, G. M. Whitesides, *J. Am. Chem. Soc.*, **124**, 5419 (2002),

[1-27] (a) C. Mao, V. R. Thalladi, D. B. Wolfe, S. Whitesides, G. M. Whitesides, *J. Am. Chem. Soc.*, **124**, 14508 (2002), (b) D. B. Wolfe, A. Snead, C. Mao, N. B. Bowden, G. M. Whitesides, *Langmuir*, **19**, 2206 (2003)

[1-28] E. L. Koschmieder, Adv. Chem. Phys., 26, 177 (1974)

[1-29] I. Prigogine, "Self-organization in Nonequilibrium Systems", John Wiley & Sons, New York (1977)

[1-30] S. Xu, E. Kumacheva, *J. Am. Chem. Soc.*, **124**, 1422 (2002)

[1-31] O. Karthaus, K. Ijiro, M. Shimomura, *Chem. Lett.*, 821 (1996)

[1-32] (a) O. Karthaus, L. Grasjö, N. Maruyama, M. Shimomura, *Chaos*, **9**(2), 1 (1999), (b) N. Maruyama, O. Karthaus, K. Ijiro, M. Shimomura, T. Koito, S. Nishimura, T. Sawadaishi, N. Nishi, S. Tokura, *Supramol. Sci.*, **5**, 331 (1998)

[1-33] (a) G. Wadawski, M. Rawiso, B. François, Nature, 369, 397 (1994), (b) B. François, P. Pirois, J. François, Adv. Mater., 7, 1041 (1995), (c) O. Pitois, B. François, Eur. Phys. J. B, 8, 225 (1999), (d) O. Pitois, B. François, Colloid Polym. Sci., 277, 574 (1999)

[1-34] O. Karthaus, N. Maruyama, X. Cieren, M. Shimomura, H. Hasegawa, T. Hashimoto, *Langmuir*, **16**(15), 6071-6076 (2000)

Chapter 2

Preparation of Nano-particles by Self-organized Precipitation

2-1. Introduction

Background

Recently, nano-particles have attracted the attention of many researchers due to those high potentials as functional materials. The wide variety of applications to drag delivery systems [2-1], sensing biomolecules [2-2], photonic crystals [2-3] and micro-lens arrays [2-4] were investigated. Because their high surface/volume ratio, the devices using nano-particle are considered to achieve high sensibility, low energy consumption, and low cost. Furthermore, on the point of view of building up the self-organized structures, they are promising materials as building blocks with various functions.

The preparation methods of organic nano-particles have already reported from many researchers in the field of powder science, polymer chemists, and materials sciences (Table 2-1). The preparation methods of organic nano-particles are classified as two categories. One is break down and the other is build up. In the case of the break down method, the bulk of organic materials are broken into small pieces by mechanical force or chemical elution. By using the mechanical fracture, μm scale particles can be obtained. However, it is difficult to produce nm scale particles by using the break down methods. In the case of build up methods, the particle properties depend on the procedures of particle formations. The build up methods including emulsion polymerization, suspension polymerization, and crystallization can be formed particles from tens nm to μm scale particles with small size distributions. These methods sometimes called "template" systems. The emulsion or stabilizers form capsules working as micro-reactors, and then, nano-particles formed in each capsules by polymerization or precipitation. However, in principle, these methods need some stabilizers (i.e. surfactants, immiscible polymers, etc.) to protect fusion of each particles. The advantage of nano-particles is their high surface/volume ratio. By using these template systems, the

surface properties only depend on the stabilizer properties. Furthermore, these methods can be applied for limited materials. To solve these problems, Nakanishi et. al. reported the re-precipitation method, which was very simple method that the poor solvent injected into the materials solution. By using this method, the organic nano-crystals can be formed spontaneously. Though this method can be applied for many materials, it has some difficulties in particle size control. To prepare uniform sized particles, the particle size should keeping small. Another method to prepare nano-particles from versatile materials is spontaneous emulsification solvent diffusion (SESD) method. The materials dissolved in their good solvent and stabilizer, and then the poor solvent of materials is added into the solution with moderate mechanical stirring. The materials spontaneously form nano-particles by addition of poor solvent. This method firstly reported by Fessi et. al. in 1989 for producing nano-particles from poly(D,L-lactide). And then, some improvements related with the stabilizer and solvent system were done by Rieger et. al and Kawashima et. al. This method can produce nano-particles from versatile materials. However, the contamination of stabilizer is inevitable and their surface properties depend on their stabilizers.

Objective

In this chapter, the novel preparation method of nano- and micro-particles from various kinds of materials named "Self-organized precipitation method" is shown. Nano-particles from engineering plastics, biodegradable materials, photo- and electro-luminescence materials, and other functional materials are prepared by using this method. Furthermore, the preparations of nano-particles from nucleic acid-amphiphile polyion complexes are shown. And their molecular recognition properties are discussed.

2-2. Nano-particle formation by "self-organized precipitation" method

Nano-particles were formed by following steps (Figure 2-1); (1) Preparation of material's solution. The materials were dissolved in good solvent. (2) Poor solvent is mixed. The poor solvent of materials, which is miscible with good solvent, is slowly added into the solution. (3) Good solvent evaporation. The good solvent is evaporated and then, the materials

type		Method	size (d: diameter)	papers
break down		collision	several microns < d	2-5
build up	template	mini-emulsion polymerization	d = 10nm-100nm	2-6
		soap free emulsion polymerization	d =100nm-1 μ m	2-7
		emulsion polymerization	d ~100nm	2-8
		SESD	d =100nm-100 μ m	2-9
		modified SESD	d ~100nm	2-10
	non-template	re-precipitation method	d < 100nm	2-11
		crystallization	10 μ m < d	2-12

Table 2-1. Various preparation methods of nano- or micro-particles.

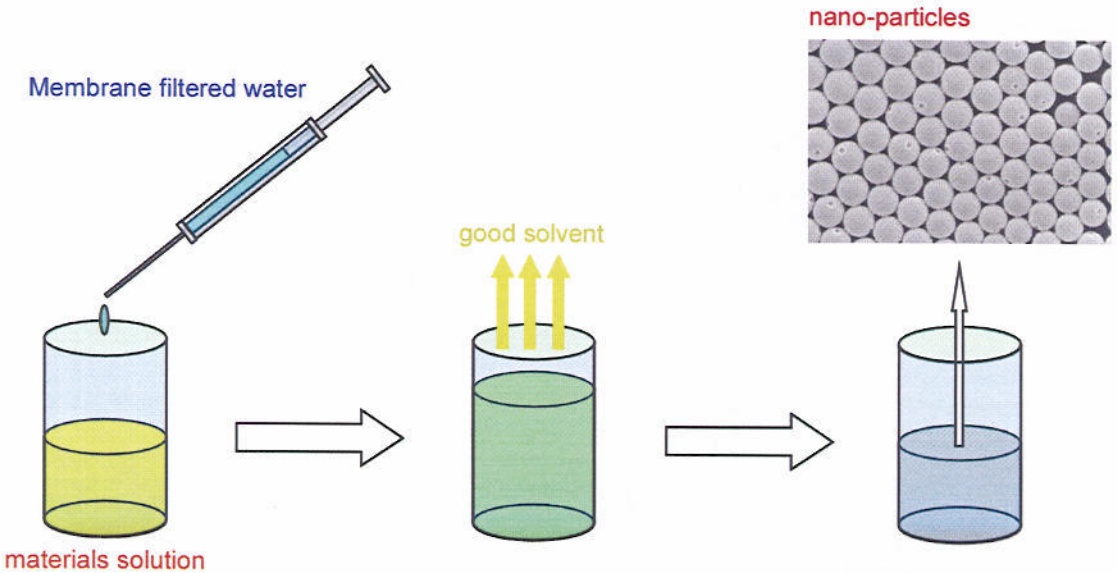

Figure 2-1. Preparation procedure of nano-particles by self-organized precipitation method.

precipitated as nano-particles.

The particle formation by using this method was firstly found in the case of tetrahydrofran (THF) solution of poly(styrene-*co*-maleicanhydride) (**2-1**, Aldrich). Same amount of water was slowly added into the solution, and then, the mixed solution was casting onto the freshly cleaved mica substrate. After evaporation of each solvent, the prepared structure was observed by scanning electron microscopy (SEM). By obtained SEM image, the particles from hundreds nanometers to several micrometers were observed (Figure 2-2). The casting solution consisted of THF and water. The boiling point of THF is higher than that of water. Therefore THF firstly evaporated and the water content of solution became higher. The polymer was precipitated in the water rich solution and finally, the particles were fixed on the substrate surface after evaporation of water. This result shows significant information about particle formation conditions. The materials should be dissolved in solvent, which has lower boiling point than poor solvent. After evaporation of good solvent, prepared particles disperse in the poor solvent. Another point is poor solvent should miscible with good solvent. In the immiscible system, the clear interface is formed and particles are not formed. In the case of the poor solvent mixing into solution with stirring, agglomeration was occurred and the polymer was reprecipitated. This result indicates this system is perfectly different from

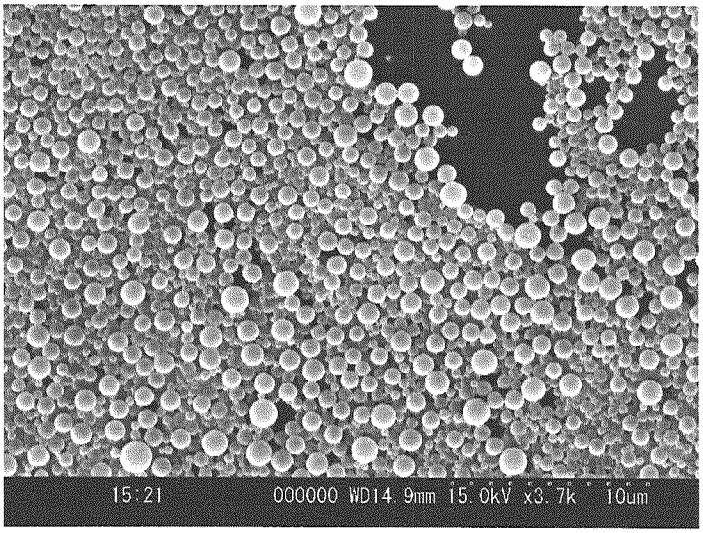

Figure 2-2. Scanning electron micrograph of nano-particles from 2-1 obtained by casting mixture of THF solution and water.

template systems.

The advantage of this method is quoted as follows; (1) this method can be applied for preparing nano-particles from various kinds of functional materials. (2) nano-particles without contamination of stabilizer or surfactant can be obtained. (3) wide range of particles can be obtained from tens nm to tens microns. In the next section, the preparations of nano-particles from functional materials are shown.

2.3. Preparation of nano-particles from functional materials

In this section, the preparation of nano-particles from functional materials by using self-organized precipitation method in detail. One of advantages of this method is application for versatile materials to prepare nano-particles. The result of nano-particles from engineering plastics, biodegradable, photo- and electro-luminescence materials, dyes, and fluorinated materials are shown.

The particles prepared from these materials by using self-organized precipitation method were observed by optical, fluorescence, and scanning electron microscopy. Preparation conditions, solvent system, and prepared particle diameters are listed on Table 2-2. Materials used for preparing nano-particles are shown in Chart 2-1. Most materials form spherical nano-particles (Figure 2-3). Nano-particles from polystyrene (Figure 2-3 (a), **2-2**,), polysulfone (Figure 2-3 (b), **2-3**), polyvinylcarbazol (Figrue 2-3 (c), **2-4**), polyion complex (Figure 2-3 (d), **2-5**), fluorinated copolymer (Figure 2-3 (e), **2-10**), and poly-ε-caprolactone (Figure 2-3 (f), **2-11**) forms spherical shape.

On the other hand, cubic, rhombic or wire shaped particles were sometimes obtained. Polyhexylthiophene (**2-9**) forms spherical and wire like precipitation (Figure 2-4 (a)). The length of wires are ranged from several μm to hundreds μm. The width of the wire is under

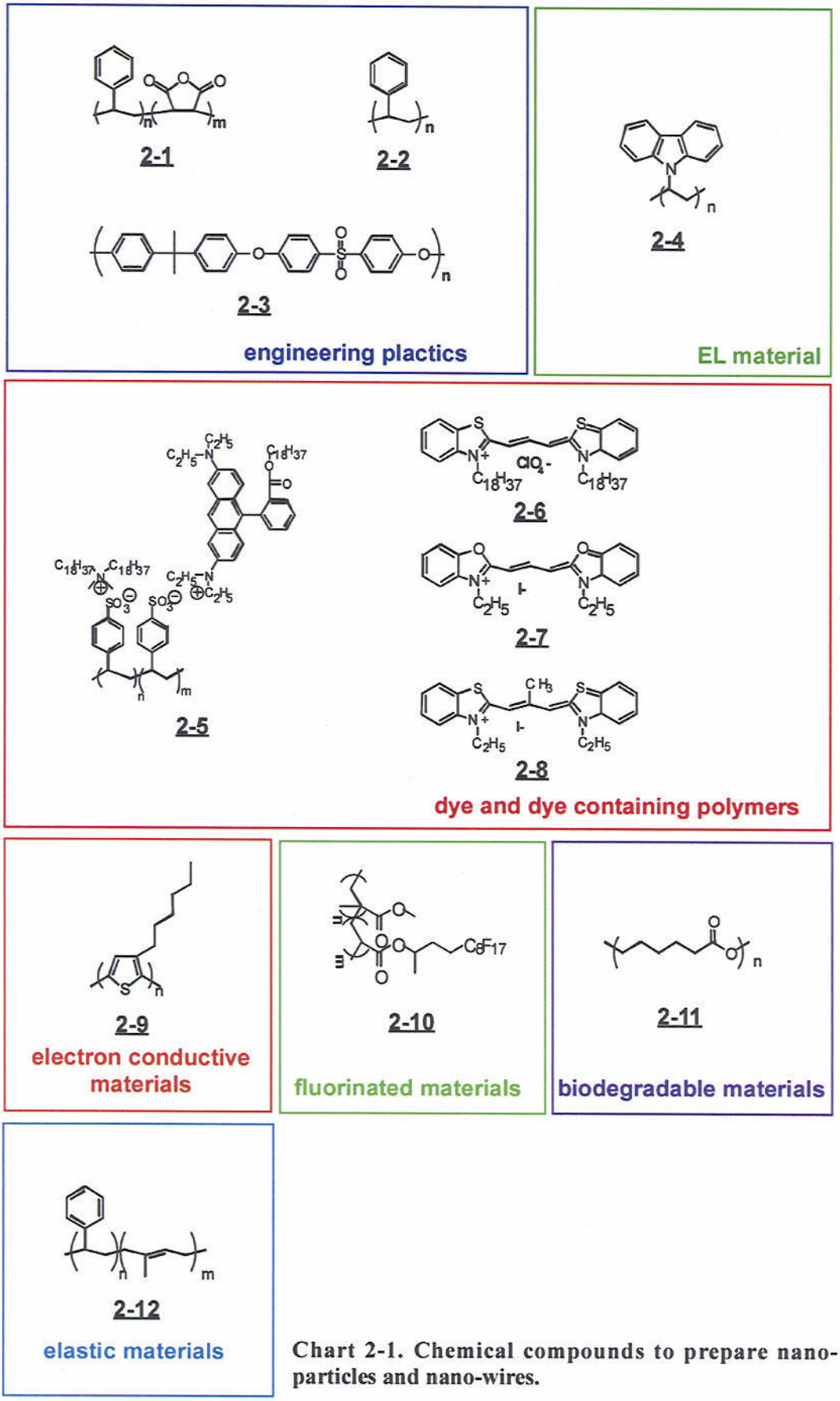

Chart 2-1. Chemical compounds to prepare nano-particles and nano-wires.

Materials	Good solvent	Poor solvent	concentration	good solvent /poor solvent	Properties of materials
2-1	THF	water	1.0g/L	1/1	Aldrich
2-2	THF	water	1.0g/L	1/1	Mw=2,316,000, Mw=2,276,000, Mw/Mn=1.02, Scientific Polymer Products, Inc.
2-3	THF	water	1.0g/L	1/1	Aldrich
2-4	THF	water	1.0g/L	1/1	Mn=c.a. 26,000, Aldrich
2-5	THF	water	1.0g/L	1/1	the preparation method described in 2.5
2-6	THF	water	1.0g/L	1/1	Nihon Kanko Shikiso, Inc.
2-7	ethanol	water	1.0g/L	1/1	Nihon Kanko Shikiso, Inc.
2-8	ethanol	water	1.0g/L	1/1	Nihon Kanko Shikiso, Inc.
2-9	THF	water	1.0g/L	1/1	radioregular, Aldrich
2-10	acetone	water	1.0g/L	1/1	Asahi Glass Corporation
2-11	THF	water	1.0g/L	1/1	Mw=c.a. 200,000, Aldrich
2-12	THF	water	1.0g/L	1/1	PSt(Mn=17,800)-PI(Mn=12,000), polymer source Inc.

Table 2-2. The list of good and poor solvents used to prepare nano-particles.

one μm. Wire structures were also observed in dye particles. Low molecular weight dyes, cyanine dye (2-6) forms rhombic or wire like precipitation (Figure 2-4 (b)).

The difference between the spherical and other shape particles is the micro-structure of materials at room temperature. Polystyrene and other polymer materials form amorphous phase at room temperature. Therefore the shape of these polymers is dominated by only surface tension. The particle surface is always suppressed by water or other poor solvents surface tension, as the result, the surface area of particle is minified. The spherical shape had smallest surface area / volume ratio. The spherical shape was chosen in such cases. On the other hand, polythiophene and low molecular weight dyes forms crystal or aggregate phase (Figure 2-5). Especially, in the case of cyanine dye particles, they form H-aggregate (Figure 2-6). The absorption spectrum of solution was blue shifted in the case of particles. Furthermore, the fluorescence emission of individual particle was measured by the laser exited microscopic spectroscopy. By the microscopic spectroscopy, the bumpy fluorescence spectrum was obtained. This fluctuation of emission was caused by the interference of aggregate structure in the particle. In these cases, the particle growth direction was dominated by the molecular arrangements of aggregates. Therefore asymmetric particles were formed.

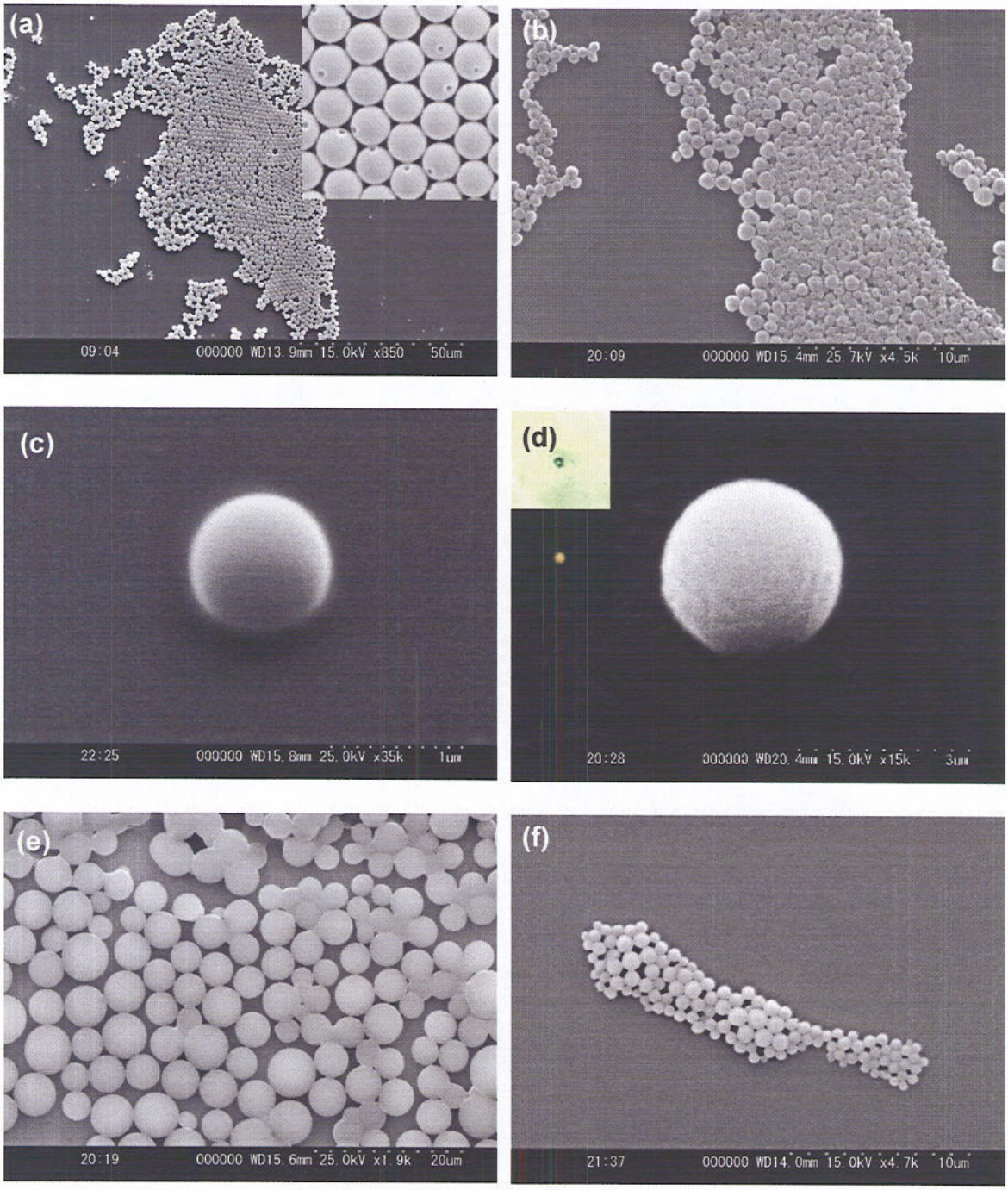

Figure. 2-3. Scanning electron micrograph of prepared nano-particles from polystyrene (a), polysulfone (b), polyvinylcarbazol (c), polyion complex containing fluorescence dye (d), fluorinated copolymer (e), and poly- ε -caprolactone (f). The close up image of array of polystyrene nano-particles is shown in an inset of (a). Optical micrograph and fluorescence micrograph of the dye labeled polyion complex particle is shown in an inset of (d).

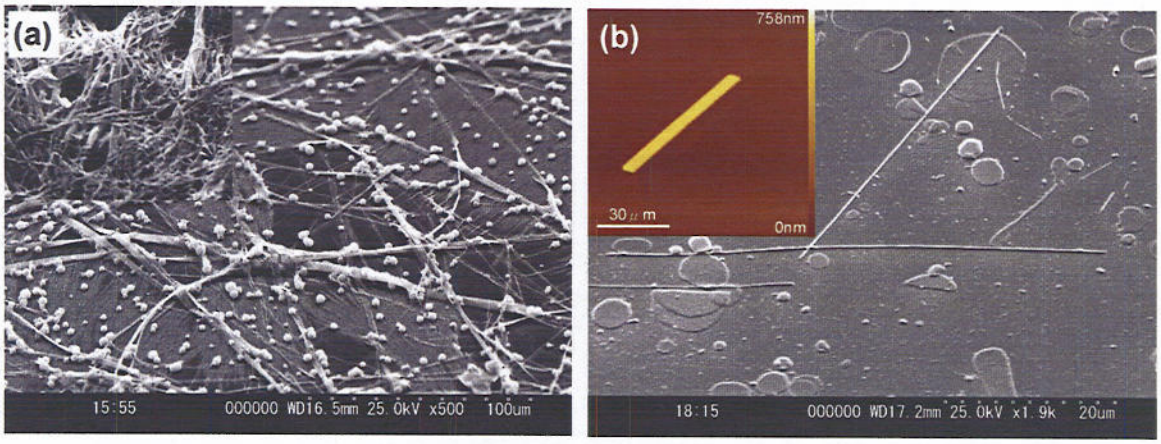

Figure 2-4. Scanning electron micrographs of micro-wires from polyhexylthiophene, and cyanine dye. Inset shows close up image of polyhexylthiophene wires (a) and an AFM image of the single wire from cyanine dye (b).

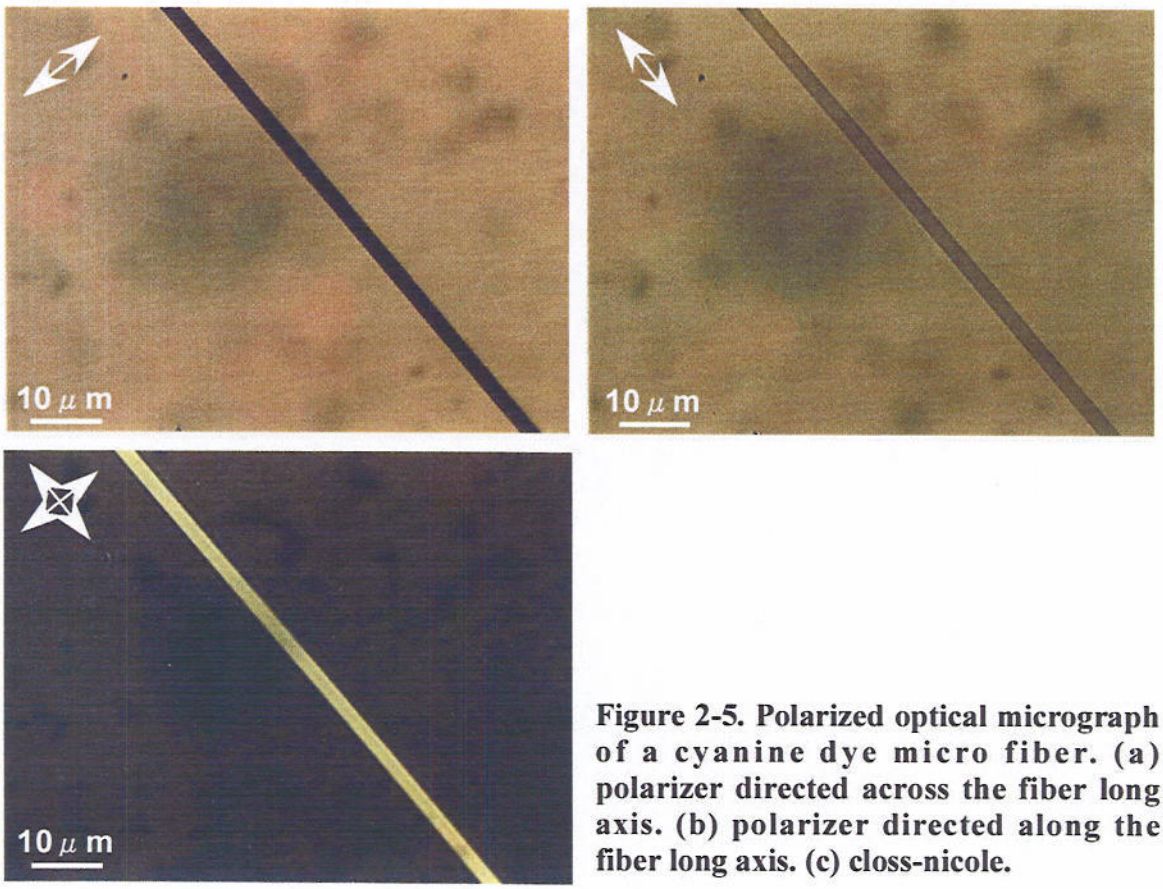

Figure 2-5. Polarized optical micrograph of a cyanine dye micro fiber. (a) polarizer directed across the fiber long axis. (b) polarizer directed along the fiber long axis. (c) closs-nicole.

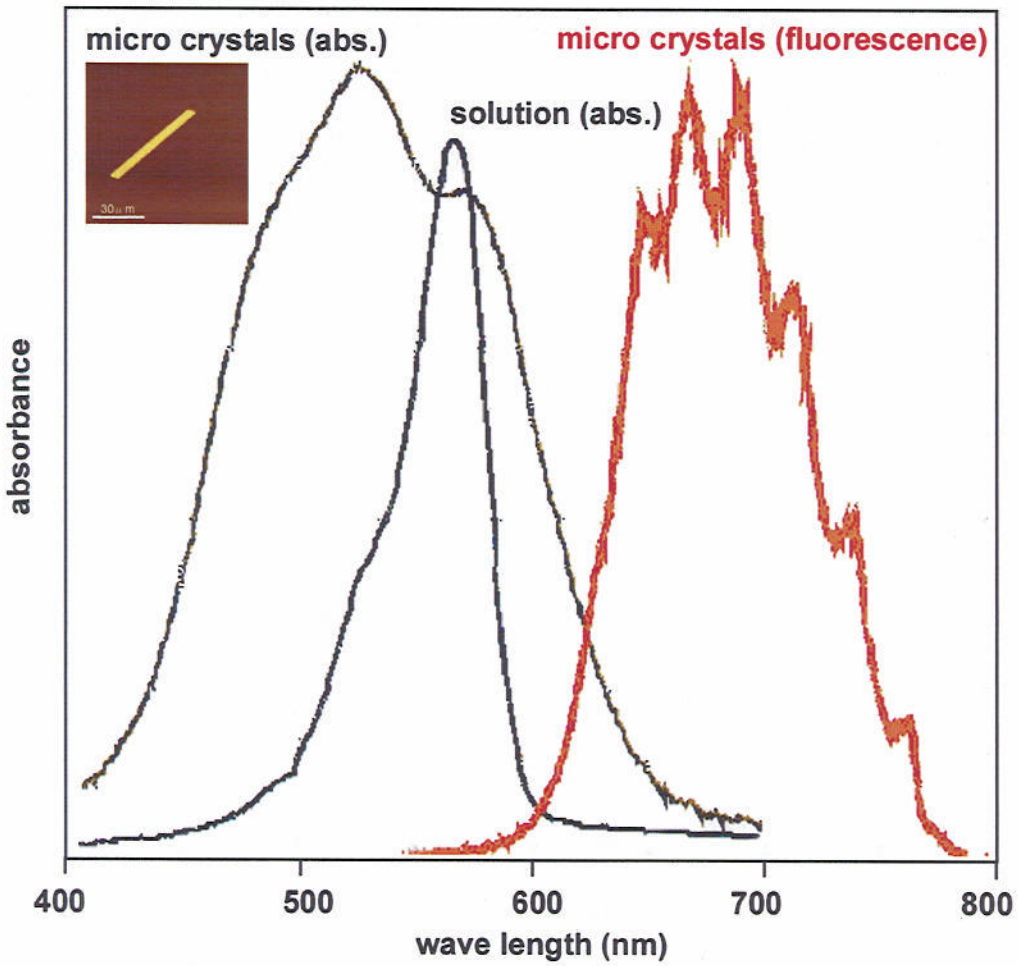

Figure 2-6. Absorption and fluorescence spectra of wires and solution of cyanine dye (2-6). The absorption peak was blue shifted in the case of wires. This result shows the H-aggregate was formed in the micro-wires (dark purple line). The fluorescence spectrum shows some interference effect of aggregate structures (red line).

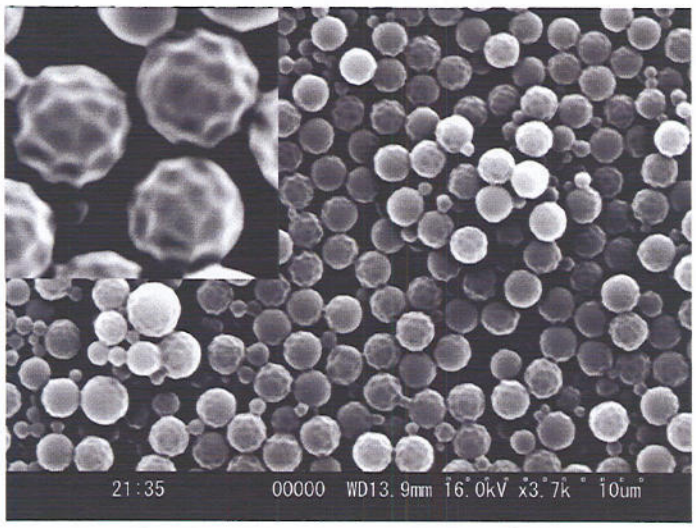

Figure 2-7. Scanning electron micrograph of particles from 2-12. The close up image of dimpled three nano-particles is shown inset of the figure.

These results indicate the shape of particles is dominated by the surface tension and cohesive force among molecules.

The most distinguish particles were obtained by using poly(styrene-*b*-isoprene) (**2-12**). In this case, the each particle surface filled by dents (Figure 2-7).

2-4. Particle formation mechanism

To discuss the particle formation mechanism, the formation process should be observed carefully. The particle formation process was observed in polystyrene system. THF solution of polystyrene was prepared as 1.0g/L solution. The same amount of water was slowly added into the polymer solution. In the case of stirring the solution after pouring the poor solvent, the agglutinates were precipitated and no nano-size particle was formed. After pouring the poor solvent without stirring, two types of samples were prepared. Five hundred micro litters of mixed solution was batched off soon after mixing poor solvent and injected into 10mL of water. This sample is considered as the early stage of particles formation. Another sample is the left mixed solution. The solution was placed for two days under ambient condition to evaporate THF.

Each sample became opaque after THF evaporation. Twenty micro litters of dispersions were casting onto freshly cleaved mica substrates. After evaporation of water, the prepared structure was observed by SEM. By SEM observations, each particle had spherical shapes (Figure 2-8). However, the clear difference of particle sizes was observed (Figure 2-9). In the case of aliquot, the particle size was around c.a. 300nm. On the other hand, the micron size particle was prepared in the case of evaporation slowly. This result shows significant information about particle formation process. In the case of template system, the template size is the maximum size of the particles. On the other hand, the particle size grew up in this system.

More detail particle formation process is discussed by using the kinds of polyion

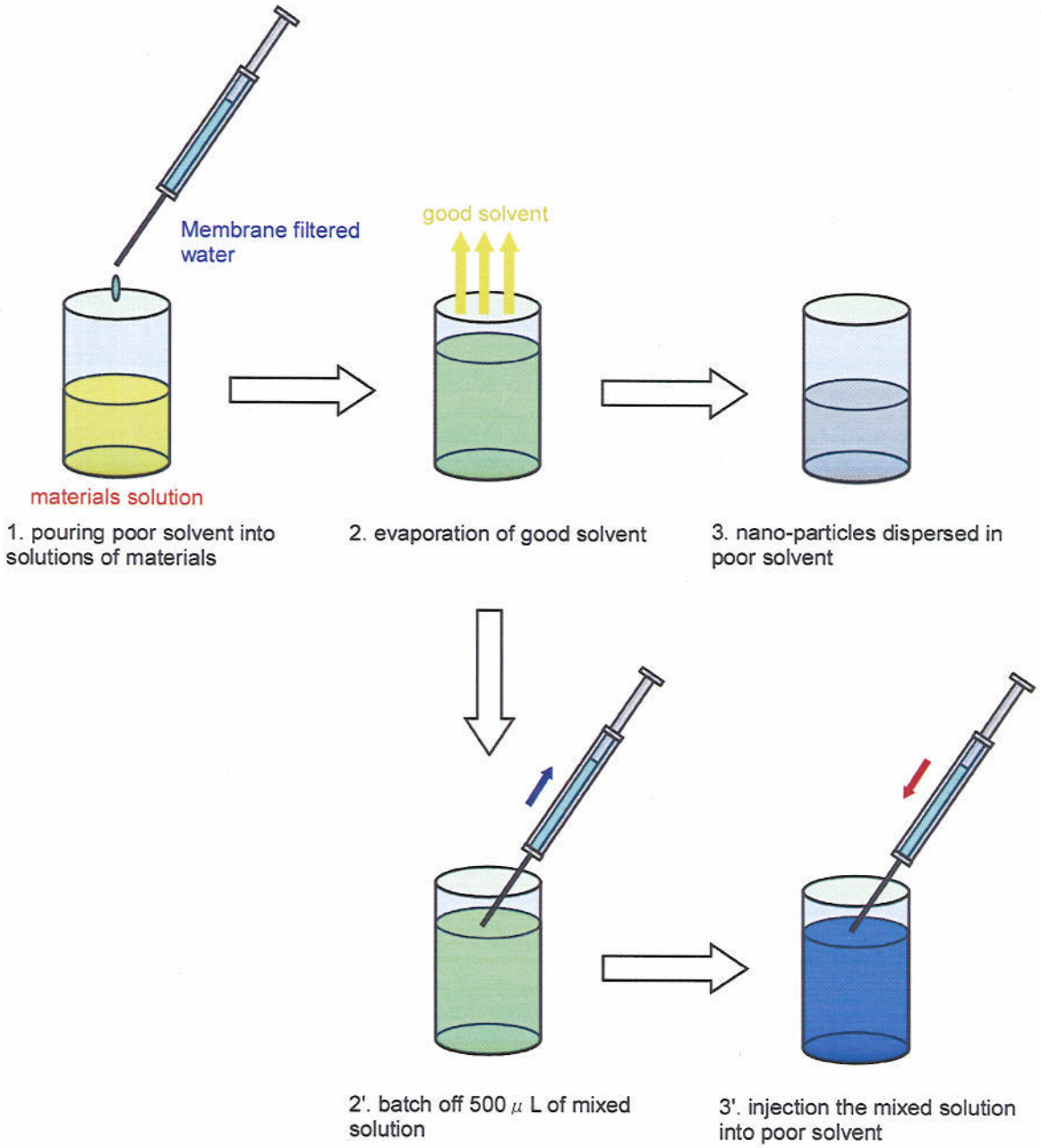

Figure 2-8. Schematic illustration of the particle formation and batch off experiment.

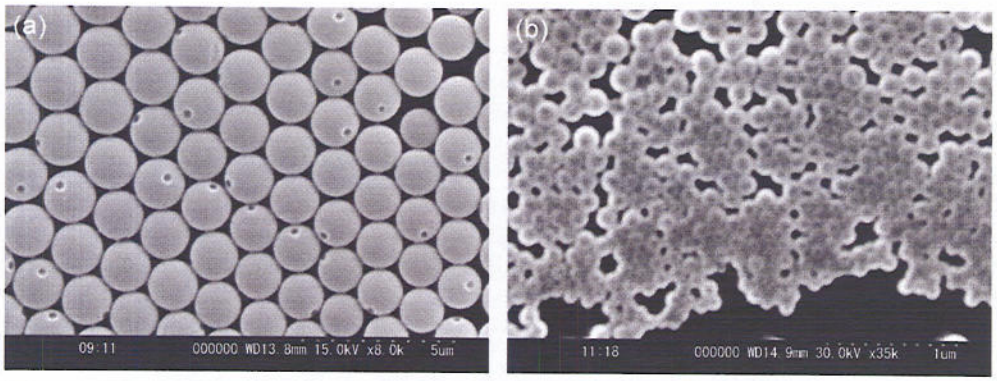

Figure 2-9. Scanning electron micrograph of polystyrene particles prepared by gently evaporated (a), and batched off (b). The size of batched off particles is smaller than that of normal evaporation.

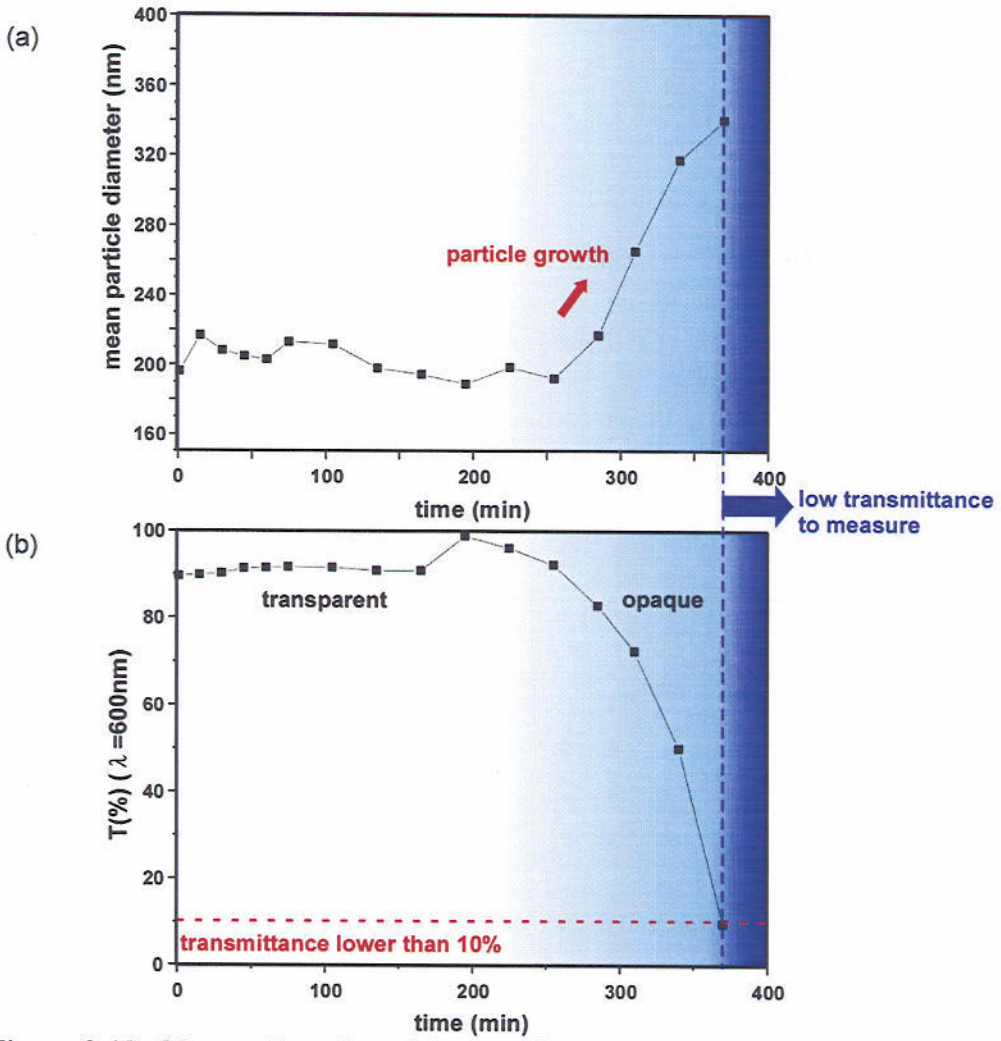

Figure 2-10. Observation of particle growth process. (a) particle size change measured by dynamic light scattering. (b) transmittance at λ =600nm of particle dispersion.

complex. Polyion complex containing polynucleic acid and amphiphile (Chart 2-1) were prepared by the procedure reported by Okahata et. al. (The detail preparation procedure was described in 2.6). Their detail properties concerning with the molecular recognition between specific base pairs are discussed in latter section. Here, the growth state of particles was observed by using polyion complex containing polyadenic acid and dimethyldioctadecyl ammonium bromide. The polyion complex dissolved in THF to prepare 0.1g/L solution. Two mL of the THF solution was injected in quartz cell (optical pass=1cm) by micro syringe. Two mL of Milli-pore membrane filtered water was added to homogeneous mixture of solution. The particle diameter was measured by dynamic light scattering (DLS, ELS-8000, Ohtsuka Denshi) half-hourly. The sample weight and transmittance were measured by electric balance and UV-Vis spectrometer (λ=600nm) as soon as measuring particles diameters.

In Figure 2-10, the particle size change (a), and transmittance of the sample solution (b) are shown. The mean particle diameter was c.a. 200nm in initial state. After 200min. later, the particle time suddenly grew up. At the same time, the transmittance of the solution decreased. The growth rate of the particle size change ranging from 200min. to 370min. was 1.3nm/min. Finally, the particle size became 350nm. However, the particle size did not measured by clouding of solution. The particle size came to wave length size, the strong scattering from particles were occurred. The sample weight linearly decreased; therefore the evaporation rate was constant. This result shows that the sudden growth of particle size was not the effect of evaporation rate change.

According to these results, the specific properties of this particle formation process are quoted as follows;

(1) Soon after mixing the poor solvent, the particle size was small.

(2) After some induction period, the particle size growth drastically.

(3) The particle growth was stopped when the good solvent was completely evaporated.

These results indicate that the particle formation process is dominated by homogeneous nucleation. The schematic illustration of formation process is represented in Figure 2-11. After mixing poor solvent, the particle size kept around 200nm. At this moment, the transmittance of the solution was high value. This state is corresponding to the formation of nuclei. The nuclei, it can be considered as globule state of polymers, are formed and collapsed in the solution. This state is considered as meta-stable state. The solution became gradually exchanged by poor solvent and a certain amount of good solvent evaporated, the particles growth was started. The molecules (polymers) still dissolved in the solution are adsorbed onto the nuclei, and then, the certain size particles are precipitated after all of the molecules spent.

The homogeneous nucleation occurs in meta-stable system. Therefore the phase diagram of the solution should be considered. The phase separation in polymer solution is studied for long years. The polymers and other organic materials usually had upper critical solution point. In phase diagram of polymer solution, the binodal and spinodal curve give significant information about solution state. The solution is single phase over the binodal curve and phase separation is occurred under the binodal curve. On the other hand, the spinodal curve is existed inner the binodal curve, the polymer solution kept single phase under the binodal curve. In the region between the spinodal and binodal, the polymer solution kept single phase but they are meta-stable state. The particle growth is occurred only in the region between the binodal and sipnodal curves. In the case of small amount of poor solvent is added, polymer solutions aged in meta-stable state, the particle size grow up. On the other hand, the large amount of poor solvent is added, the solution penetrated both curves, as the result, the polymer was precipitated. The difference between reprecipitation method and self-organized precipitation method is whether the solution aged in meta-stable state or not.

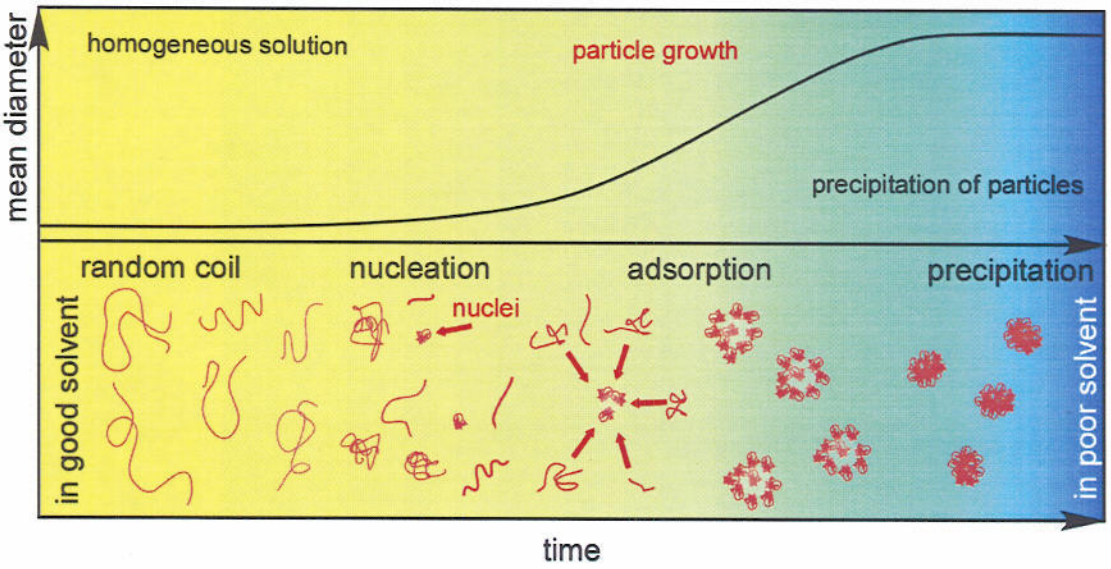

Figure 2-11. The formation mechanism of nano-particles by using self-organized precipitation method.

2.5. Size and size distribution control

The particle size and size distribution controls are significant issue of nano-particle formations. In the case of the conventional template method (i.e. emulsion polymerization etc.), the size of template size dominated the size of nano-particles. On the other hand, the self-organized precipitation method is a non-template system. The parameter of the controlling the particle formation is quote as follows;

(a) The concentration of solution

(b) The ratio between good solvent and poor solvent

(c) Preparation temperature

(d) Combination of good solvent and poor solvent.

In these parameters, (a) and (b) is easy to control. The effects of the solution concentration and the ratio between good solvent and poor solvent are discussed.

Experimental. Polystyrene was used as a model material. Polystyrene (Mw=2,316,000, Mn=2,276,000, Mw/Mn=1.02, Scientific Polymer Products, Inc, U.S.A.) was dissolved in

tetrahydrofran (THF, with stabilizer, WAKO Chemical Industry). From 0.1g/L to 5.0g/L solution was prepared. The poor solvent, water (Milli-pore membrane filtered, 18kΩ resistance) was added into 2mL of the homogeneous solution. The amount of water was changed from 1mL to 20mL. The mixed solutions were gently placed for two days to evaporate the good solvent, THF.

After evaporation of THF, the particle size was measured by dynamic light scattering (DLA, ELS-8000, Ohtsuka Denshi). The ζ potential of the particles was also measured by electrophoretic dynamic light scattering. The morphologies of particles were observed by SEM (S-3500N, Hitachi).

Results and discussion. The shape of the particles was spherical. The characteristic property of prepared particles is a dent existing on the surface of particles. These dents observed on each particle surfaces. The particle size was changed by changing the preparation conditions. The particle size decreased by decreasing the concentration of the starting THF solution. The particle size also decreased by increasing the amount of water contents (Figure 2-12). The particle size was controlled from c.a. 100nm to tens micrometer. These results related the formation process of particles. The particle formation mechanism of this method depends on the formation of nuclei and growth of particles. In the case of lower concentration, enough amounts of polymers to grow up the nuclei were not existed. Therefore only small size particles, near the size of nuclei or single polymer chains can be precipitated. According to the literature describing the particle size of single polymer chain, the particle size from single polymer chain is considered c.a. 37nm calculated by using the molecular weight [2-13]. The minimum size of the particles obtained by using this method under low concentration condition was c.a. 80nm. This size will be consisted of only two or three polymer chains. In the case of pouring amount of water, the situation is more complex. The effect of the addition much amount of water is the spontaneously precipitation from homogeneous phase.

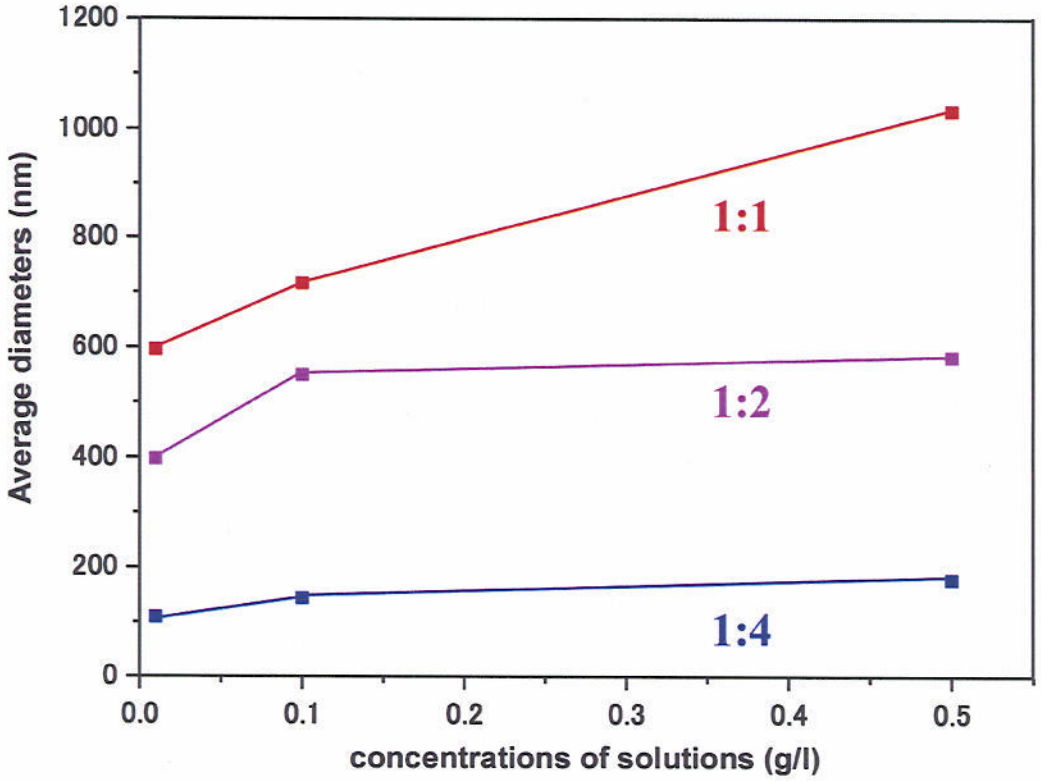

Figure 2-12. The particle size change of polystyrene particles by changing solution concentration and amount of poor solvent (water).

The surface potential of the particles give important information about the stability of the nano-particles. On the surface of particles, the electric double layer is formed depending on the functional groups on the particle surfaces and ion adhesions. Above the layer of adhesion ions, the surface called Stern plane, and the potential of the Stern plane is called Stern potential. On the other hand, the Stern potential is difficult to be measured in actual cases. The slipping plane above the Stern plane is affected by hydrodynamic stimulations. The potential on the slipping plane is called ζ potential. By electropholisis, the particles move depending on the ζ potential of each particle. This means the ζ potential is easily determined by electropholisis. In most cases, the surface potential can be approached by the ζ potential. In the case of using polystyrene, the ζ potential was charged minus. The value of charged potential is less than -34mV. This value is competitive value of commercially available sulfonic acid stabilized polystyrene nano-particles (diameter=300nm). This high surface potential kept the particles disperse for months.

2.6. Molecular recognition of nano-particles of polynucleic acid-amphiphile polyion complexes.

Polyion complexes, **2-13**, **2-14** and **2-15** (Chart 2-2) were prepared from polyA, polyU and polyC and dioctadecyl-dimethyl-ammonium bromide according to the conventional method, respectively [2-11]. Polyion complex formation of the polynucleic acids and the amphiphile was confirmed by elemental analysis for all products [2-12]. Water was added in each prepared polyion complex / THF solution. The solution was transparent initially, but it became gradually clouded according to the THF evaporation. After completely evaporation of THF, aqueous dispersions of nano-particles were obtained. Figure 2 shows a scanning electron micrograph of the nano-particle of **2-13** The nano-particle has an almost completely spherical shape (Figure 2-13).

After completely evaporation of THF (2days after mixing), the particle size was measured again with dilution the prepared particle dispersion. In this case, the average particle size grew up for 500nm at this final state. In this experiment, the average diameters of the prepared nano-particles of **2-13**, **2-14** and **2-15** were controlled as 64nm, 42nm and 1466nm, respectively (Figure 2-14 (a), (b) and (e)).

It was great interesting whether the surface of the nano-particles still had molecular recognition of base-pairing or not. When polyA nano-particles of **2-13** and polyU nano-particles of **2-14** were mixed in water, a drastic change of particle size from tens nm to 217microns diameters was occurred (Figure 2-14.(c)). This indicates aggregation was formed by mixings of polyA and polyU nano-particles. However, in case of polyA nano-particles of **2-13** and polyC particles **2-15**, there was no aggregation. The particle size was not changed after mixing (Figure 2-14. (f)). These results indicate that nucleobase existed on the surface of

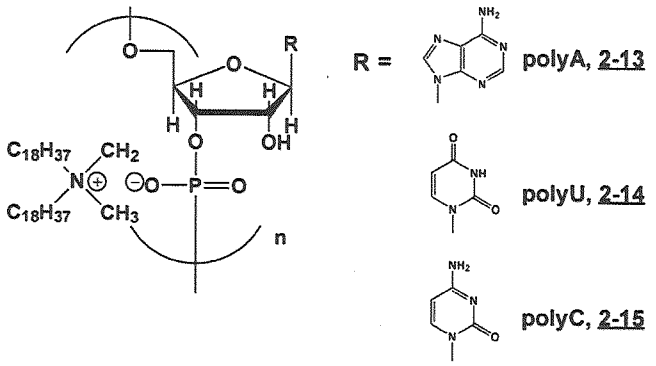

Chart 2-2. Chemical compounds used in this experiment.

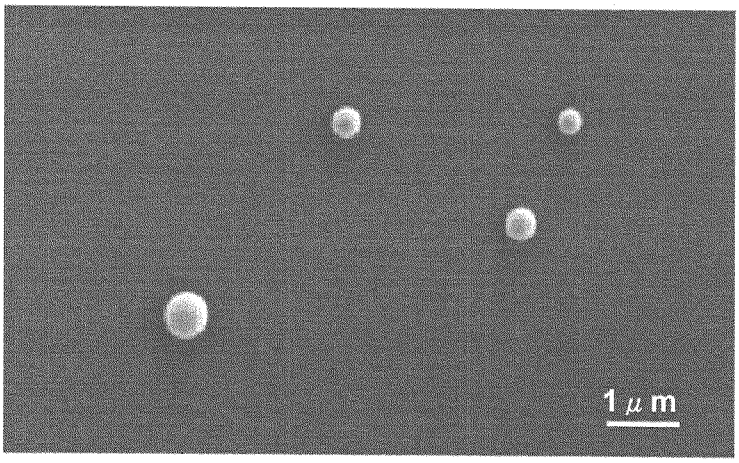

Figure 2-13. Scanning electron micrograph of 2-13 nano-particles

nano-particles and they could form complementary base-pairs between polyA and polyU.

In order to confirm hydrogen bonding formation among the nano-particles melting properties of mixed **2-13** and **2-14** nano-particles in water by UV-Vis absorption spectroscopy (V-530, JASCO) [2-15]. The absorption changed at 400nm, which was attributed to scattering from aggregates was monitored as a parameter of the aggregation size. When the temperature was increased, absorbance at 400nm decreased (Figure 2-15). At 52°C, drastic decrease of absorption was observed. This indicates dissociation among nano-particles was occurred by increasing temperature. The melting curve shows two steps of decreasing absorbance were

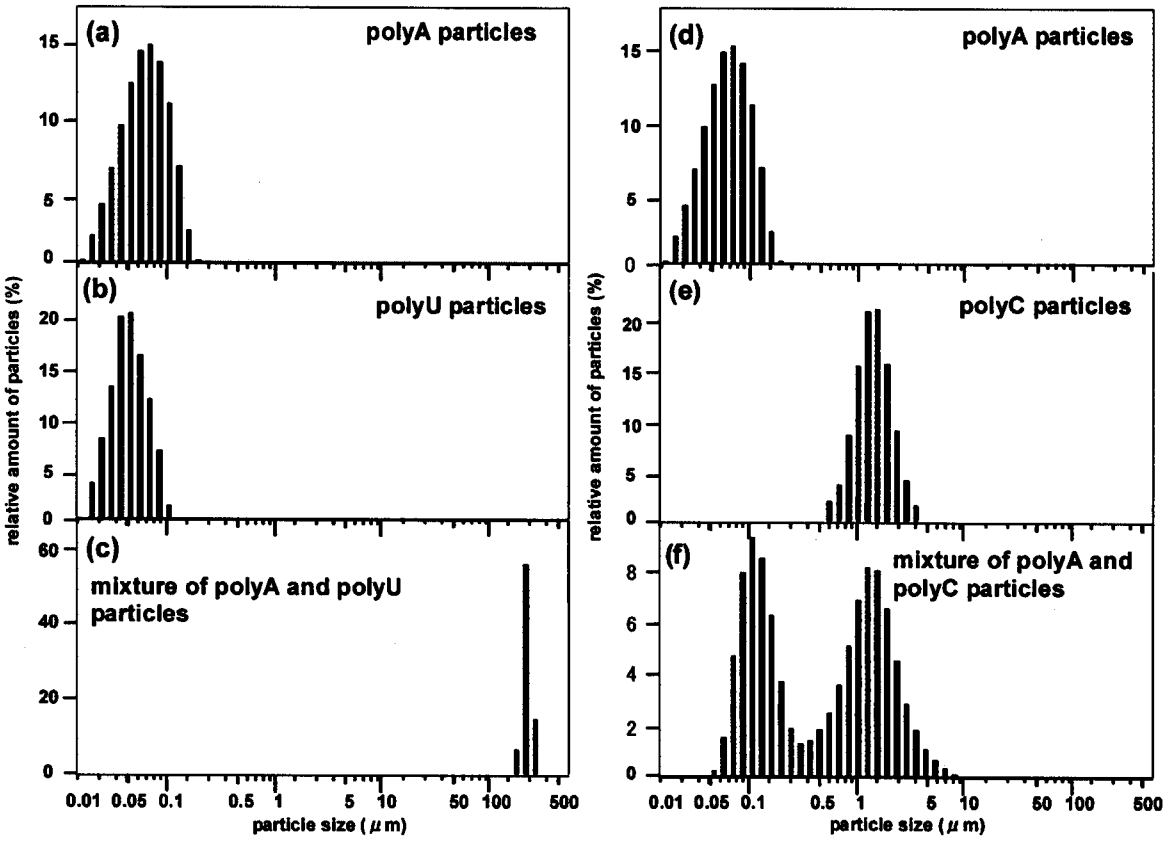

Figure 2-14. Distributions of diameters of nano-particles from polynucleotides-amphiphles polyion complex. Diameter distributions from polyA (a), (d), polyU(b) and polyC(e) nano-particles were shown. The results of mixture of polyA and polyU nano-particles and polyA and polyC nano-particlecs were shown (c) and (f), respectively.

existed. Melting point of double-stranded poly adenilic acid and poly uridiric acid sodium salt is 58°C in the same conditions [2-16]. Lower melting point of the aggregate of poylA and polyU nano-particles than ds-polyA-polyU indicates hybridization between polyA and polyU of the surface of the nano-particles was not perfect due to less number of base pairs or steric hindrance.

We showed preparation of the nano-particles from polynucleotide-cationic amphiphile polyion complex by solvent replacemet. The nano-particles diameter was controlled by concentration of the polyion complex solution from nanometer scale to micrometer scale. Hybridization of polynucleotides located at the surface of the nano-particles allowed forming the specific aggregation. This experiment is preliminary to organize the three

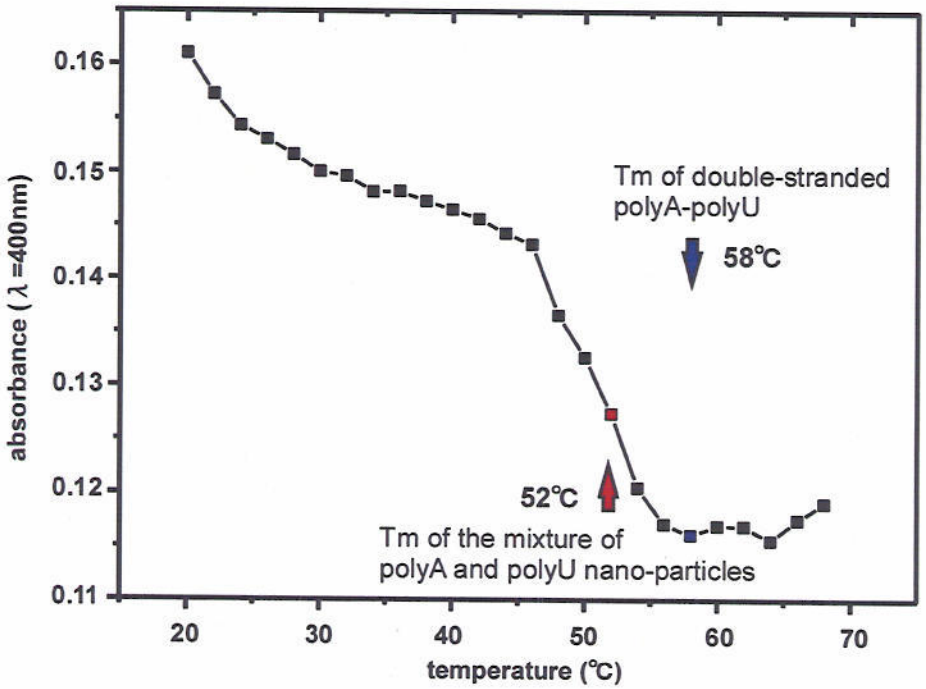

Figure 2-15. Melting properties of 1 and 2 nano-particle aggregation. Clear decrease of 400nm absorption was observed from 46℃ to 68℃. The melting temperature of the aggregation was 52℃. This is lower than the melting temperature of double strand polyA-polyU, 58℃ estimated from 260nm absorbance of the water solution.

dimensional architectures out of the nano-particles by specific molecular recognition (Figure 2-16). These nano-particles can also be utilized for diagnosis for hereditary diseases and vectors for gene therapies [2-17].

Experimental. Polyion complex containing polynucleic acids and amphiphile was prepared by the procedures reported by Okahata et. al. Polyadenic acid (polyA), polyuridic acid (polyU), and polycytosic acid (polyC) (Yamasa) were dissolved in Milli-pore membrane filtered water, respectively. The same molar of dimethyldioctadecyl ammonium bromide (Sogo Pharmaceutics, Inc.) was dispersed in Milli-pore membrane filtered water by the probe type ultra sonic generator (UD-20, Tommy Seiko) for 2 hours. The polynucleic acid solution and amphiphile solution was mixed and then, the white precipitation was spontaneously dispersed in mixed solution. Each white product was extracted by chloroform and reprecipitated in acetonitrile. The reprecipitated products were accumulated by centrifugation (3600r.p.m.,

15min.). After drying *in vaccuo*, the elemental analysis was performed for all compounds [2-15].

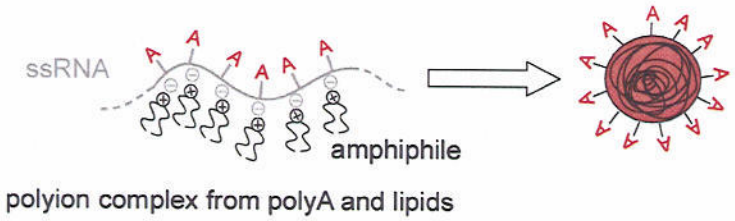

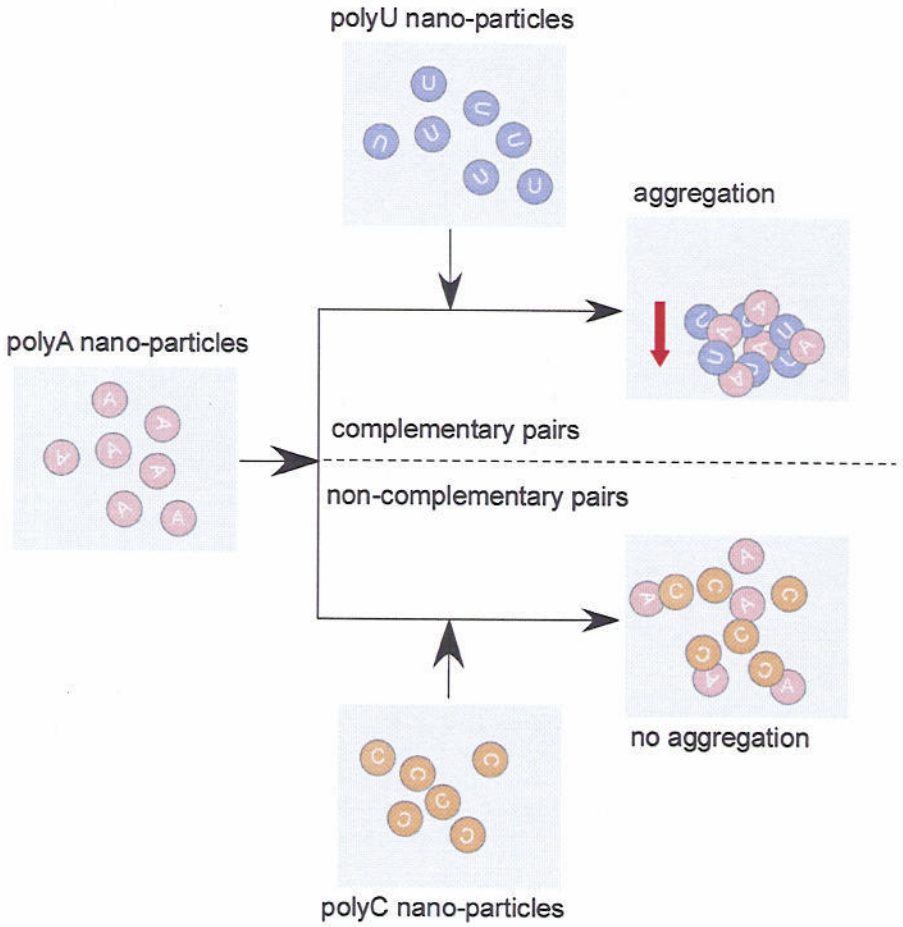

Figure 2-16. Schematic illustration of molecular recognition between particles containing different nucleic acids.

Reference

[2-1] G. D. Zhang, A. Harada, N. Nishiyama, D. L. Jiang, H. Koyama, T. Aida, K. Kataoka, *J. Control. Release.*, **93**(2) 141 (2003)

[2-2] B. Yoza, M. Matsumoto, T. Matsunaga, *J. Biotech*, **94**(3), 217 (2002)

[2-3] (a) Y. A. Vlasov, X.-Z. Bo, J. C. Sturm, D. J. Norris, *Nature*, **414**, 289 (2001), (b) T. Cassagneau, F. Caruso, *Adv. Mater.*, **14**(1), 34 (2002), (c) L. M. Goldberg, J. Wagner, J. Stumpe, B.-R. Paulke, E. Görnitz, *Langmuir*, **18**(8),3319 (2002)

[2-4] Y. Lu, Y. Yin, Y. Xia, *Adv. Mater.*, **13**(1), 34 (2001)

[2-5] Y. Kuga, S. Endoh, H. Chiyoda, K. Takeuchi, *Powder Tech.*, **66**, 85 (1991)

[2-6] B. S. Casey, B. R. Morrison, R. G. Gilbert, *Prog. Polym. Sci.*, **18**, 1041 (1993)

[2-7] Y. T. Moon et. al., *J. Am. Ceram. Soc.*, **78**(10)2690 (1995)

[2-8] M. L. Steigerwald, A. P. Alivisatos, J. M. Gibson, T. D. Harris, R. Kortan, A. J. Muller, A. M. Thayer, T. M. Duncan, D. C. Douglass, L. E. Brus, *J. Am. Chem. Soc.*, **110**, 3046 (1988)

[2-9] H. Fessi, F. Puisieux, J. P. Devissaguet, N. Ammoury, S. Benita, *Int. J. Pharm.*, **55**, R1-R4 (1989)

[2-10] (a) H. Murakami, M. Kobayashi, H. Takeuchi, Y. Kawashima, Int. J. Pharm., **187**, 143 (1999), (b) M. Jobmann, G. Rafler, *Int. J. Pharm.*, **242**, 213 (2002)

[2-11] S. K. Triphathy, H. Katagi, H. Kasai, S. Balasubramanian, H. Oshikiri, J. Kumar, H. Oikawa, S. Okada, H. Nakanishi, *Jpn. J. Appl. Phys.*, **37**, L343 (1998)

[2-12] K. Matsuno, *Pharm. Tech. Jpn.*, **11**, 1215 (1995)

[2-13] J. Kumaki, *Macromolecules*, **19**, 2258 (1986)

[2-14] W. Saenger, Principles of Nucleic Acid Structure, Springer-Verlag, New York (1984)

[2-15] **2-13**; yield 43% ; Anal. Calcd. for $C_{48}H_{91}N_6O_7P_1$: C,65.6; H, 10.4; N, 9.57%. Found: C, 59.2; H, 9.73; N, 10.07. polyA : amphiphile=1.0 : 0.73. **2-14**; yield 56%; Anal. Calcd. for $C_{47}H_{90}N_3O_7P_1$: C, 66.0; H, 10.5; N, 4.91%. Found: C, 62.9; H, 10.6; N, 4.56%. polyU : amphiphile = 1.0 : 0.82. **2-15**; yield 45%; Anal. Calcd. for $C_{47}H_{91}O_7N_4P_1$: C, 66.0; H, 10.7; N, 6.56%. Found: C,62.34; H,10.28; N,5.13%. polyC : amphiphile = 1.0 : 0.75.

Chapter 3

Honeycomb-patterned Films

3.1. Introduction of the honeycomb-patterned films

In this chapter, the fabrications of the "honeycomb films" with hexagonally arranged, sub-micron or micron sized pores are shown. In many micro-patterned films, micro-porous polymer films with high regularities are attractive materials of potential application in the fields of electronics, photonics and biotechnology [3-1~3-2]. Recently, new class of micro-porous polymer films by using self-organization of condensed water droplets on the polymer solution surface as templates. The honeycomb-patterned porous polymer films are prepared by simple casting of polymer solutions of water immiscible solvent under high humidity (Figure 3-1) [3-3~3-20]. Hexagonally packed water micro droplets are formed by evaporation cooling on the solution surface and then transferred to the solution front in the convectional flow or by the capillary force. After solvent evaporation, the honeycomb patterned polymer film is formed with the water droplets array as template. Finally micro-porous polymer films are obtained after water evaporation (Figure 3-2). These micro-porous film formations are considered as one of the typical examples of the self-organized meso-structures. On the other hand, the honeycomb-patterned films from water miscible materials, super engineer plastics, and other functional materials have not reported yet. Furthermore, the detail formation processes, precise controlling of the honeycomb-pore sizes and fabrication methods have not been discussed.

In this chapter, the fore capital issues are discussed. The honeycomb-patterned films of polymer blend from ampihphilic copolymer and matrix polymers (section 3.3.). The phase separation in the honeycomb-patterned films from two components provides novel micro-structures. The formation mechanism of the honeycomb-patterned film will be reconsidered. Thermal and chemical stabilities, controlling surface properties and structures are significant for practical applications of the honeycomb-patterned films. Therefore the

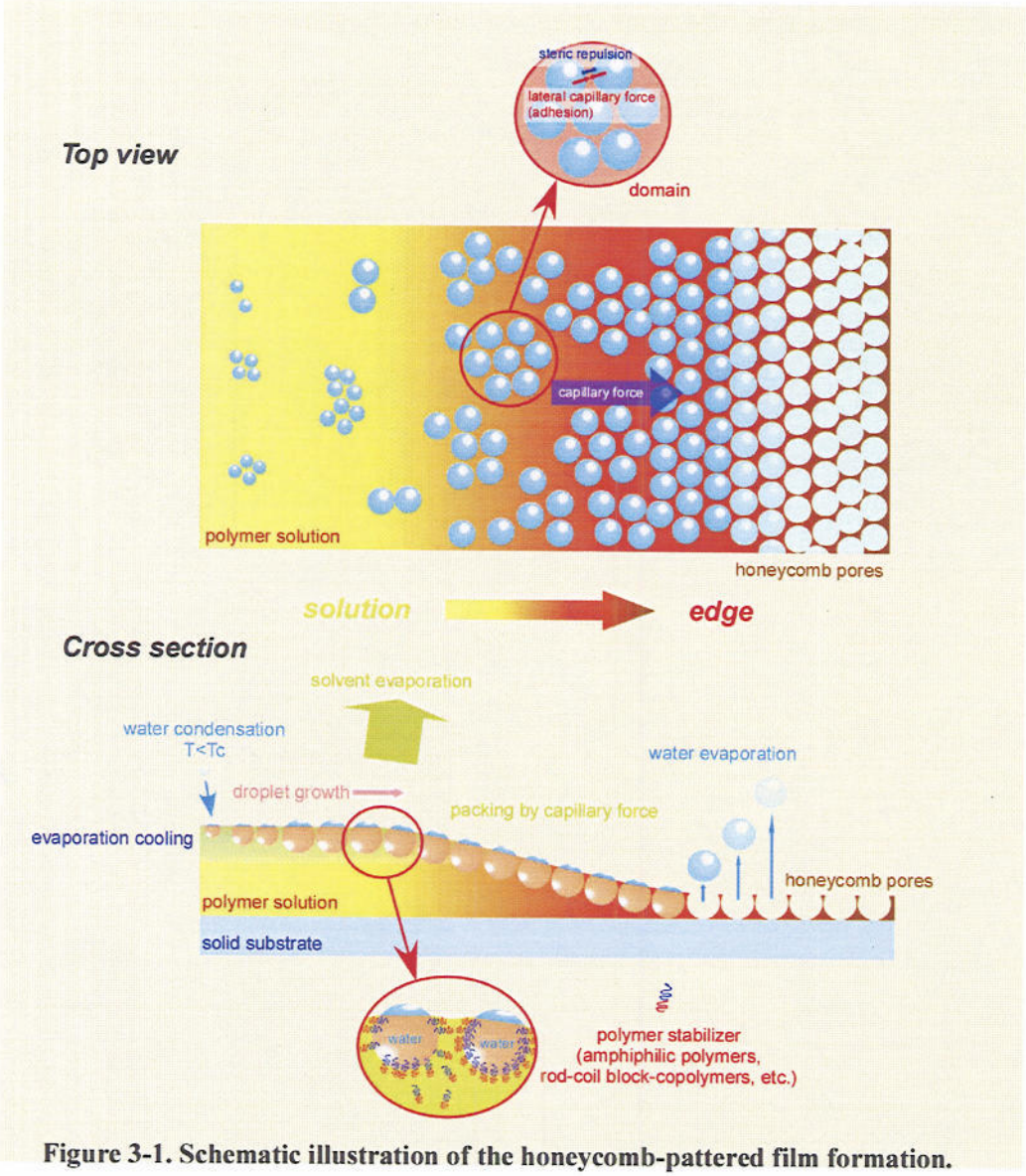

Figure 3-1. Schematic illustration of the honeycomb-pattered film formation.

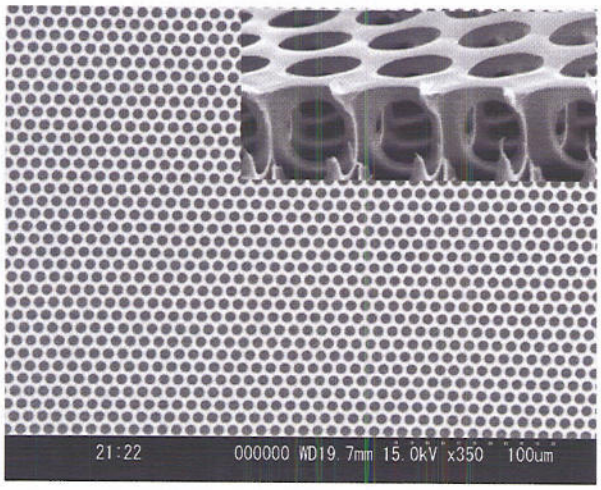

Figure 3-2. Scanning electron micrograph of the honeycomb structure. Inset image show the cross section of the film.

properties of the honeycomb-patterned films from functional or high performance materials are focused in the section 3.4. The controlling of pore size is one of the most significant issues to apply the honeycomb-patterned films. Effect of flow rate of humid air and the preparation of submicron sized honeycomb pores are shown in the section 3.5. Another approach is preparation of micro-structures by using the honeycomb-patterned films as templates. Micro lens, micro particles, pillars, and other characteristic micro-structures can be formed by molding and deformation of the honeycomb-patterned films. The third issue is the micro structure in the honeycomb-patterned films (section 3.6.).

3.2. General experimental conditions

The preparation methods of the honeycomb-patterned films used in this chapter include two methods. The experimental set up of batch method is shown in Figure 3-3. The glass dish of 9cm was filled with polymer solution, and then, the compressed humid air (40~70%) prepared by letting through the gas washer filed with water was applied vertically. The temperature and relative humidity of surrounding atmosphere is always monitored by hygrometer. The flow velocity was monitored by flow meter. The gap between the funnel and the glass dish was fixed from 5cm to 10cm. The honeycomb-patterned films were obtained as opaque round shape films. The advantage of the batch method is easy to change the preparation conditions. The formation process of the honeycomb-patterned films much are affected by the preparation conditions because the condensation of template water droplets influenced by the temperature, evaporation speed, surface tension of the solution, and so on. The batch method can easily change these parameters. Chemical compounds used in this chapter are shown in Figure 3-4. The amphihpilic copolymer **3-1** is blended in the polymer solution to stabilize the condensed water droplets.

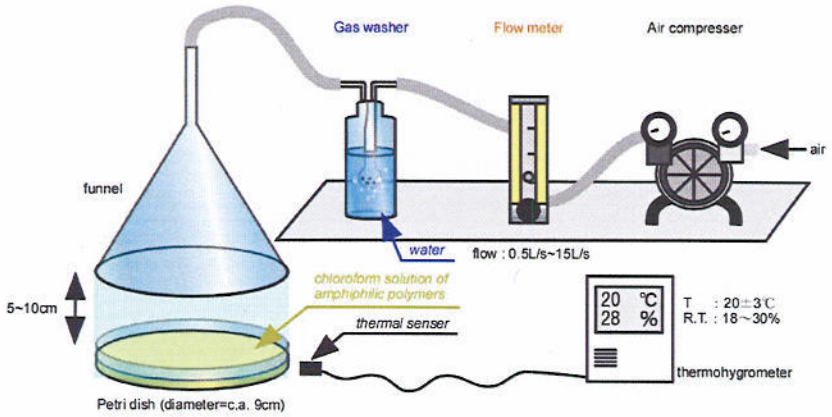

Figure 3-3. Schematic illustration of experimental set up.

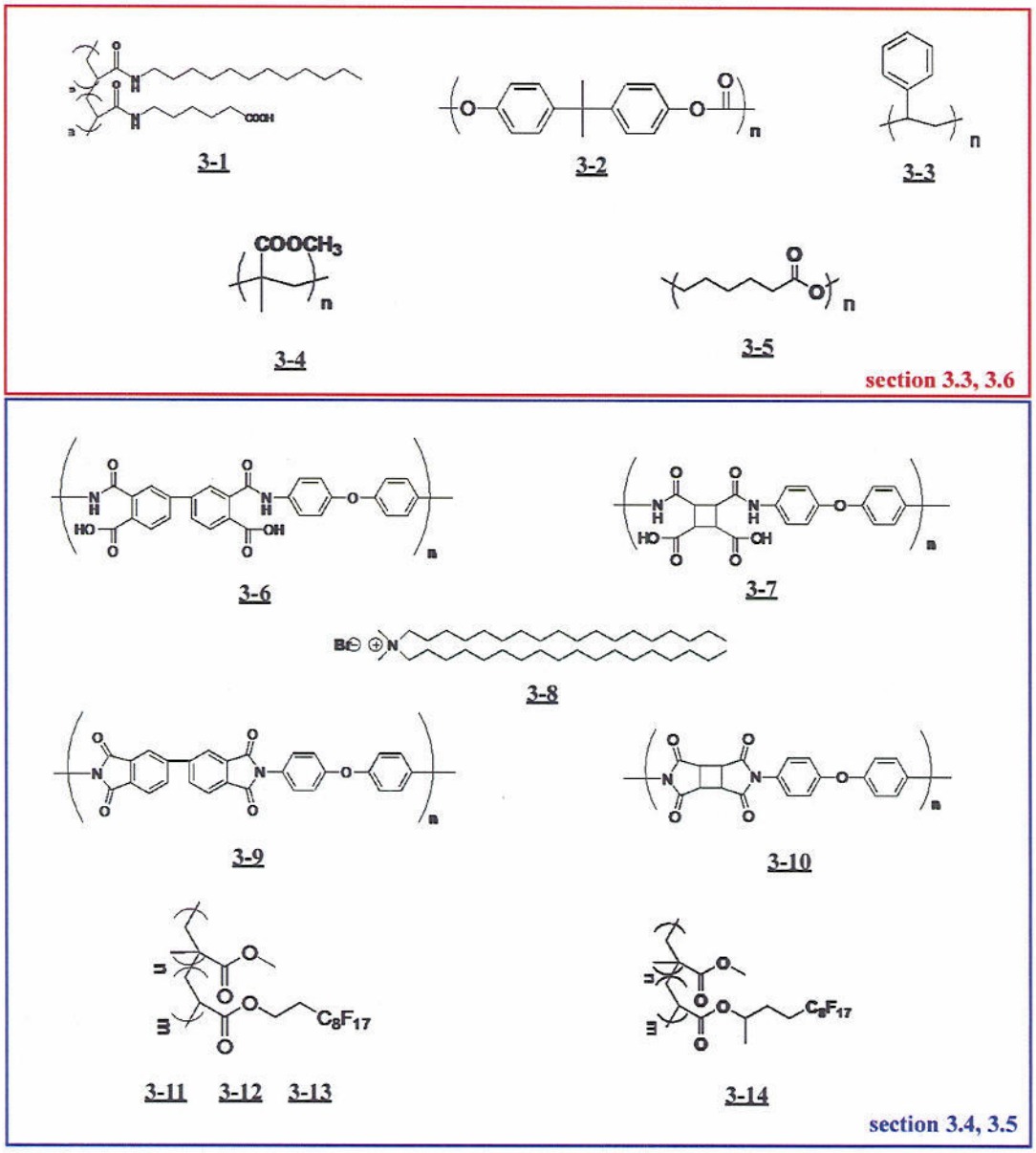

Figure 3-4. Chemical compounds used to prepare honeycomb-patterned films.

3.3. The polymer blend system of amphiphilic polymer and matrix compounds

3.3.1. The polymer blend honeycomb-patterned films

In the honeycomb-patterned film formation, the amphiphilic molecules can be act as a stabilizer of the condensed water droplets. If not amphiphilic molecules exist in casting solution, the film had irregular arrangement of variety size of pores (Figure 3-5 (a) and (b)).

It is difficult to fabricate the honeycomb-patterned films from normal hydrophobic polymers. Because the honeycomb-patterned films are formed by using condensed water droplets, the stabilizer of the water droplet is indispensable. In the case of mixing the certain amount (c.a. 10%wt.) of amphiphilic polymer into the hydrophobic polymer solution, the highly ordered honeycomb-patterned films from polymer blends of amphiphilic polymer and matrix polymers are obtained.

The Figure 3-6. shows the examples of polymer blend system. In each case, the highly ordered hexagonal arrays of micro-pours were formed in the films.

However, it was not clearly revealed that where the amphiphilic polymers were distributed in the honeycomb-patterned films. In this section, fabrication of micro-ring and micro-dot structures by annealing the honeycomb-patterned micro-porous films of amphiphilic copolymer and poly(bisphenolA-carbonate) **3-2** blend on a solid substrate are shown. FT-IR reflection absorption spectroscopy (RAS) measurements of prepared micro-structures and amphiphilic copolymer specific fluorescence dye staining experiment revealed that only amphiphilic copolymer was transferred onto solid substrate by the annealing process. DSC measurement also reveals the phase-separation state of the amphiphilic copolymer and poly(bisphenolA-carbonate) in the honeycomb-patterned films.

3.3.2. Experimental

Preparation of honeycomb-patterned films. Chloroform solution of amphiphilic

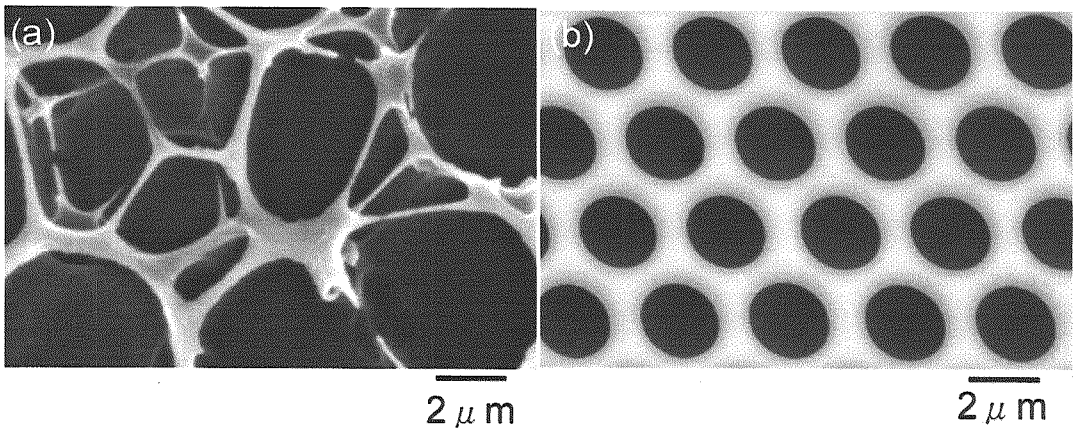

Figure 3-5. The film with irregular micro-pores was obtained from only polystyrene case (a). The honeycomb-arranged micro-porous film was obtained from polystyrene/amphiphilic blend (b).

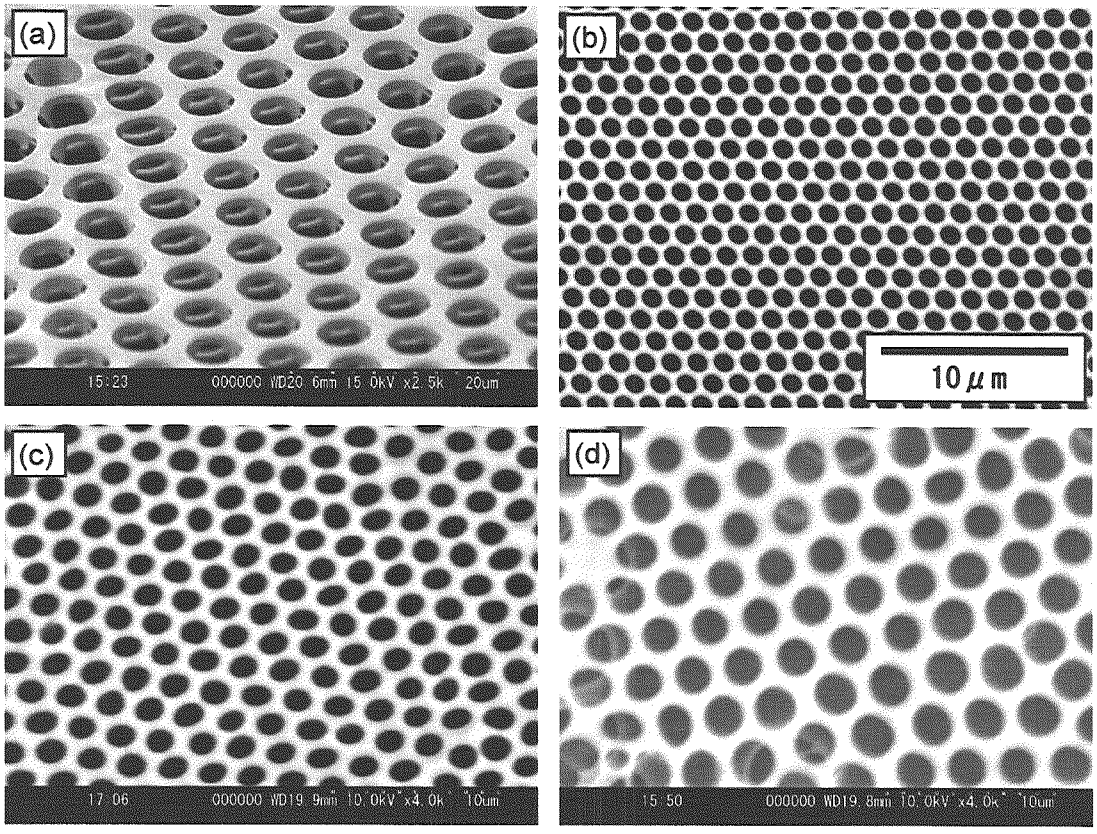

Figure 3-6. Scanning electron micrograph of honeycomb-patterned films from polymer blend of amphiphilic copolymer 3-1 and other materials. (a) poly(bisphenolA-carbonate) 3-2. (b) polystyrene 3-3. (c) poly(methymethacrylate) 3-3. (d) poly- ε -caprolactone 3-4.

copolymer **3-1** and poly(bisphenolA-carbonate)**3-2** (Mw=c.a.64,000 , Aldrich, U. S. A.) was prepared. The weight ratio between copolymer and poly(bisphenolA-carbonate) was 1:9. The solution concentration was 2.5g/L. Homogeneous solution of the polymer blend was dropped on a glass substrate (a glass Petri dish with 90mm diameter and 10mm height) with applying humid air (40~70% relative humidity) vertically on the solution surface. After complete evaporation of solvent, a white turbid polymer film with interference colors when it illuminated by white light was formed. The morphology of the prepared film was observed by optical microscopy, scanning electron microscopy.

Transferring structures onto ITO electrode by annealing process. ITO electrode was washed by chloroform and ethanol with sonication. After dried under ambient condition, the electrode surface was treated by ozone for 30 minutes in ozone cleaner (NL-UV253, Nippon Laser Denshi, Japan). By this treatment, the electrode surface became highly hydrophilic (The water contact angle became less than 30 degrees). The prepared honeycomb-patterned film was cut as 10mm squire sheets by surgical knife. A sheet of cut film was peeled off from the glass substrate in water, and then, the film floated on the air-water interface. The floating film was turned over upside down by tweezers. The cleaned ITO electrode was immersed in the water and scooped up the film onto the electrode surface. The prepared sample was dried *in vacuo*.

The sample was annealed ranging from 120℃ to 200℃ for 5~60 minutes on a hot-stage (RINCAM600, Japan Hi-tech, Japan). After cooling under ambient condition, the film was peeled off by a sheet of adhesive tape (Scotch tape, 3M, Japan). The transferred pattern was observed by the OM, SEM and atomic force microscopy (AFM, SPI400, Seiko Instruments, Japan). By AFM, the two-dimensional distribution of current conduction of the electrode surface was imaged. The samples were fixed on the sample stages of AFM by silver conductive paste (Dotite, Doujin Chemical Industry, Japan). The bias voltage from 5.00V to

9.99V was applied between the sample stage and an gold coated AFM tip. The topography and current image was simultaneously measured.

FT-IR RAS spectroscopy. The cleaned ITO electrode was coated with Au by ion sputter (VPS-020, Sinku Kiko, Japan). The honeycomb-patterned film and transferred patterns were prepared on the Au coated ITO electrodes by the same as the ITO electrode case. FT-IR RAS measurement was carried by FT-IR200 spectrometer (JASCO, Japan) with polarizing reflection unit (PR-500).

Specific staining of amphiphilic copolymer. Fluoreseine-5-isothiocyanate (**3-5**, FITC-1, Chart 1) was dissolved in dimethylformamide (DMF). And then, the 1mL of FITC-1/DMF solution was mixed in 9mL of aqueous solution of sodium carbonate (c.a. pH9). The transferred structures on ITO electrodes were immersed in the solution in ice bath for 1 hour and then the sample was kept in the solution for 10 hours at r.t. After rinsing by deionized water and ethanol, the samples were dried under ambient condition. The fluorescence image was obtained by B-exitation fluorescence microscopy (FM, BH-2, Olympus, Japan).

3.3.3. Results and discussion

A typical scanning electron micrograph of the prepared honeycomb-patterned film is shown in Figure 3-7(a). Well-arranged and uniform sized micro-pores were formed. The pore size was controlled from sub-micron scale to tens-micron scale by changing casting volume (15)

The cross-section of the film was shown in Figure 3-7(b). This micrograph indicates the honeycomb-patterned film consisted of double layers supported by pillar structure. The hexagonal lattices and dents are connected vertically by pillars at the vertex of hexagons. This structure apparently reflected the template water droplets. The pin-cushion like structure was

obtained by peeling off the top layer of the film by a sheet of adhesive tape under cooling in liquid nitrogen (Figure 7(c)). In liquid nitrogen, the polymer is stiff and their elasticity was lowered. Therefore the pillars were easily broken by the applied mechanical force.

After annealing and peeling off the honeycomb film placed on the ITO or gold electrodes, interference colors were observed on the surface of the electrodes annealing at any temperature (Figure 3-8). However, the two-types of micro-structures were formed depended on the annealing temperature. In the case of annealing ranging from 120V to 180°C, a hexagonal arranged ring structure was clearly imaged by AFM (Figure 9(a)). This structure was formed within 5 minutes after annealing starts. And the same structure was obtained when the annealing time was elongated. The current image of the hexagonal ring structure was obtained by conductive AFM measurements (Figure 9(b)). The inversed image of topography was obtained. Therefore no polymers remained on the substrate except for micro-rings. In the case of annealing over 180°C, micron-sized dots were formed (Figure 9(c)). The arrangement of the dot structure was reflected the hexagonal arrangement of honeycomb pores. The conductive AFM image showed clearly that the area except for the micro-dots is bare ITO electrode (Figure 9(d)). No structure was transferred annealing under 120°C.

The AFM images of the micro-rings prepared by using the honeycomb-patterned films with different pore size were shown in Figure 10(b). The periodicity and diameters of the micro-rings were changed by changing template honeycomb pore size. On the other hand, the heights and widths were not changed.

To reveal chemical composition of the prepared micro-structures, FT-IR RAS spectroscopy was performed. Figure 11(a)-(c) show the FT-IR spectra of the honeycomb-patterned film, the hexagonal micro-ring structure and the hexagonal micro-dot structure, respectively. The absorption attributing to the C=O stretching of the poly(bisphenolA-carbonate) was measured at 1790cm^{-1}. On the other hand, the micro-ring

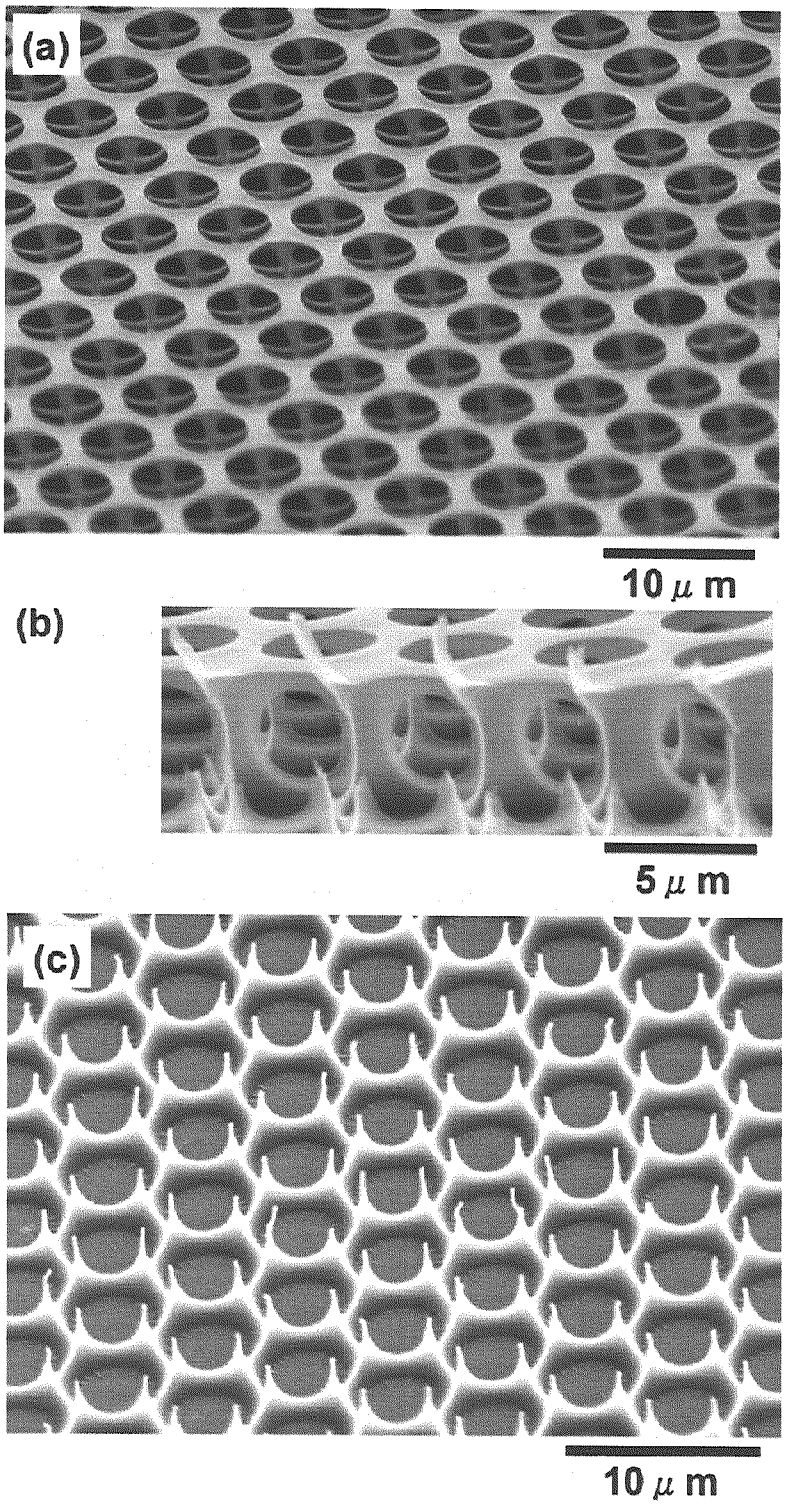

Figure 3-7. Scanning electron micrograph of honeycomb (a), cross section of honeycomb (b) and pillars (c), respectively.

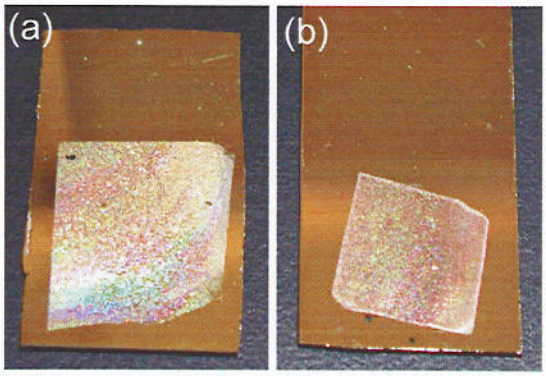

Figure 3-8. Photograph s of transferred structure. (a) annealing at 140℃, (b)annealing at 180℃

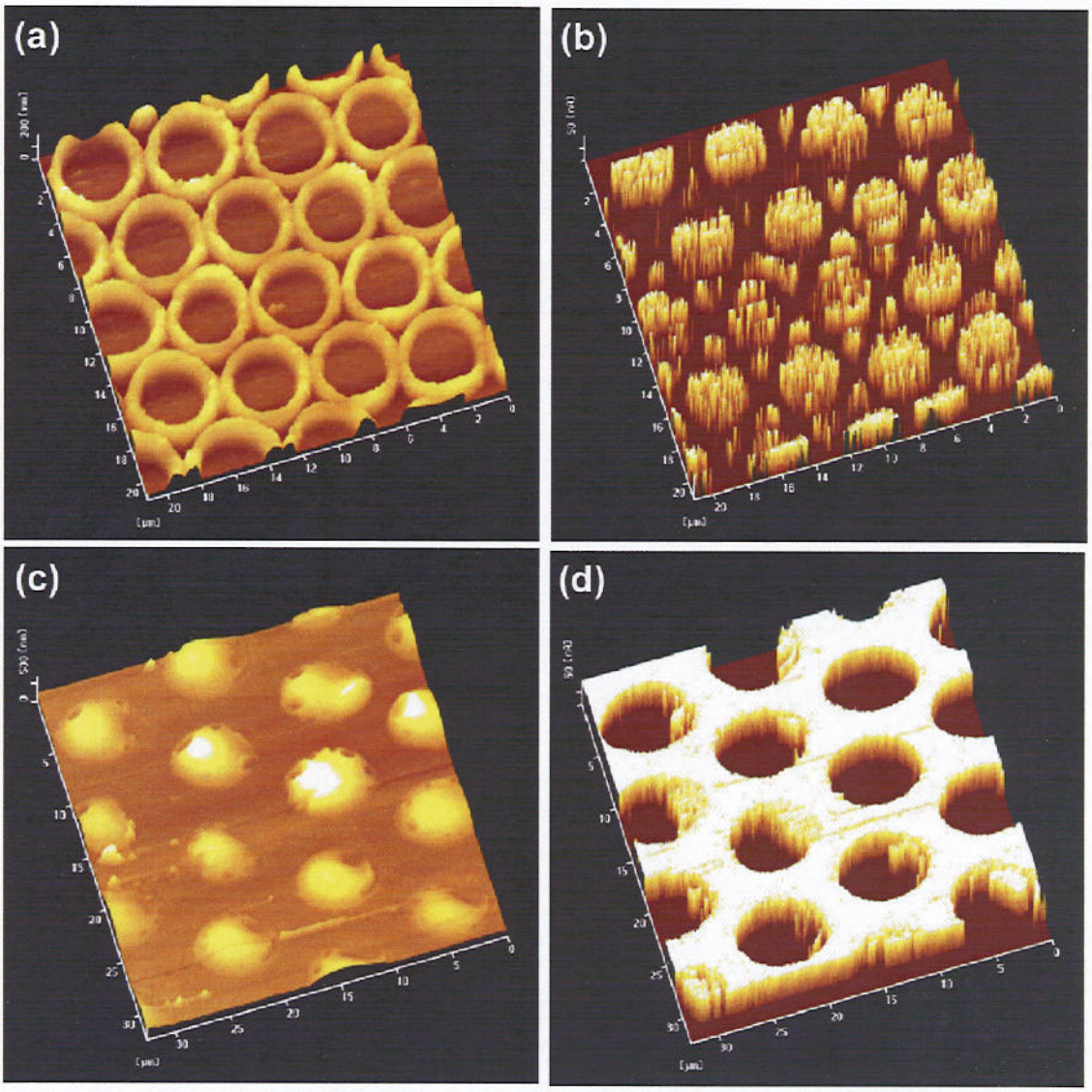

Figure 3-9. AFM images of micro-ring structure (a) and micro-dot structures (b). The electric current image of each sample was obtained simultaneously by applying voltage between a sample stage and gold coated AFM tip (b), (d). The applied bias voltage was 5.00V (b) and 9.99V (d), respectively. The inversed images of the micro-ring structures and micro-dot structure are clearly imaged.

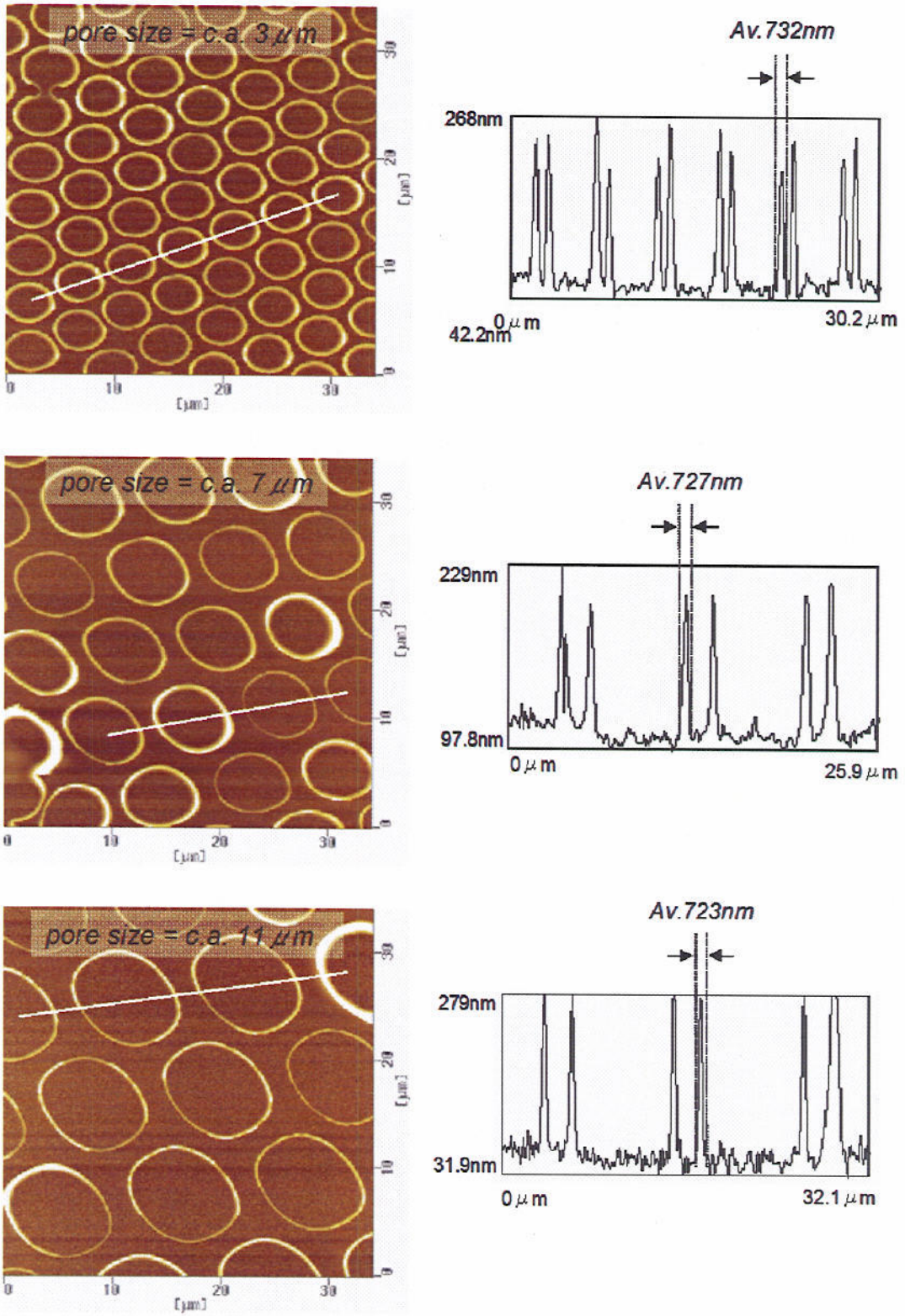

Figure 3-10. The size change of micro-ring structures by changing the size of pores of the template honeycomb-patterned films.

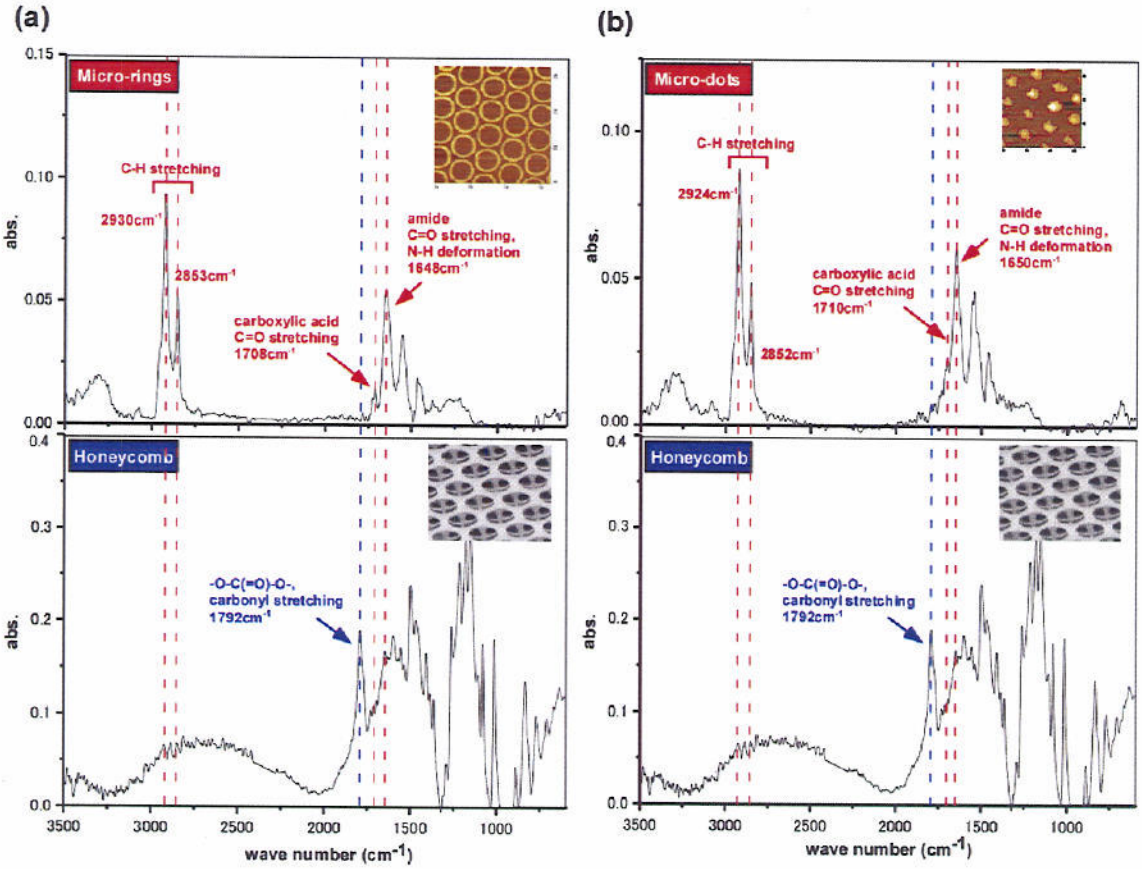

Figure 3-11. FT-IR RAS spectra of the honeycomb (the two bottom spectra), rings (a) and dots (b), respectively.

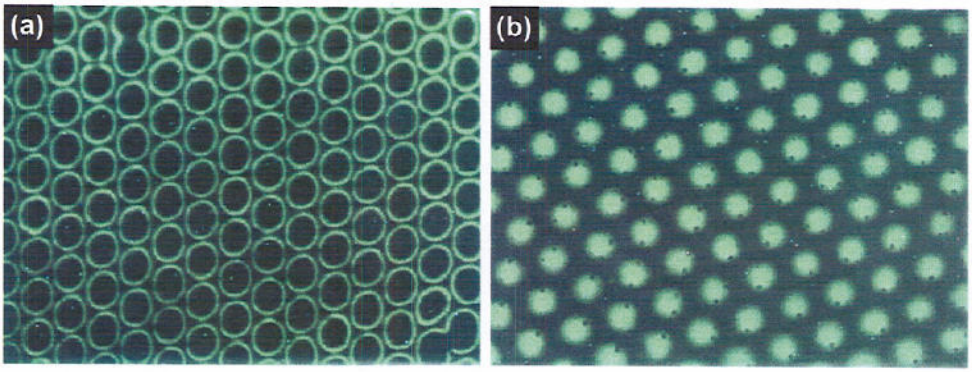

Figure 3-12. FITC labeled micro-rings (a) and dots (b), respectively/.

structure and the micro-dot structure did not have absorption at 1790cm^{-1}. Moreover, the absorptions at 1648cm^{-1} and 1708cm^{-1} attributed to the stretching of the amide C=O group and N-H group were observed. The absorptions of the stretching of the C-H group were also measured on 2930cm^{-1} and 2853cm^{-1}. These absorptions were not clearly observed on the absorption spectra of the honeycomb-patterned film. These results indicate that the main component of the honeycomb-patterned films is poly-(bisphenolA-carbonate) and the one of the hexagonal rings and dots is acrylamide polymer, **3-1**.

FITC-1 is a dye with isothiocyanate group, which is one of the reactive functional groups for amine, alcohol and carboxylic acid groups. This dye reacts with the carboxylic acid of the copolymer **3-1**. On the other hand, the dye does not react with poly-(bisphenolA-carbonate). Therefore it can be revealed which components consisted of the transferred structures. By this staining experiment, the micro-rings and micro-dots were clearly imaged by fluorescence microscopy (Figure 12(a), (b)). These results also support the result of the results of FT-IR RAS spectroscopy.

The difference between the formation of micro-rings and that of micro-dots is annealing temperature. Therefore, the thermal stabilities of the honeycomb-patterned films should affect the rings and dots formations. By DSC measurements, the glass transition point (Tg) of the poly(bisphenolA-carbonate) is around 144°C (Figure 3-13). The amphiphilic copolymer had three transition points under 100°C, and melt at 194°C. The amphiphilic molecules have many types of micro structures as liquid crystals in their bulk conditions. The micro structures reflected on DSC curves, and then the some transition points were measured. These results indicates the amphiphilic polymer is soften easier than the poly(bisphenolA-carbonate). However, by only these results, the reason of the difference between rings and dots formations is not cleared. The DSC curve of the honeycomb-patterned film, which is the mixture of amphiphilic polymer and poly(bisphenolA-carbonate), provides

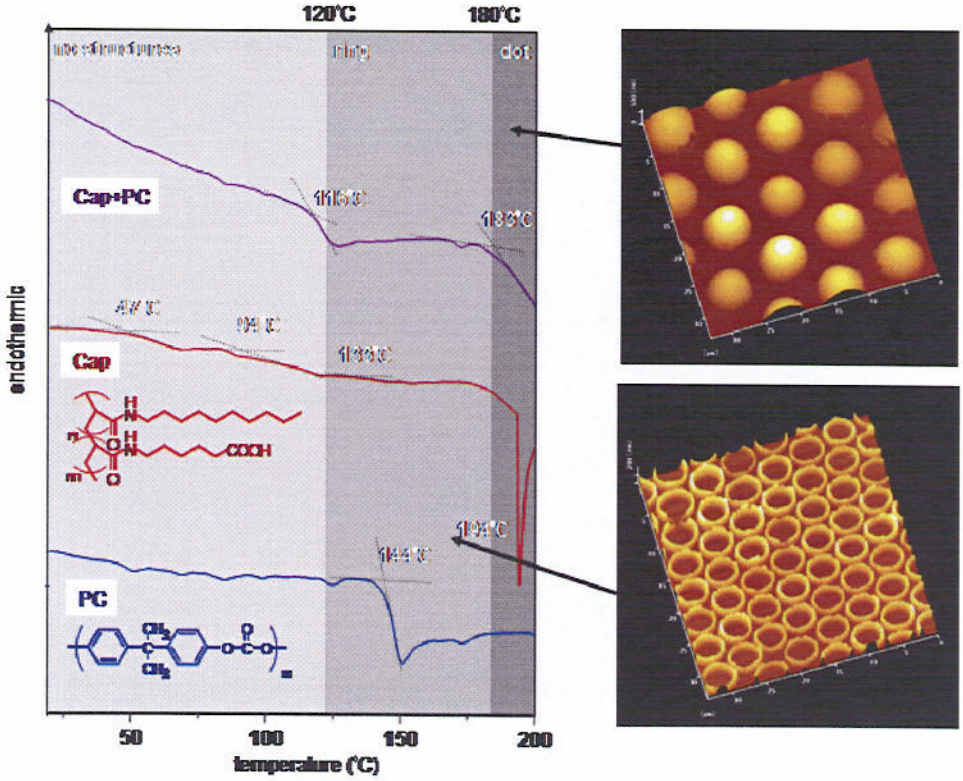

Figure 3-13. DSC curves of poly(bisphenolA-carbonate) (blue), 3-1 (Cap, red), and honeycomb film (purple), respectively. The glass transition temperature (Tg) and melting point (Tm) are shown as white letter.

the information about the inner structure of the honeycomb-patterned film. The DSC curve shows clear two transition points at 116°C and 183°C. The 90% of the honeycomb-patterned film is consisted of poly(bisphenolA-carbonate). Therefore the first clear transition point is considered as the Tg of the matrix poly(bisphenolA-carbonate). The temperature of Tg is lessen because the matrix and amphiphilic polymer, which had lower transition temperatures, are well blended. The upper transition temperature corresponds to the Tm of the amphiphilic polymer. The film melts over this temperature. Noteworthy, these temperatures are same as the temperature of the ring and dot formations, respectively. By reconsidering the formation mechanism of the honeycomb-patterned films, the honeycomb-patterned films were formed by using the condensed water droplets as templates. To stabilizing the condensed water

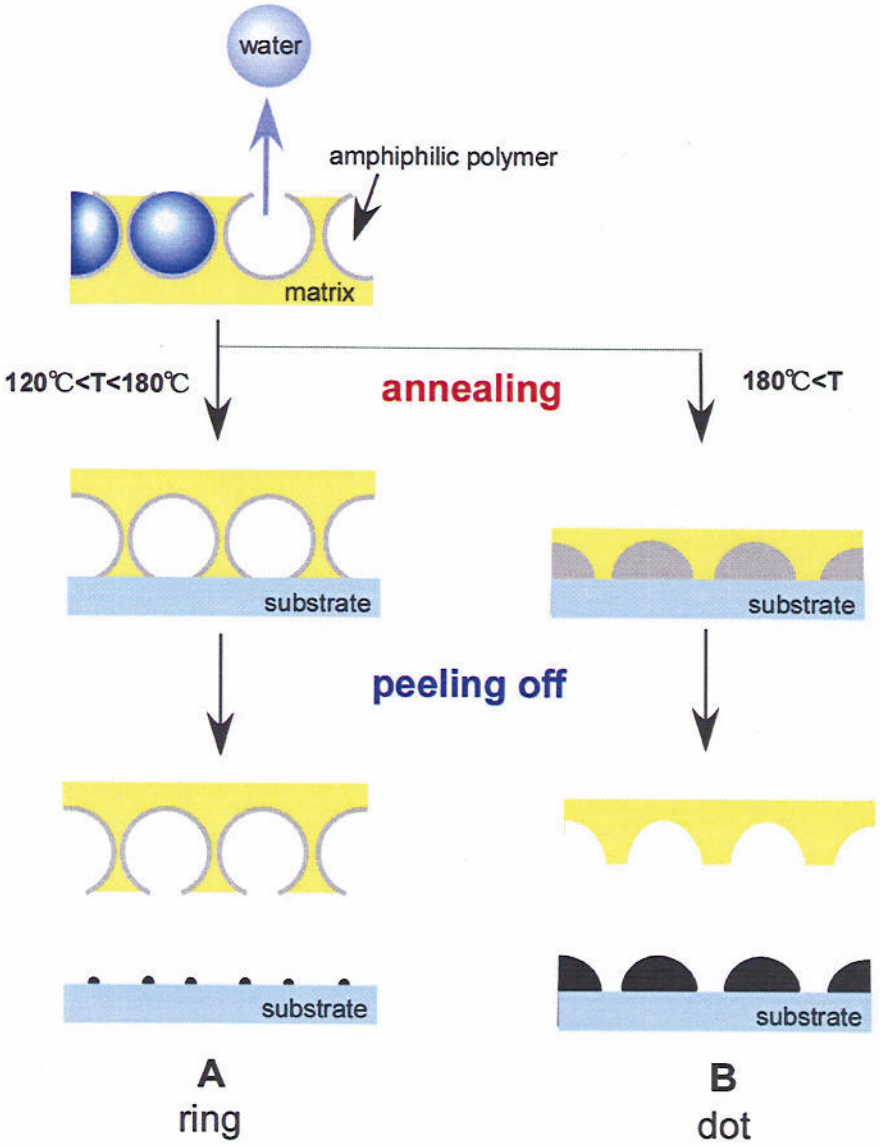

Figure 3-14. Schematic illustration of the micro-ring and micro-dot pattern formations.

droplet, the amphiphilic copolymers shold be highly condensed at the water-solution interface. The amphiphilic copolymer should work as a kind of the protective colloids. After formation of the honeycomb-patterned film, the amphiphilic copolymer will be located at the surface of the pores (Figure 3-14). When the honeycomb-patterned film was annealing ranging from 120°C to 180°C, the matrix of poly-(bisphenolA-carbonate) became soften, but it still kept the honeycomb structure. Meanwhile, Tg of amphiphilic copolymer was lower than 100°C. As the

result, only amphiphilic polymer located at the edge of the micro-pores was transferred on the electrode surface (Figure 3-14A). The transferred edge formed the hexagonally arranged micro-rings reflecting the arrangement of the honeycomb-patterned film. In the case of annealing over 180°C, the poly-(bisphenolA-carbonate) started to plasticize. The spherical pore was collapsed into hemispherical shape and the amphiphilic polymer melts and fills the pores (Figure 3-14B). After cooling, amphiphilic copolymer with hemispherical shape was transferred onto electrode surface as a dot structure. The small pores observed on the each dots were the trace of enclosed air. The ring width and heights are depending on the thickness of the stabilizing water droplets. The thickness of the protective colloid is usually not much changed. Therefore the width and heights kept similar value.

3.3.4. Conclusion

The hexagonally arranged micro-rings and micro-dots were formed by thermal treatment of honeycomb-patterned films on ITO electrode. The diameter, space and periodicity of the structure depended on the dimension of the honeycomb-patterned films though the height and width of the structures were independent. The FT-IR RAS spectroscopy and staining experiment showed only the amphiphilic copolymer was transferred onto the electrode surface. This was caused by the difference between the Tg of poly-(bisphenolA-carbonate) and that of amphiphilic copolymer. These patterns can be prepared by other amphiphilic polymers with having lower Tg than matrix compounds.

3.4. The high-performance honeycomb-patterned films

3.4.1. Preparation of the honeycomb-patterned films with thermal and chemical stabilities.

The thermal and chemical stabilities of the micro-porous films are one of the most significant properties for practical applications. The super-engineering plastics are known as high performance materials with thermal and chemical stabilities. Polyimide is one of the well known super engineering plastics with highly thermal and chemical stabilities. Due to the poor solubility of polyimide in most

solvent, polyamic acid, the precursor of the polyimide, is used for the pattern formation. Most polyamic acid, however, can be dissolved only in water and water miscible solvent, eg. N-methylpyrrolidone. The solubility of the polyamic acid to organic solvents was reported to be improved by forming the ionic complex with amphiphilic cations, which does not affect the imidation reaction. Polyion complexes of polyamic acids and dialkyl ammonium salts are firstly prepared to dissolve them in water immiscible organic solvents. Then, honeycomb-patterned films of the polyion complexed precursor are prepared by the simple casting under humid condition. The precursor films are converted to the corresponding polyimide by chemical treatment. The cyclization reaction of polyamic acid to polyimide with removal of the amphiphiles is confirmed by FT-IR measurement. The thermal and chemical stability of the honeycomb patterned films are discussed.

Experimental section. Amphiphilic polyion complexes were obtained as precipitates after mixing of aqueous solution of polyamic acid **3-6**, **3-7** (Nissan Chemical Industry, Japan, Figure 3-4) with aqueous dispersion of N,N-dimethyldioctadecylammonium bromide **3-8** (Sogo Chemical Industry, Japan). The white precipitates were extracted in chloroform, and then purified by reprecipitation in ethanol and acetnitril.

Chloroform soluions of the polyion complex were dropped on a clean glass substrate. Applying humid air (relative humidity 50~70%) flowed vertically to the solution surface, chloroform was gradually evaporated and water droplets condensed on the solution surface. The interference color emerged on solut 60 urface that indicates regular packing of uniform-sized water droplets. After complete evaporation of the solvent, the film was soaked into mixed solution of benzene, pyridine and acetic anhydride (volume ratio; 3: 1: 1, respectively) for over 12 hours to convert polyamic acid to polyimide [3-21].

Optical micrograph and scanning electron micrograph were taken by BH-2 (Olympus, Japan) and S-3500 (Hitachi, Japan), respectively. Pore size was measured by laser light diffraction experiment. Red laser beam (Sigma Koki InGaAlP laser, 3mW power, wave length

670nm, spot size 400μm) was passed vertically through the center of the self-standing polymer film. The diffraction pattern was projected onto a paper screen placed horizontally 93mm apart from the film center.

FT-IR RAS measurement was carried by FT-IR200 spectrometer (JASCO, Japan) with polarizing reflection unit (PR-500). The patterned films were prepared from 20μl of 1.0g/l solution on an Au coated ITO substrate for the FT-IR measurement.

The polyimide films were heated on a hot stage equipped to an optical microscope, RINKAM RH-600 (Japan Hi-Tech, Japan) to observe the thermal stability. Thermo-gravimetric analysis (TGA) up to 600℃ with heating rate of 20℃/min was carried by TA-60 (SHIMADZU, Japan).

Results and discussion. It was reported that polyion complex of protonated long chain alkylamine and polyamic acid were dissolved in chloroform to prepare Langmuir-Brodgget film. The polyion complexes of polyamic acids **3-6**, **3-7** and dialkyl ammonium salts **3-8** prepared in this experiment was soluble in chloroform, too.

The typical SEM image of honeycomb patterned polyion complex film is shown in Figure 3-15(a). Well-arranged hexagonal lattice was observed. Tilting the SEM sample stage at 70 degrees, double-layer structures of the patterned film is clearly imaged. Two hexagonal lattices are connected vertically by pillars at the vertex of hexagons (Figure 3-15(b)). A schematic model of double-layered structure is shown in Figure 3-15(c).

To control pore sizes of honeycomb structures, casting volume of solutions was changed. When the volume of the casting solution increased from 20μl to 5ml, pore sizes of honeycomb structures were increased from c.a. 500nm to 9μm (Figure 3-16). The solvent evaporation time, which is equal to the water condensation time, is a main controlling factor of pore sizes in any case. Larger amount of casting solution requires longer time for complete

solvent evaporation, and then the water droplet grows larger. Casting temperature is another

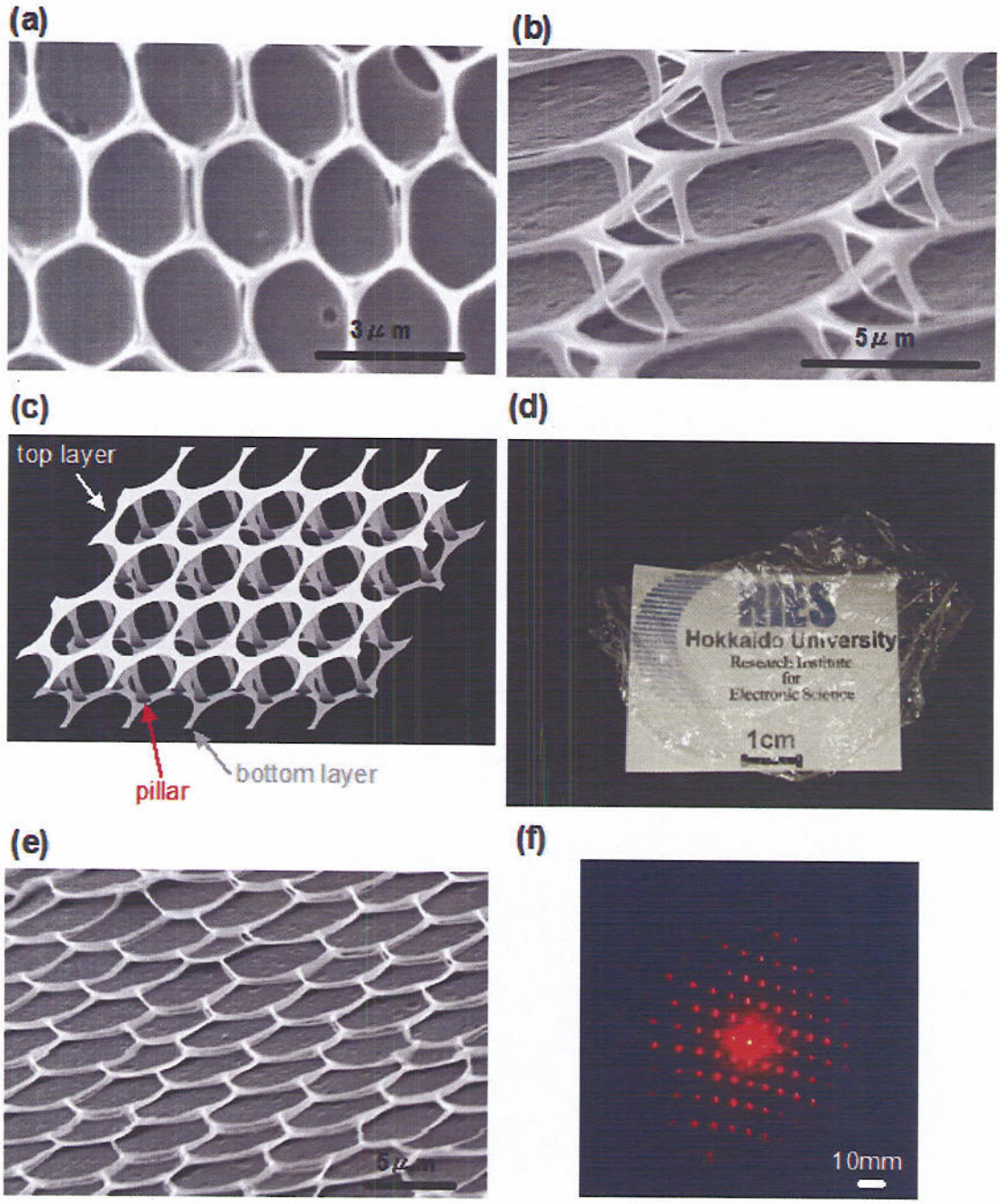

Figure 3-15. Scanning electron micrograph of the honeycomb-patterned film from polyion complex from 3-6 and 3-8 are shown (top image (a) and 70° tilted image (b)). A representative illustration of the honeycomb-patterned film (c) is reconstructed from the tilted image of the film. A sheet of the honeycomb-patterned films after chemical imidization of the polyion complex film from 3-7 and 3-8 is shown in (d). The scanning electron micrograph and the laser diffraction pattern of the film of (d) are shown (e) and (f), respectively.

controlling factor of the pore size. When the substrate was cooled at 4℃, diameters of pores were drastically increased to 18μm from 5.2μm (20℃). The solution surface was cooled rather than the case of casting at room temperature and solvent evaporation was suppressed. Therefore large amount of condensed water was provided for longer time. As the result, the pore size grew larger.

The precursor films were too fragile to be peeled off from substrate. While after soaking in the mixed solution of benzene, pyridine and acetic anhydride, the film can be peeled off as a self-supported film from a substrate (Figure 3-15(d)). Mechanical property of the honeycomb film was improved by imidization reaction. After chemical treatment, the color of the film of **3-6** and **3-7** was converted from white into yellow. This color change was ascribable to the imide formation with elongation of π-electron conjugate length. The infrared absorption attributed to the C-H stretching disappeared in the FT-IR RAS spectra of films, and the carbonyl group absorptions appeared at 1780 cm^{-1} and 1720cm^{-1}(Figure 3-17(a), (b)). This measurement revealed that polyamic acids **3-6**, **3-7** were completely converted into polyimides **3-9**, **3-10**, respectively. SEM observation clearly shows that double layers structure was collapsed after chemical treatment, but the honeycomb structure was still kept after chemical treatment (Figure 3-15(e)).

The ordered arrangement of micro-pores was clearly indicated by a light scattering experiment. A laser with a beam diameter of 400 microns was used as a light source. The diffraction pattern was projected on a white paper screen and imaged by a video camera. The diffraction pattern with hexagonally arranged spots was obtained from the honeycomb patterned film of **3-10** (Figure 3-15(f)). According to the Bragg's low,

$$n\lambda=2d\sin\theta$$

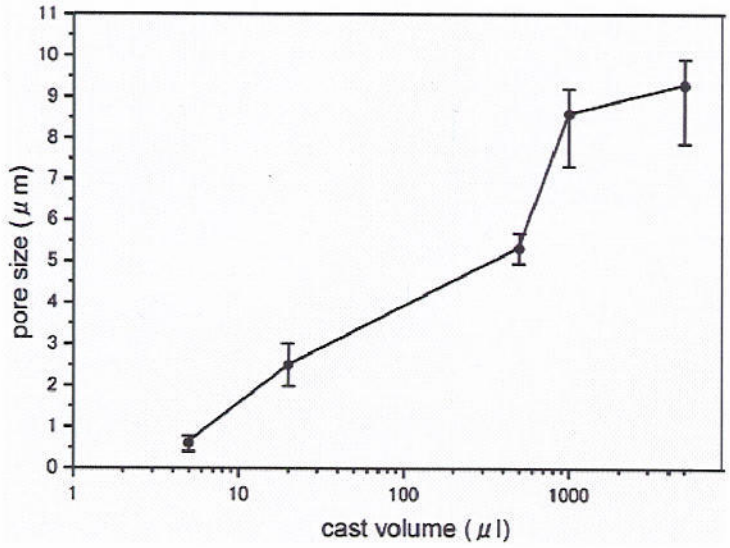

Figure 3-16. The relation between casting volume and pore size of the honeycomb-patterned films.

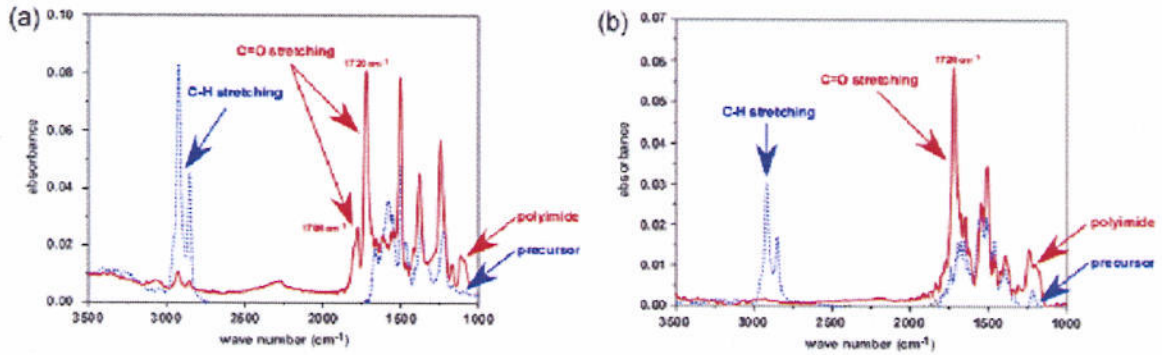

Figure 3-17. Change of FT-IR RAS spectra by imidization reaction. (a) Honeycomb-patterned films of precursor (3-6, 3-8) and polyimide 3-9. (b) 3-7, 3-8 and 3-10.

here λ is the wave length of the incident light, d is the lattice constant of the scattering centers, and θ is the angle of diffraction, the lattice constant d was calculated as a function of camera length. In the case of the film prepared from 1ml of the sample solution, the average lattice constant of the micro pore was calculated 3.1μm. This value was consistent with the pore size estimated from optical microscopy and scanning electron microscopy. The higher order diffractions (up to 7 orders) indicate the micro-pore lattice in the film has highly ordered hexagonal arrangement.

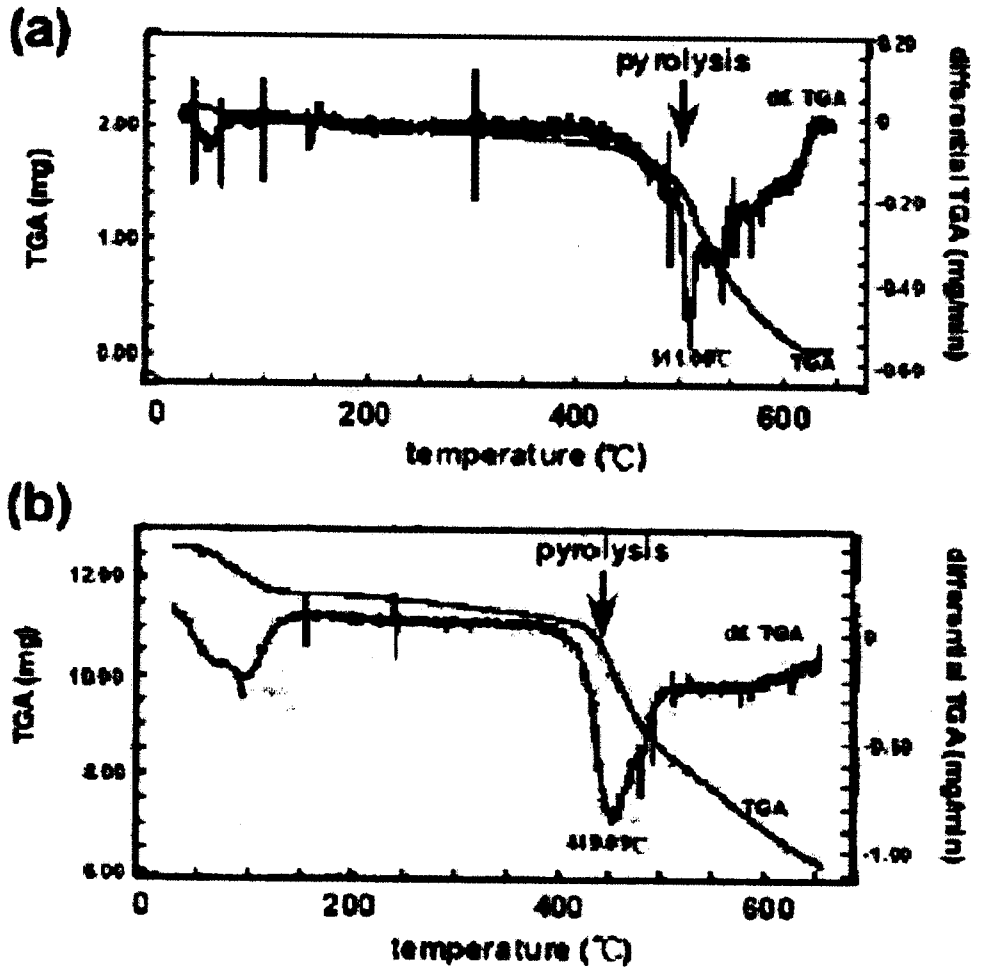

Figure 3-18. Thermal stability of the honeycomb-patterned films of the polyimides. TGA and differential TGA curves of the patterned polyimide films of 3-9 (a) and 3-510(b).

To evaluate thermal stability of the honeycomb film, the precursor and imidized films were annealed on a hot stage up to 300℃ for 1 hour, respectively. *In situ* optical microscopy revealed that the polyimide film kept its honeycomb structure at 300℃, while the polyion complex precursor film melted at about 150℃. The TGA measurement shows that the pyrolysis of polyimide films **3-9** starts at 400℃ and the decomposition completes at 511℃ (Figure 3-18(a)). The pyrolysis of the film of **3-10** starts at 400℃ and the decomposition completes at 449℃ (Figure 3-18(b)). After soaking the patterned polyimide films in chloroform, tetrahydrofuran, and conc. H_2SO_4, respectively for two weeks, the SEM

investigation revealed the films kept their honeycomb structures. These results indicate that the honeycomb-patterned structure does not affect thermal and chemical durability of polyimide film.

3.4.2. The honeycomb and pin-cushion structures from fluorinated polymers

Super hydrophobic and lipophobic surfaces have been received great interest from the point of practical applications, i.e. self-cleaning surface, preventing snow sticking, oxidation, current conduction and so on [3-22]. Both chemical feature and topological feature of materials surface affect on the surface properties. Fluorocarbon groups are usually used to introduce water and oil repellencies to materials surfaces [3-23]. Preparing rough, micro-structured surfaces is also important point. In nature, it was well known that some plant reeves repels water. This was caused by micron sized wax dots were formed on the surface of reeves. In artificial systems, recent developments of photolithography techniques allow to investigating the effect of surface topology on the surface wettabilities [3-24]. It was also reported that fractal structure of surfaces prepared by crystallization of wax shows high water contact angle [3-25]. By using chemical vapor deposition (CVD) of polytetrafluoroethylene (PTFE) [3-26], coating hydrophobic silanes onto sublimated aluminum acetylactonate [3-27], UV irradiation of TiO_2 coated crater like film [3-28], aligned carbon nano-tubes and walls [3-29], inversed opals [3-30], and aggregations of polypropylene fibers [3-31], the rough surfaces of hydrophobic materials were reported. In this report, we show the simple preparation of ultra water and oil repellent surface by self-organization.

Experimental section. Fluorinated copolymer used in this experiment was shown Figure 3-4 The copolymer **3-11**~**3-14** had methylmetacryrate (n) and fluorinated residue (Asahi Grass Company, Japan). Their n:m ratio was 9:1(**3-11**), 7:3(**3-12**), and 1:1(**3-13**), respectively. Another fluorinated copolymer had branched methyl group in fluorinated residues (**3-14**). The

ration of n and m2 was 1:1. The copolymer was dissolved in AK-225 (Tokyo, mixture of $CF_3CF_2CHCl_2$/$CClF_2CHClF$, Asahi Grass Company, Japan) to prepare 10g/L solutions. In all cases homogenous solution of the compounds was dropped onto glass substrates at ambient temperature. Humid air (relative humidity: 40~60%) was applied by an air pump (current velocity: 80~200ml/min). The pin-cushion structures were prepared by peeling the top of the film off by Scotch tape™. The pin-cushion structures were also investigated in the same way as the honeycomb films (Figure 3-19).

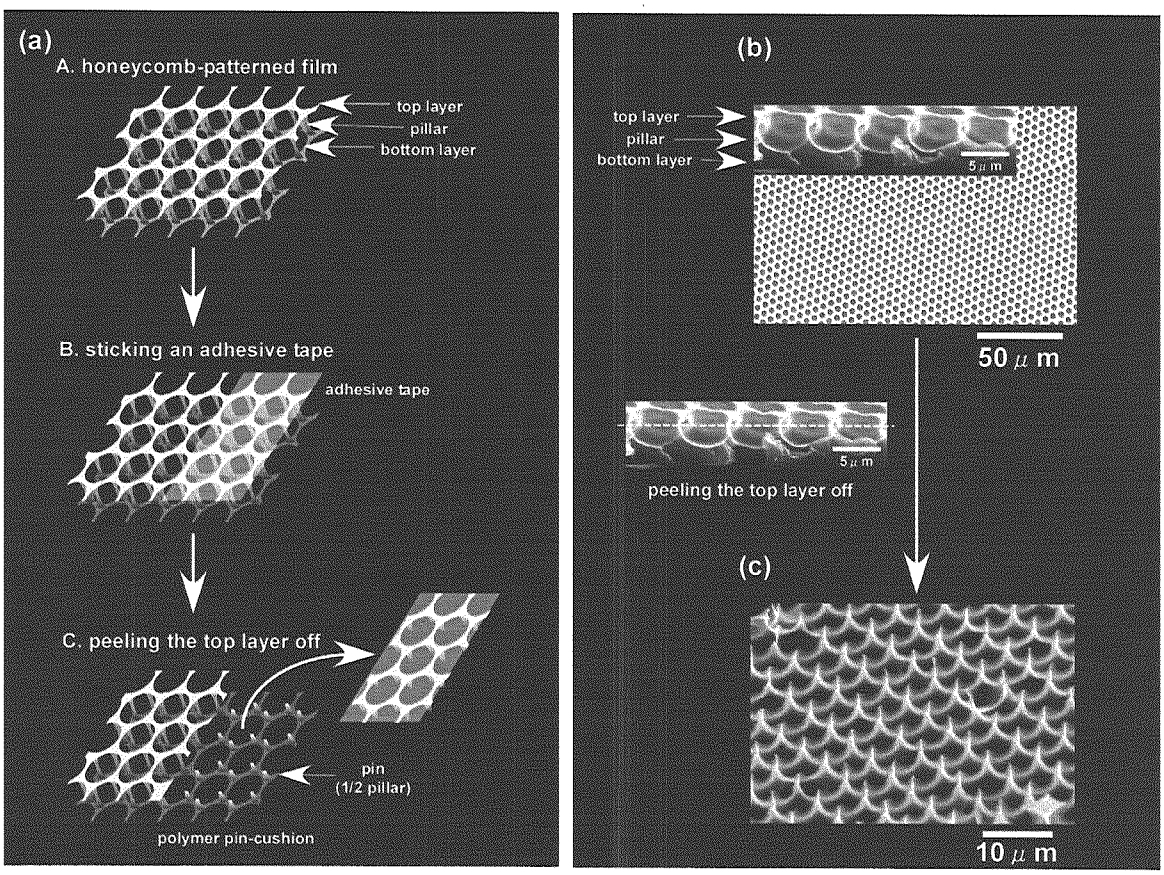

Figure 3-19. A schematic illustration of "pin-cushion" structure formation (a). The typical scanning electron micrographs of the honeycomb-patterned films (b) and prepared pin-cushion structure (c).

The surface morphologies of the films were observed by optical microscopy (BH-2, Olympus, Japan), atomic force microscopy (AFM, SPI-400, Seiko Instruments, Japan), and scanning electron microscopy (SEM, S-3500N, Hitachi, Japan). Pore sizes of the films were measured by these micrographs by using imaging software, NIH image (NIH, U.S.A.). The image of SEM was changed from a grayscale image into a monochrome image. And then, the diameter of pores, width of rims, the center distance of the pores, and surface area fraction of the polymers were measured. Contact angles of water and benzene on the prepared films were measured by a contact angle analyzer (G-1, ERMA Inc., Japan). A liquid droplet of five micro litters was gently placed onto the films. Contact angles were measured 30s after placing a liquid drop before evaporation of liquid. As a control experiment, the polymers were coated onto a glass slide by spin coating at 1,000r.p.m.

Results and discussion. The different structures were obtained by changing copolymers. Optical micrographs of the surface structure of the obtained films are shown in Figure 3-20. Random arrangements of pores are observed in the film from **3-11**, which is the highest fluorinated residue composition (3-20(a)). The arrangements of pores became more regular in the case of reduce the content of fluorinated residues. By the 2 dimensional Fourie transform shows the regularity of pore arrangement changed from halo to hexagonal arranged dots. In the high fluorinated conditions, the condensed water droplets are not stable because of the low surface free energies of fluorinated materials. The water droplets easily fuse with neighbor droplets and as the results, the random arranged, different size water droplet formed on the solution surface. The ratio between fluorinated residue and MMA was 1:1, the water droplets was able to stay independently on the solution surface. The most regular patterned film from **3-13** was used to measure the water and oil contact angles. In the case of using **3-14**, the regularity of the pores was higher than that of **3-13**. However, the **3-14** film was soft and brittle. The film shrunk and winkles were formed on the film surfaces (3-20(d)).

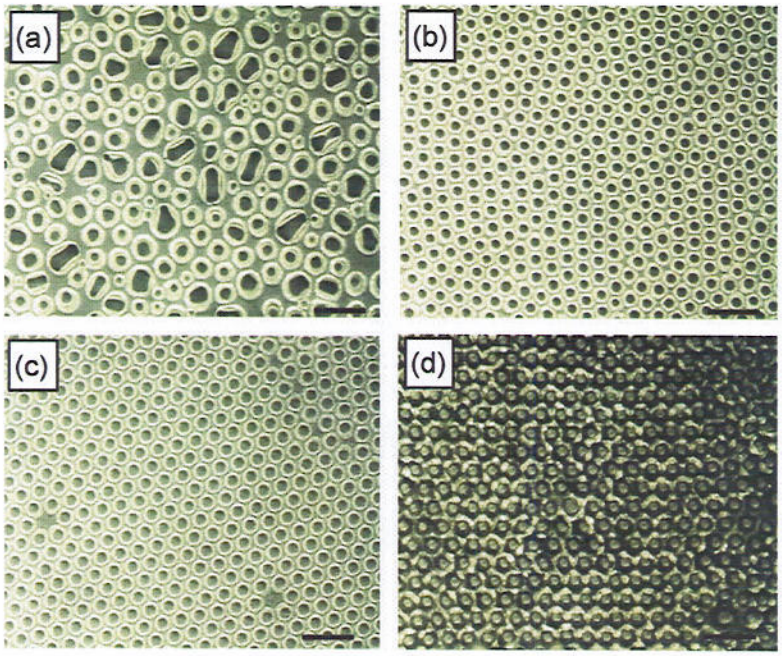

Figure 3-20. Optical micrograph of films from fluorinated copolymers. (a) 3-11, (b) 3-12, (c) 3-13, (d) 3-14. (black bars indicate 10 μ m.)

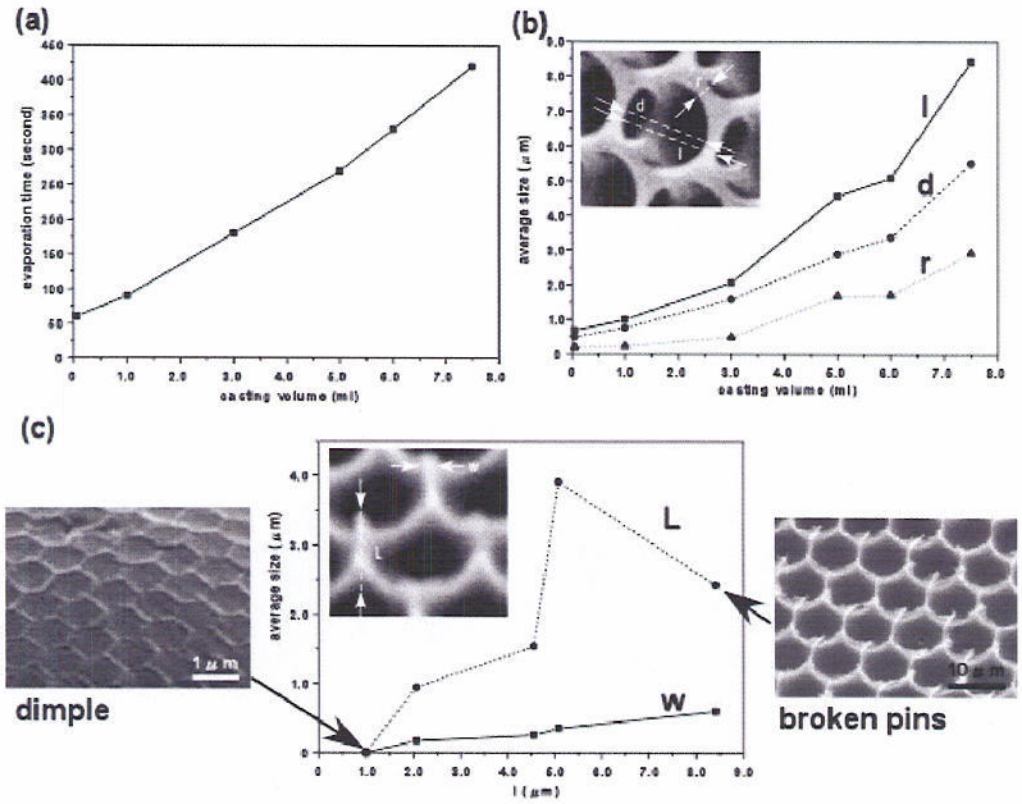

Figure 3-21. (a) Relation of casting volume and evaporation time. (b) Rim width r, pore diameter d and repeat length l of honeycomb structure with casting volume. (c) Pin height L and width w with l.

typical scanning electron microscopy (SEM) image of a honeycomb-patterned **3-13** film is shown in Figure 3-19(b). Hexagonally arranged lattice was observed. The cross section of the film was obtained when the film was tilted. The spherical shape of the cross-section of the pores was reflected in template water droplets (inset of Figure 3-19(b)) (16). Two layers of hexagonal lattices are stacked vertically by pillars at the vertex of hexagons. The model of the honeycomb-patterned film is shown Figure 3-19(a)A.

A pin-cushion like structure was obtained (Figure 19(a)C, (c)) after peeling off the top layer by a sheet of adhesive tape (Figure 19(a)B). Mechanical stress was applied on the center of the pillars, and then, pillars broke up to two sharp pins. One is stuck on the upper layer; the other remained on the bottom layer. The size of honeycomb and pillar structure was easily controlled by casting volume. Figure 21(a) shows the relation between casting volume and evaporation time. This result means the evaporation time was changed by changing casting volume. The relation between casting volume and pore size (d) and rim width (r) of honeycomb-patterned films is presented on Figure 2(b). The averages of pore size, rim width and center distance of the films became large when large amount of polymer solution was casting. The average center distance of the hexagonally arrayed micro pores was ranged from 500nm to 8.0μm by changing casting volume from 20μL to 7.5mL. The AFM image of the honeycomb-patterned films with the smallest pore size is shown in Figure 3-. The pore size of honeycomb-patterned film depends on the size of template water droplets. The size of the water droplets is dominated by the solvent evaporation time, which is equal to the water condensation time (see section 3.4.1.). The width of pins, which were prepared after peeling off, correspondingly increased from 90nm to 420nm (Figure 21 (c)). The height of the pins increased with the pore size of the honeycomb-patterned film increasing. However, the pin height of the I=8.5μm case lower than I=5.2μm. Scanning electron micrograph shows the pins were eliminated near the bottom layer (inset of Figure 21(c)). Because the long pillars are

mechanically week for stresses, the pins are broken by the peeling process. Furthermore, In case of l=1.0μm, the honeycomb pillar was completely eliminated from the bottom layer. As the result, dimple like structure was formed (inset of Figure 3-21(c)).

The water contact angle of a flat film of **3-13** was 117°. This value was higher than the flat surfaces from other hydrophobic materials. Super hydrophobic surface is defined that the water contact angle of the surface was over 150°. Therefore the flat film had not enough high contact angles to accept this film as super hydrophobic. In case of honeycomb structured films of **3-13**, they had higher contact angles than flat films (Figure 3-22 (a)). The contact angles on honeycomb films increased with decreasing their pore periodicity. The maximum was 145° in the case of l=1.0μm. Furthermore, it was noteworthy that contact angles on the pin-cushion films higher than on the honeycomb films. In this case, the maximum of contact angle was 170° on the pin-cushion structure prepared from honeycomb film with 2.1μm average center distance. This film had pins with less than 170nm width and 0.95μm height. The contact angles of water increased with decreasing the size of pins. In the case of dimple structure, the topology of the dimple structure is very much like honeycomb structure. Therefore the water contact angle on the dimple film had similar value of the honeycomb-patterned film.

It has been discussed water repellency of rough hydrophobic surfaces for several decades. The superficial contact angle of the surface consisted by two components (i.e. air and polymer) was described as a formula of fraction of surface areas of each parts reported by Cassie and Baxter [3-32]. According to the Cassie's low;

$$\cos\theta_c = A_1\cos\theta_1 + A_2\cos\theta_2 \qquad [1]$$

here, θ_c is superficial contact angle; θ_1 and θ_2 are contact angles of flat film of fraction 1 and 2,

respectively. A_1 and A_2 are surface area fraction of polymer and air, respectively. When the fraction 2 is air, $\cos\theta_2$ is substituted -1. And area faction A_2 equal to (1- A_1). For this reason, the formula [1] is changed as follows:

$$\cos\theta_c = A_1(\cos\theta_1 + 1) - 1 \qquad [2]$$

According to the equation [2], large air void required to achieve high contact angle. Using the measured values and the equation contact angles were plotted again in Figure 22(c). To determine the surface area fraction A_1, the scanning electron micrographs are analyzed by NIH image. The plot indicates that theoretical calculation and the experimental results are matched in the case of the polymer fraction in the honeycomb-patterned regime. On the other hand, the experimental results not matched in the pin-cushion regime. This was caused by the nonuniformity of the pin structures such as the dimple structure.

Another important advantage of using fluorocarbon materials is lipophobic properties based on their low surface free energies. It is also expected that surface topologies enhance the lipophobicity as well as hydrophobicity. The contact angles of lypophilic solvent, benzene on the each film were also measured (Figure 22(b)). The contact angles against benzene on pin-cushion structures were higher than honeycomb patterned films. The highest contact angle of benzene was 135° measured in this experiment. Benzene has lower surface tension comparing with water. Therefore, there are few lipophobic materials having contact angles higher than 100° against benzene. The contact angle of the dimple structure was same as the case of measuring water contact angles.

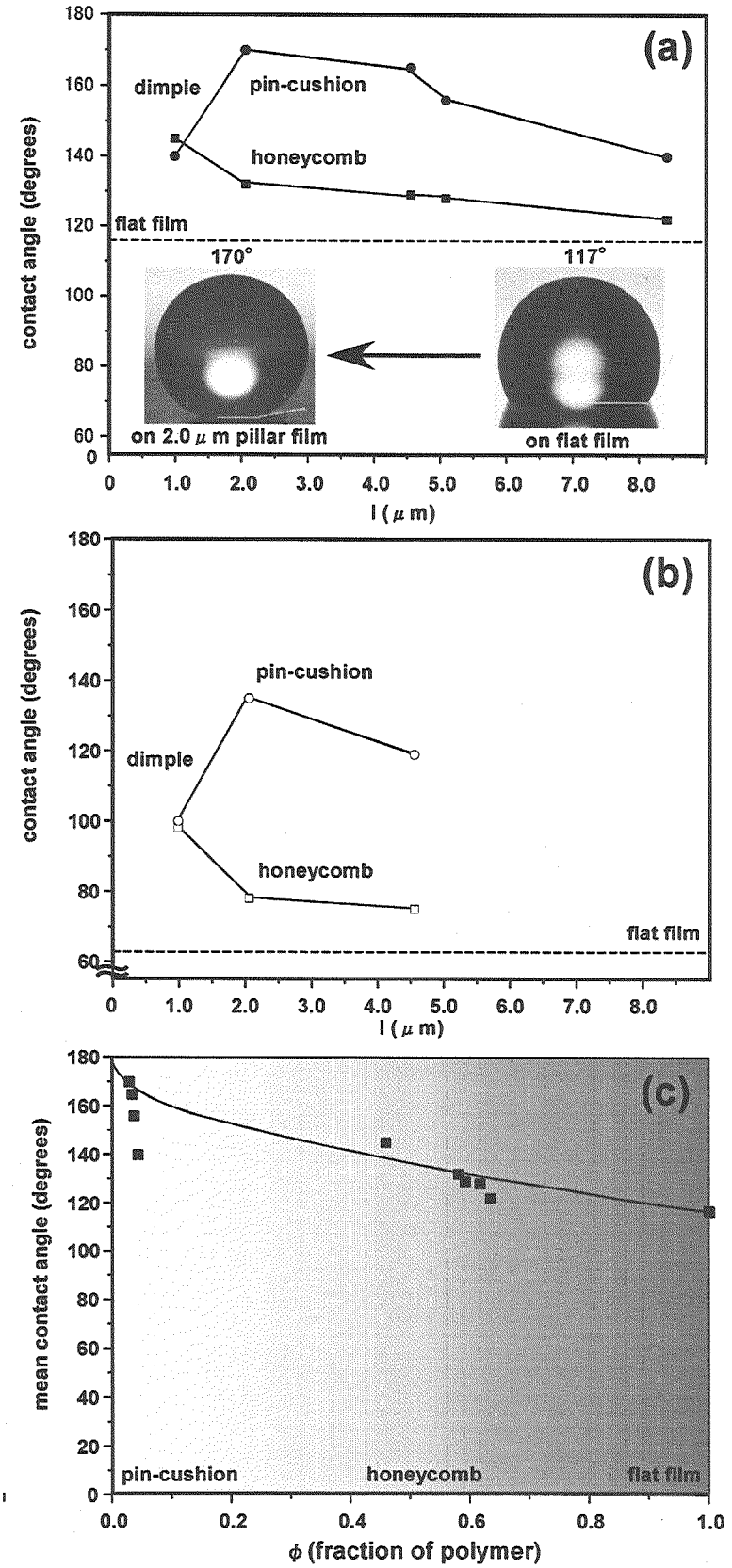

Figure 3-22. Variation of water contact angle with average repeat length l. Inset photograph shows drastic contact angle change between on spin coated flat film and needle structured film (a) . The water contact angles were re-plotted with fraction of air void (b).

This is the first report of preparation of super hydrophobic and lipophobic surface from fluorinated polymers by self-organization. The honeycomb-patterned film was prepared by casting fluorinated polymer solution on solid substrate under humid condition. After peeling off the top layer of honeycomb structure, the pin-cushion structure was formed. The prepared films showed the super hydrophobic and lipophobic properties. The super hydrophobic and lipophobic films can be utilized for dust free, low friction coating. The honeycomb and pin-cushion structures can also be utilized for not only hydrophobic coating but also photonic crystals [3-1] and other applications.

3.5. Pore Size Control of the Honeycomb-patterned Films

3.5.1. The water condensation mechanism

The honeycomb-patterned films are formed by using condensed water droplet on the solution surface as templates. Water condensation is one of significant issues in the fields of climate physics, surface sciences, and lubrication. In daily life, we can see the condensation of the water droplets onto the window glass as dew. In lubrication processes, the dew is one of the reasons of roughing the lubricant surfaces. Moreover, the condensation of dew is the most unwanted phenomena in preparation of flat and transparent polymer films. Condensation of dew forms tiny holes on the film surfaces. As the results, the light scattering was generated on these holes and then, the film became opaque.

The water condensation process was investigated by climate physicists [3-33~3-38]. The condensation process is consisted of two stages. In the first stage, nucleation onto a substrate from supersaturated atmosphere is occurred. The water changed from vapor to water droplets reached at critical temperature and critical nucleation diameter. In the ideal condition (water condensed onto completely flat, no defect substrate), homogeneous nucleation is occurred. In this case, the critical temperature is about 0°C and critical nucleation diameter is

c.a. 30Å. On the other hand, there is no substrate without defect. Actually, the tiny defect is always observed on glass, silicon, and other substrates. Moreover, the surface tension of the substrate affects the nucleation rate. Furthermore, in the case of liquid substrate, the thermal fluctuation also affects the nucleation rate. In such cases, the heterogeneous nucleation is occurred. Because the effect of surface tension and the thermal fluctuation of the substrate, the critical nucleation temperature are higher than 0°C and the critical nucleation size become larger than 30 Å. By using thermograph, the temperature of the solution surface evaporating solvent was c.a. 8°C (see supporting information). This result indicates the water condensation was enough to occur at least cooling at 8°C.

In the next stage, the growth of individual droplet is occurred. The droplets grow up to fill the substrate surface until the coverage becoming 100%. Therefore the controlling factor of the size of water droplets is the critical nucleation diameter and water condensation time. In actual experiment, the parameters including humidity, temperature, velocity of applied air flow and casting volume are affected the size of pores. By using the experimental equipment shown Figure 3-2, the humidity and temperature are difficult to be controlled. Furthermore, the applied flow changes local temperature by solvent evaporation cooling. Therefore in this experiment, the casting volume was changed to control the size of the pores and other parameter was fixed.

The specific problem of liquid substrate is the mobility of the solvent. The mobility of the liquid induces the change of arrangements of these droplets. The condensed water droplets accounts for the spherical particles floating on the surface of the liquid. The local arrangement of the droplets is affected by the interaction between the neighbor particles. The particle-particle interaction is consisted of the adhesion from the capillary force, which is generated by the inter-particle surface tension of solvent, and repulsion from steric hindrance of particles and Brownian motion. Because these interactions are totally summed up to long

range adhesion force, the particles are closely packed locally and the packed particles form many islands of domains on the liquid surface. In lager scale, these domains are affected by dynamic motions of solvent. The capillary force on the solution edge, thermal and Marangoni convections [3-39] are forced the domains to packing or breaking each other. To obtain large size domain or mono-domain of particles, it is needed to control these dynamic phenomena.

3.5.2. Effect of flow rate

To control the pore size, especially in submicron scale, is significant issue to apply the honeycomb-patterned films for photonics [3-1, 3-40~3-43]. The pore size of the honeycomb-patterned films can be controlled by changing the casting volume (see section 3.3., 3.4.). This treatment changes the evaporation time, which is the growth time of condensed water droplets. When the evaporation time is reduced, the condensed water droplets kept small size, which approximately same size of water condensed on the solution surface. Another parameter of changing the evaporation time is the flow rate of applying humid air. When faster velocity of humid air is applied, the solvent evaporates instantaneously.

To apply humid air with high velocity, the compressed air was applied through the gas washer with water and outputted from the glass capillary (Figure 3-23), the inner diameter of the glass capillary was 0.8mm). The flow rate of the compressed air was 10L/min. Fifty micro litters of polymer solution was casting onto the glass and then, the humid air was applied horizontally to the substrate. The solution spread c.a. 1cm, the half region of the solution near the output of humid air evaporated in a sprit second and form transparent film (Figure 3-24). The other side of the solution became opaque, and the opaque film was formed after completely evaporation of solvent.

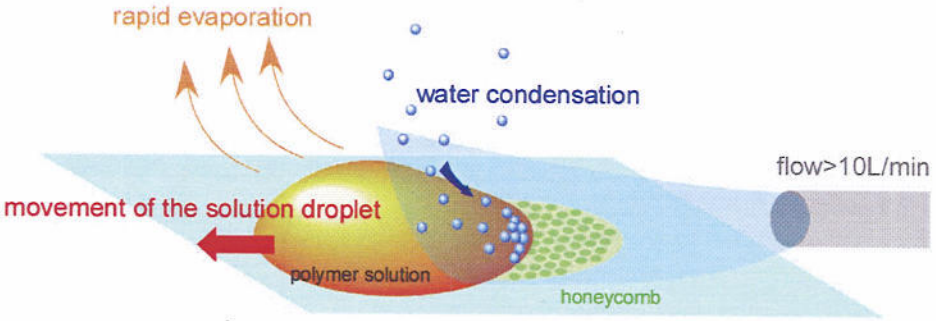

Figure 3-23. Schematic illustration of fast air flow experiment.

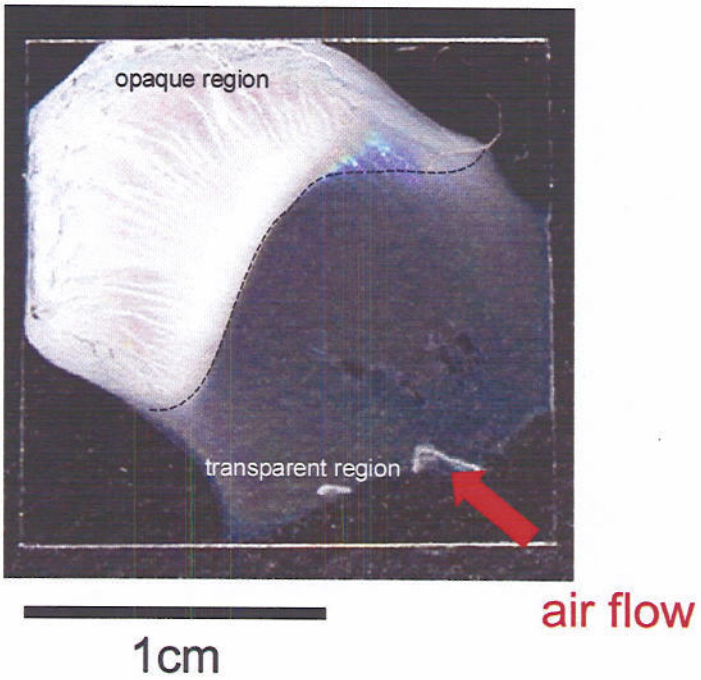

Figure 3-24. Photograph of the film prepared by applying fast air flow.

Scanning electron microscopy revealed that the size of the honeycomb-pore was changed from the edge near the output of the humid air to the other side of the edge (Figure 3-25). In the edge, the small, irregular size and arrangement of pores were formed. The smallest size of pores is in the tens nm scale. This result indicates the water condensed on the solution surface in the range of tens nm scale. On the other hand, the evaporation time was too

short to rearrangement of the water droplets. The pore size changed from 100nm to 550nm from the edge to the center of the film. After reaching the 550nm, which is the region staying 1mm away from the edge, the pore size was not changed. This is considered as the effect of the shape of casting solution. When solution is casting onto solid substrate, the solution form lens like shape. The capillary force on the solution edge affects shape of the solution in capillary length [3-44]. Therefore the thickness of the solution at the edge is thinner than the inner part of the solution. The solvent at the edge evaporated faster than the inner part, the smaller size water droplets were fixed on the film. In the opaque region, the micron sized pores were observed.

These results indicates that it is necessary the high flow rate to reduce pore size. To prepare the honeycomb-patterned films with submicron scale pores on wide surface area, the method of continuous formation of honeycomb-patterned film was fabricated (Figure 3-26). The solid substrate was fixed on the substrate holder, which can move straightly with controlling its speed by a computer. The microtome blade was placed over the substrate with the certain gap, the solution was casting onto the substrate. The substrate was moved straightly and applied humid air, the honeycomb-patterned film was continuously produced.

By using this method, the film with homogeneous sized submicron pores was obtained (Figure 3-27). When the pore size became under light wave length, the film was transparent. Furthermore, the water contact angle on the prepared film was higher than 160°. By using this method, the transparent super hydrophobic surface is easily produced on solid substrate.

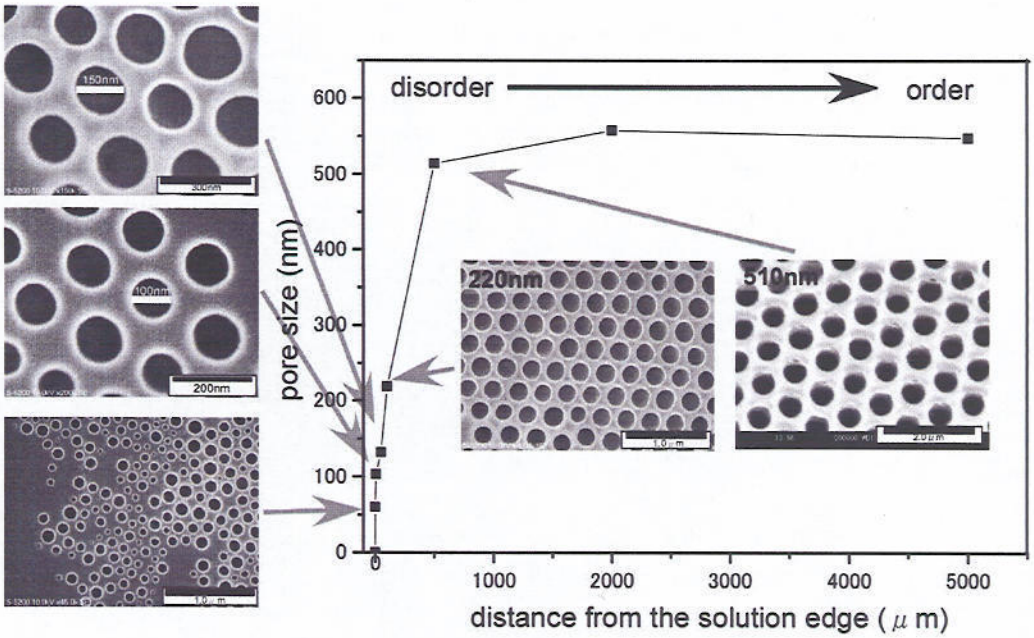

Figure 3-25. Scanning electron micrograph and influence of the edge on honeycomb pore sizes.

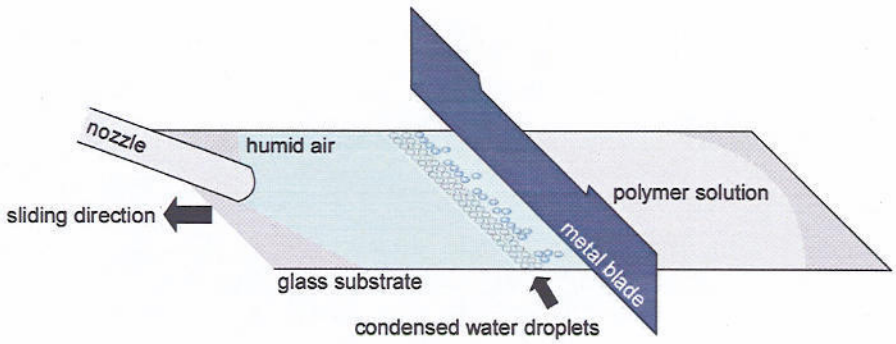

Figure 3-26. Schematic illustration of continuous fabrication of honeycomb-patterned films.

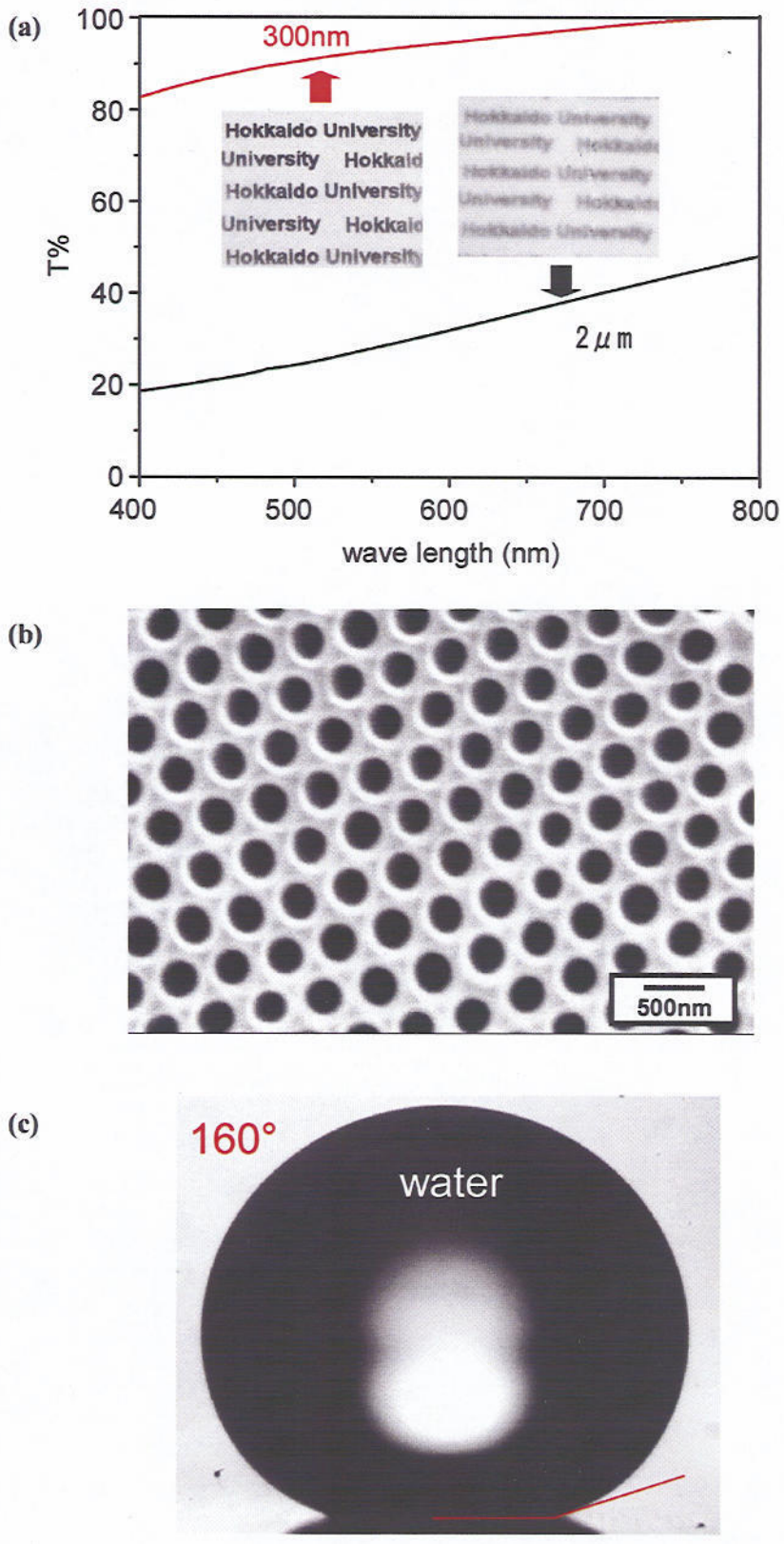

Figure 3-27. (a) Transmittance from the honeycomb-patterned films with 300nm pores (red) and 2.1 μ m pores (black), respectively. (b) Scanning electron micrograph of submicron honeycomb-patterned film. (c) Water contact angle on the submicron honeycomb-patterned films.

3.6. Micro-structures prepared by using the honeycomb-patterned films as templates

In this section, the new class of micro- and nano-structures fabricated by using the self-organized micro-structures as templates. The negative images of the self-organized micro-structures were prepared by simple molding. Thermal and photo-chemical curing agents were used as molding materials. The solution of biodegradable polymers, photo-luminescence materials, and engineering plastics were also used.

3.6.1. Preparation of negative mold of the honeycomb-patterned films

The honeycomb-patterned films were prepared by casting chloroform solution of polystyrene (PSt, Mw=280,000, Aldrich) and amphiphilic copolymer **3-10** by the procedure shown in section 3.2.1. The prepared honeycomb-patterned film had hexagonal arrangement of micron pores revealed by SEM (Figure 3-20). The cross section of the honeycomb-patterned film shows the double layer structure same as other materials case (inset of Figure 3-20).

One significant property of molding agent is immiscible with the template honeycomb materials. Polydimethlysiloxane (PDMS, Dow Cornig, Inc., U.S.A.) is one of the well known molding agents. This molding agent does not miscible with PSt and **3-10**. The prepolymer of PDMS (prePDMS) and catalyst solution was mixed (prePDMS:cat=10:1wt.). The mixture was casting onto the prepared honeycomb-patterned film. The sample placed *in vacuo* to remove air bubbles in the honeycomb pores. After removing the air bubbles, the sample annealed at 300°C for 2 hours in an electric oven. After cooling to room temperature, the annealed film was rinsed by the chloroform to remove the template honeycomb-patterned film. The surface structure of the negative mold was observed by SEM. The negative mold had the arrays of micro-dots with hexagonal arrangement (Figure 3-20). The cross section of the negative mold shows the each dots consisted of a micro-sphere connected each other

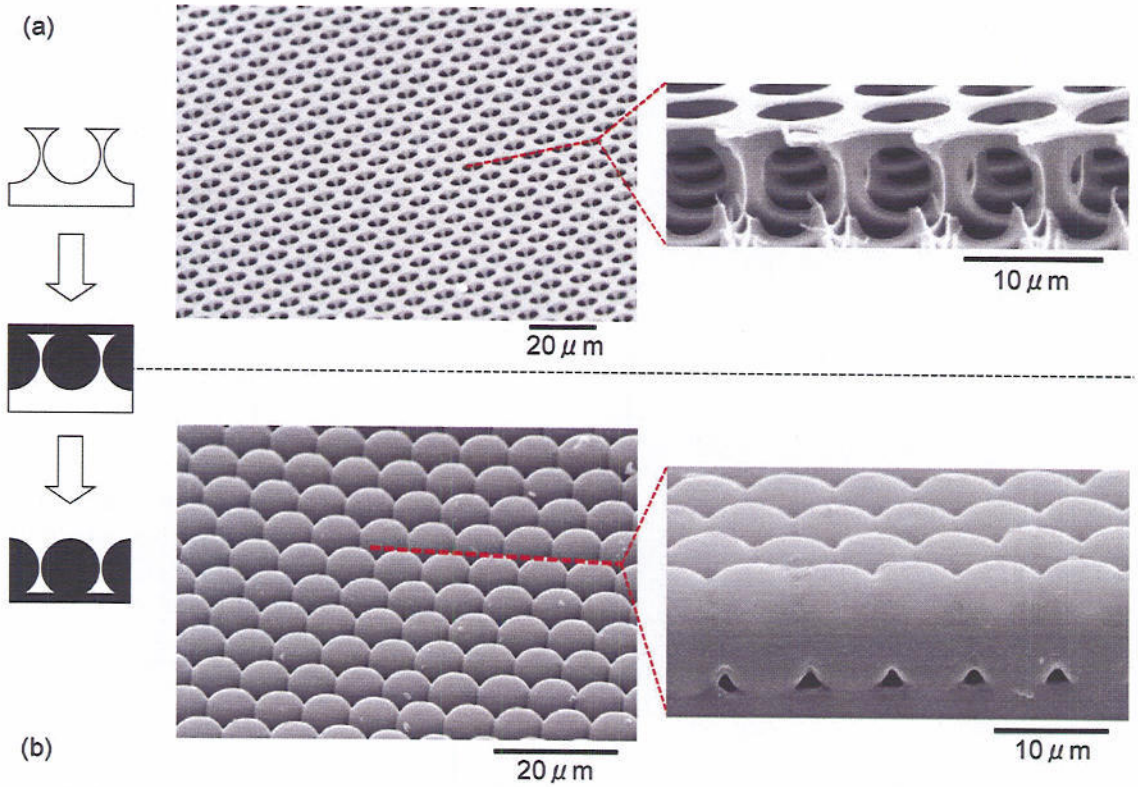

Figure 3-28. The well arranged hexagonal micro-pores can be observed on the scanning electron micrograph of the honeycomb-patterned film and their cross section (a). The inversed image of the honeycomb-patterned film was obtained by molding (b).

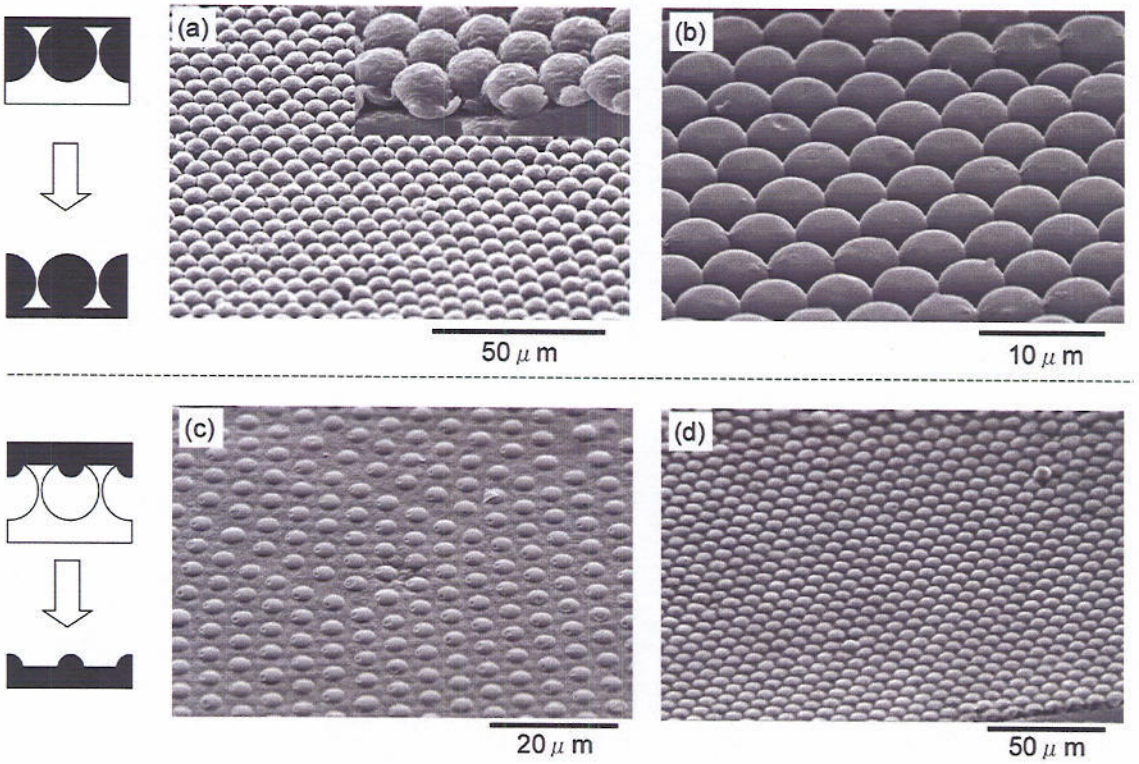

Figure 3-29. Two types of negative molds were obtained. The molding agent filled the template by vacuum treatment ((a) and (b)). Only the hemi-sphere structure was transferred in the case of curing or solvent evaporating under ambient conditions ((c) and (d)).

(upper scanning electron micrograph of Figure 3-20). The template honeycomb-patterned films had laterally connected spherical micro-pores. These structures completely reflected the template honeycomb structures. The laser diffraction experiments shows the negative mold had similar hexagonal periodicity (inset of Figure 3-20).

The other negative molds were obtained by casting photo-cross linking agents (Figure 3-21 (a), (c)), collagen (Figure 3-21(b)) and water dispersion of gold nano-particles (Figure 3-21 (d)). In each case, the dispersions or cross-linking agents were simply casting without any vacuum treatments. As a result, different structures were obtained. In the case of preparing the negative mold under ambient condition, only the hemi-spherical dot structure was formed. This is caused by the imperfection of filling molding agents in the pores. Without the vacuum treatment, the molding agents keep their liquid film state and do not penetrate into the honeycomb pores. The infiltration force affecting liquid on the porous medium is capillary force. The dimension of the capillary force making liquid move into the pores are calculated as follows;

$$\Delta P=\gamma\cos\theta/2r$$

here, ΔP is the dimension of capillary force, γ is surface tension of the liquid, θ is the contact angle of liquid on the flat solid substrate, and r is the pore radius [3-44]. This relation shows the liquid with low affinity to the porous materials does not filtrate into the pores. Therefore only air pressure and gravity are driving force to filtrate molding agent into the honeycomb pores when the sample prepared under ambient condition. To fill the honeycomb pores, the vacuum treatment is effective.

3.6.2. Application the negative mold for micro lens arrays (MLAs)

Micro lens arrays are one of important devises in the fields of photonics and electronics. Many applications of MLAs (i.e. coupling lenses of optical telecommunications, a

light homogenizer of liquid crystalline display (LCD) projectors, image sensors and so on) have already reported [3-45~3-50]. Commercially available MLAs are usually prepared by ion exchange technique, modified LIGA process or photo-lithography. So many elaborate processes including preparation of photo-mask, UV light exposure and anisotropic etching were needed to fabricate three dimensional lens structures. Therefore more easy and simple fabrication method was needed to prepare MLAs.

Whitesides et. al. reported that micro contact printing or template directed polymer dewetting on patterned substrate work as MLAs [3-51]. It was also reported that colloidal array was prepared by filling colloid suspension into patterned substrate by Xia et. al. [3-52]. But these methods still require many steps and pre-patterned surface prepared by photolithograpy or soft-lithography. Monolayer assembly of fine polystyrene micro-spheres prepared onto was also used as MLA. However, mono-disperse microspheres from favorable materials are essential to the method.

The simple preparation of MLA by molding these honeycomb patterned films. Using these spherical pores as templates, negative images of the honeycomb films were prepared by molding these micro-pores (Section 3.4.2.). Moreover, hexagonal array of pillar structure was prepared by peeling the top layer of the honeycomb-patterned film (Section 3.3.1.). A hemi-spherical MLA can be prepared by molding this pillar structure. Optical properties of prepared MLA were discussed.

The reflective index of PDMS is c.a. 1.4. Moreover, PDMS is almost transparent in the range of visible light, which was the wavelength from 400nm to 600nm. Therefore PDMS had enough properties to work as lens. The schematic illustration of preparation procedure is shown in Scheme 1. Honeycomb films were prepared from casting 1.0ml~5.0ml of 5.0g/l chloroform solution of polystyrene (Chart 1, 1, Aldrich, Mw=280,000) and amphiphilc copolymer 2(Chart 1, 1:2=9:1) in a 9cm Petri dish. After casting, moist air (relative humidity

~50%) was applied vertically onto solution surface. The prepared film was observed by optical (BH-2, Olympus, JAPAN) and scanning electron microscopy (SEM, S-3500N, Hitachi, JAPAN) after completely evaporation of solvent and condensed water. A sheet of adhesive tape (Scotch Tape, 3M) was stuck on the surface of a honeycomb film. And then, a peeled honeycomb films were prepared by peeling the top layer of honeycomb structure off.

The two types of negative molds were prepared from the honeycomb films and peeled honeycomb films (Figure 3-22). Polydimethylsiloxane (PDMS) prepolymer (Sylgard184, Dow Corning Inc., U.S.A.) was simply casting onto the prepared honeycomb films (A) or onto a peeled honeycomb films (B). And then, the sample cured at 300°C for 1hour in an electric oven. After curing, the template honeycomb film was peeled off. The prepared film was rinsed by chloroform and ethanol (sample A). Another type of negative mold was prepared by molding peeled honeycomb films. After peeling, PDMS prepolymer was casting on the peeled honeycomb film and cured (sample B). The prepared structure was investigated by SEM.

Two-dimensional arrays of spherical micro particles were obtained after curing (Figure 3-23(c)). Each spheres were connected each other on 6 surface points of the lateral position of the spheres. Because these PDMS micro-spheres were connected each other, these micro-spheres were obtained as a sheet. On the contrary, hemi-spherical micro lenses were obtained (Figure 3-23(d)). The hexagonal array of dents was acted as template of these hemi-spheres. Each Mold structure still kept periodicity of template honeycomb films. Highly ordered hexagonal array of spheres or hemi-spheres were formed. The highly ordered laser diffraction spots were also observed from the PDMS molds (insets of Figure 3-23(c) and (d)).

The projection experiment was performed under an optical microscope. Figure 3-24 shows the experimental set up of micro lens projection. In the case of sample A, a hexagonal arrangement of bright spots was observed. But the letter "F" was not clearly observed in each

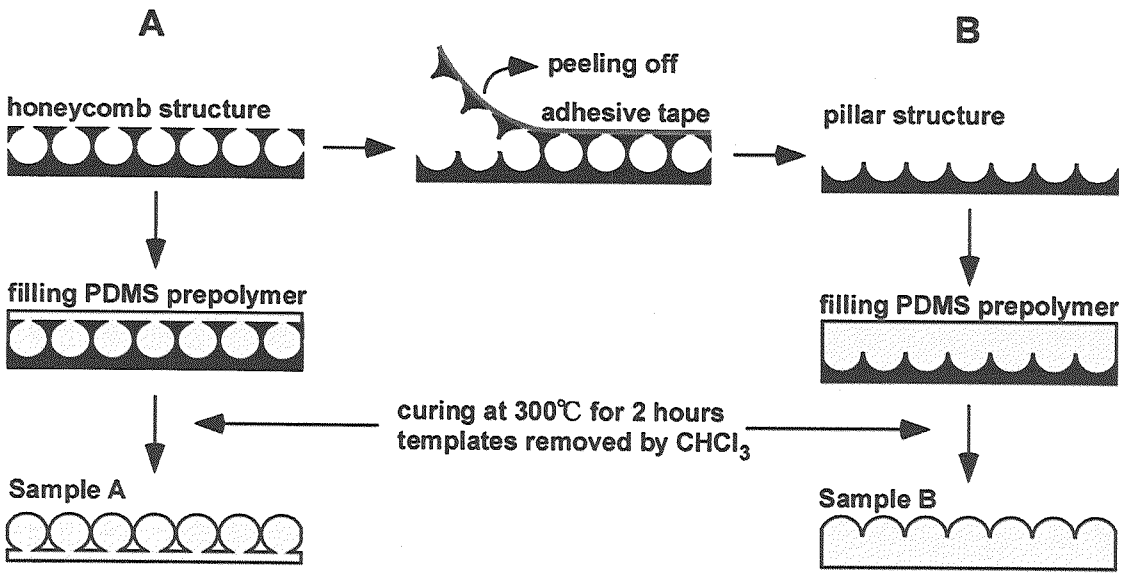

Figure 3-30. Schematic illustration of spherical and hemi-spherical micro lens arrays (MLAs). The spherical MLA was prepared by simple molding process (A). The hemi-spherical MLA was prepared by molding the pillar structure (B).

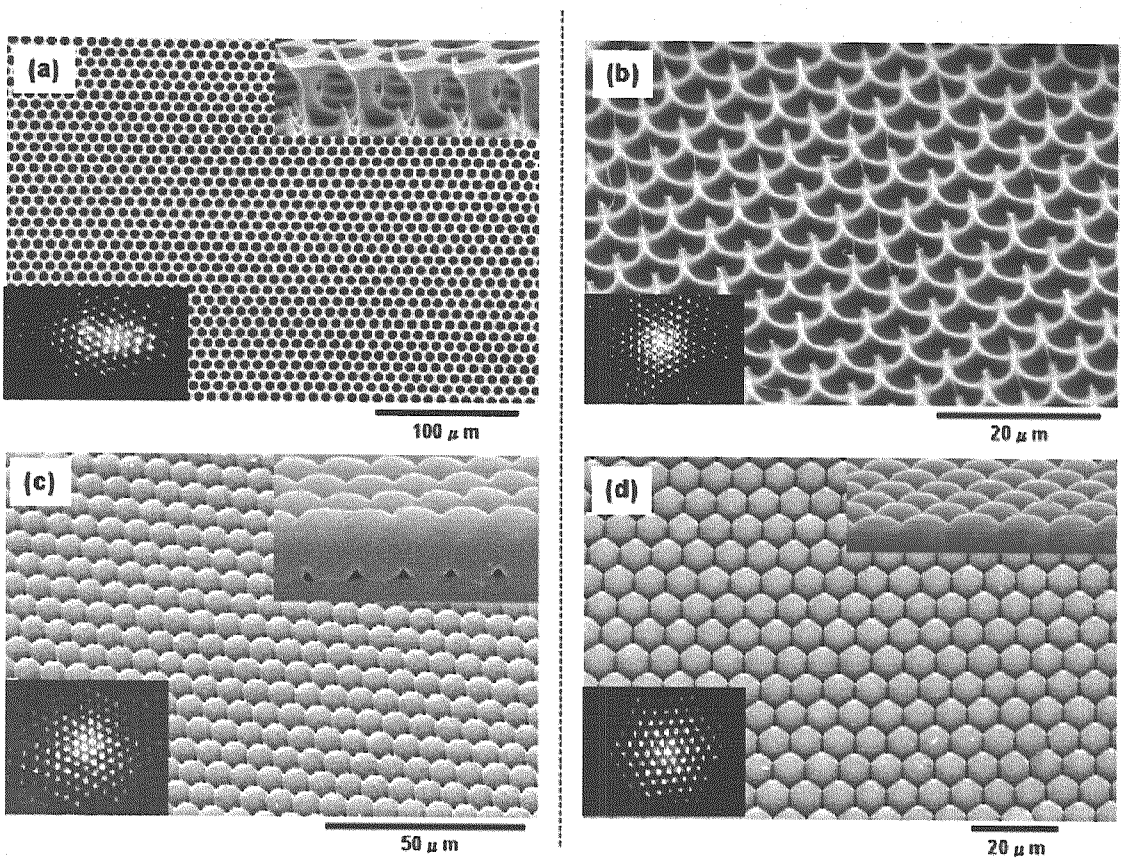

Figure 3-31. Scanning electron micrographs of the template honeycomb and pin-cushion structures ((a), (b)) and negative molds of each templates ((c), (d)).

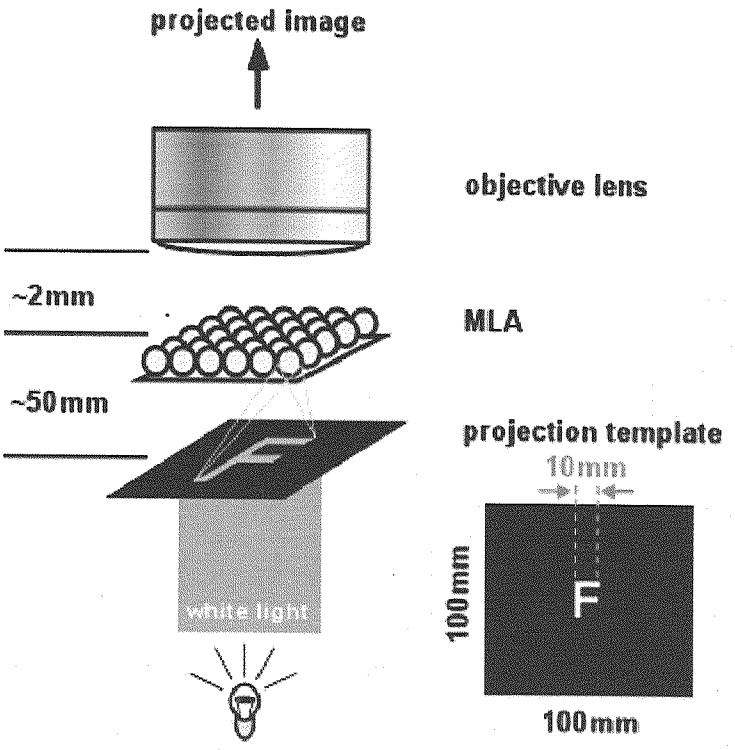

Figure 3-32. Schematic illustration of projection experiment.

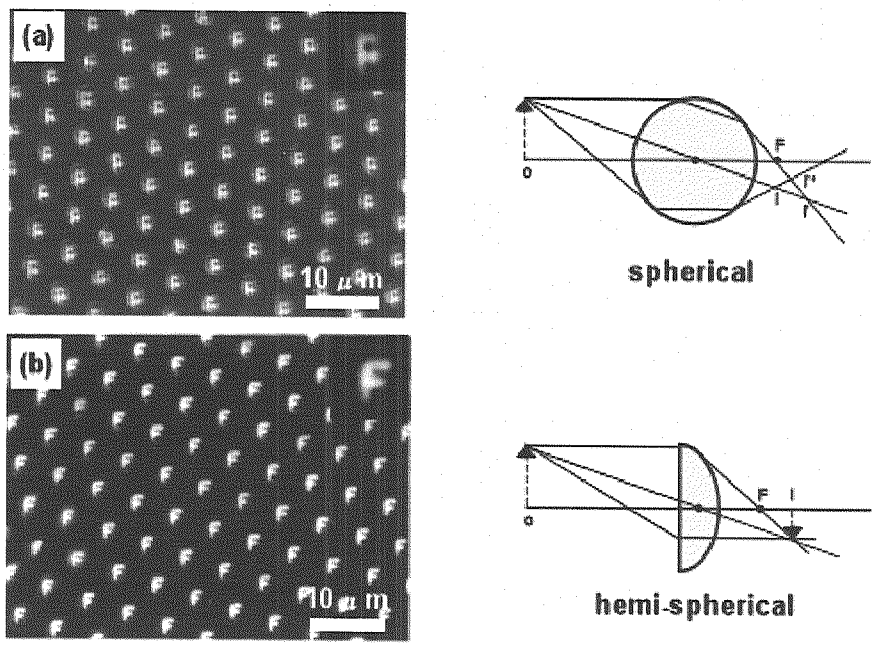

Figure 3-33.Projected images through the spherical (a) and hemi-spherical MLAs, respectively. The schematic illustration of production of image is also shown.

spots (Figure 3-25.(a)). It was reported that spherical lens projected blur images because it had some optical aberrations. A major influence on the aberration is spherical aberration. In the case of sample A, the spherical aberration was much occurred because the sample A has spherical shape of lenses. In comparison, a hemi-spherical lens is favorable for projection. It can focus light on one spot originated from same light source. Using hemi-spherical lens array (sample B), the hexagonally arranged letter "F" was clearly observed (Figure 3-25.(b)).

Some other examples of using different projection templates are shown in Figure 3-26. Clear images of hexagonally arranged dot, cross, rectangle and star images were obtained. In each case, the obtained image was miniaturized c.a. 3μm. Therefore the prepared MLA enables to reduce the template image as c.a. 1/3000 scale.

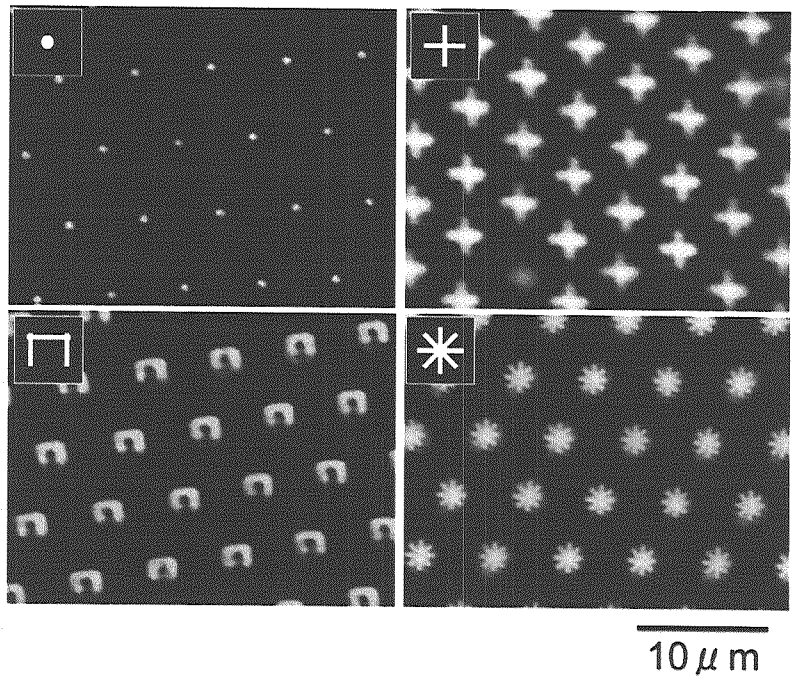

Figure 3-34. Various kinds of projection template and their projected images.

3.6.3. Micro-spheres prepared from negative molds by ultra sonic treatment

Negative molds consisted of connected micro-spheres. If individual micro-spheres divided into the liquid medium, the micro-spheres from various kinds of functional materials can be obtained from the negative molds. The negative molds consisted of two components; one is structured layer, the other is not structured layer. The structured layer was formed in the honeycomb pores, the other was not. By using the PDMS negative molds, the re-dispersed PDMS micro-spheres can be prepared.

The connecting points between the unstructured layer and the micro-spheres shaped like an hourglass. Therefore the points are week against the mechanical force. The structured layer was removed from the unstructured layer by surgical knife. By this treatment, sheets of monolayer micro-sphere arrays were obtained (Figure 3-27). When this sheet of the micro-spheres stretched perpendicular to the lattice directions by tweezers, the 1dimensional array of micro-spheres obtained. The isotropic force was applied, the mechanical force break only the connection between micro-spheres perpendicular to the direction of applied force. As the result, the "necklace structure" was obtained.

In the case of anisotropic force was applied, the all connecting point will be broken. To applied anisotropic force, the monolayer was immersed in water and ultra sonic (20kHz) was applied by probe type ultra sonic generator (UD-20, Tommy Seiko, Japan) for 2 hours. After ultra sonic treatment, the dispersion of the micro-spheres was casting onto the freshly cleaved mica substrate and dried under ambient condition. By scanning electron microscopy, the individual micro-spheres are clearly observed (Figure 3-28). The micro-spheres had a straw bag shape. The round signature of connected area was observed on the surface of the micro-sphere.

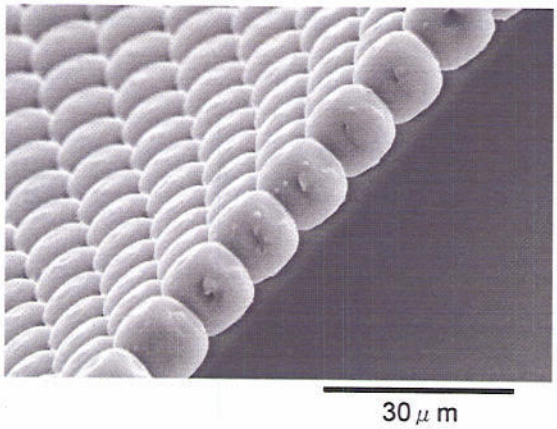

Figure 3-35. Scanning electron micrograph of monolayer of PDMS micro-spheres.

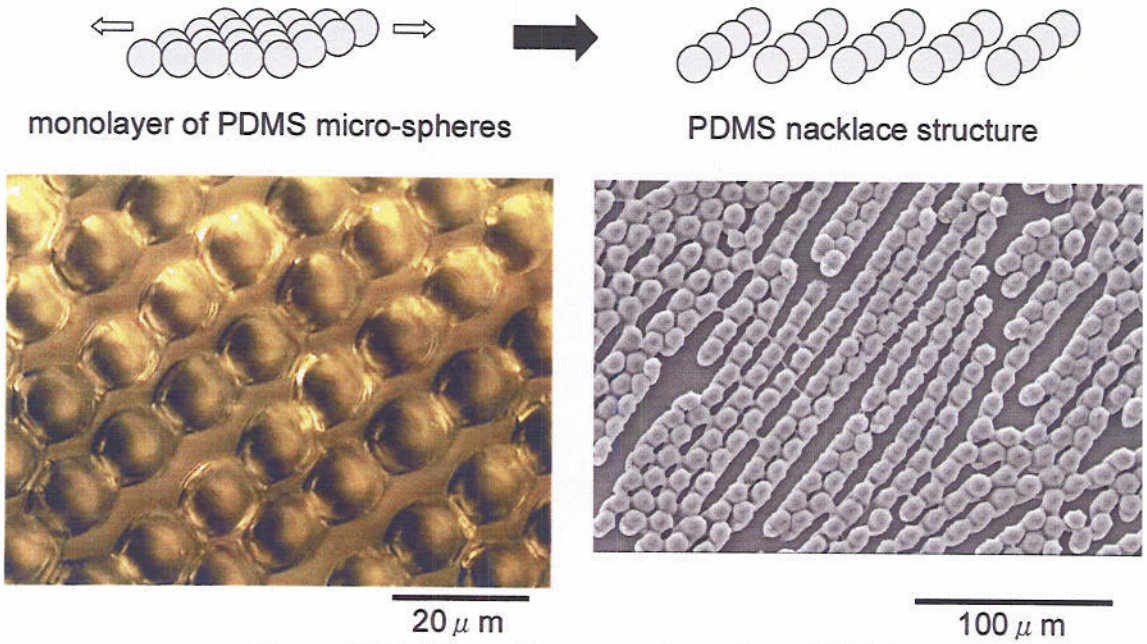

Figure 3-36. The necklace structures from PDMS.

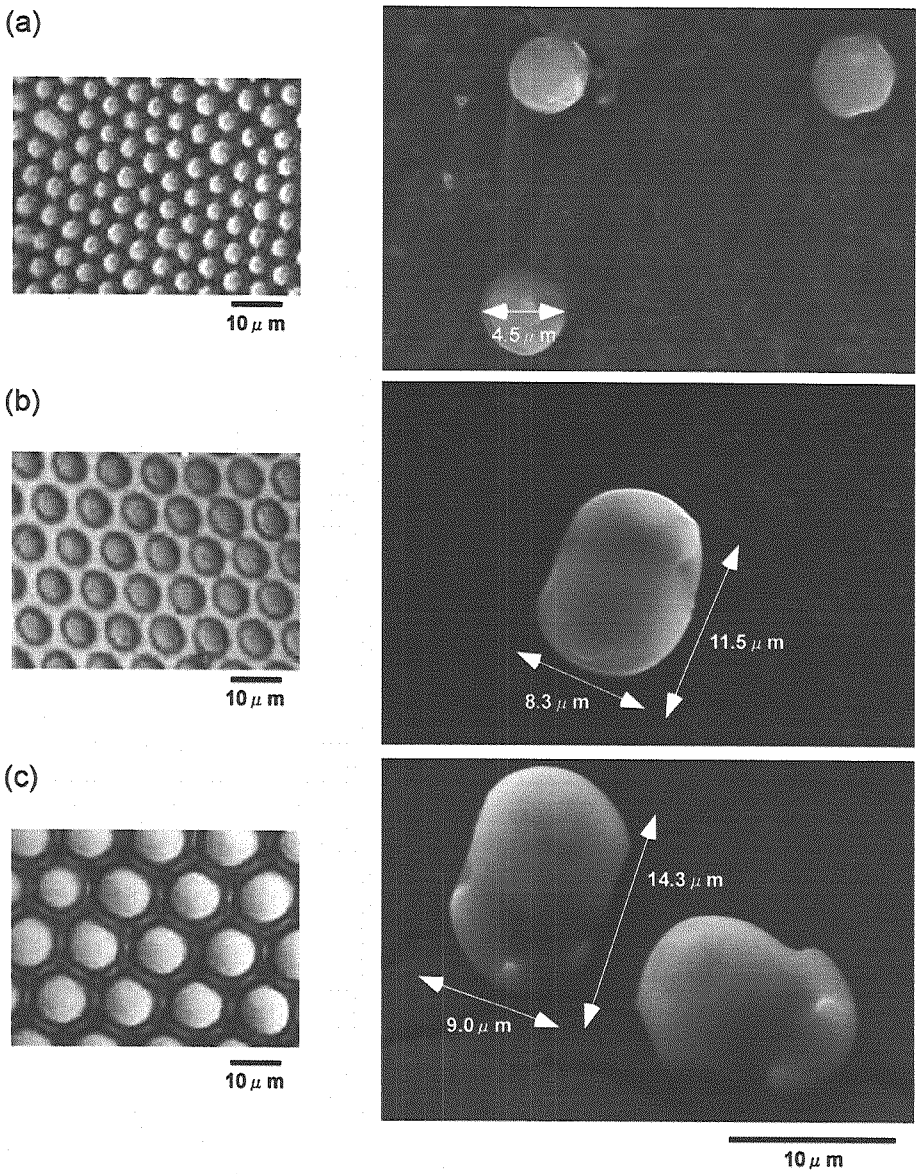

Figure 3-38. Various size particles prepared by changing the size of template honeycomb pores (ϕ). (a) ϕ =5 μ m, (b) ϕ =7.5 μ m and (c) ϕ =13 μ m.

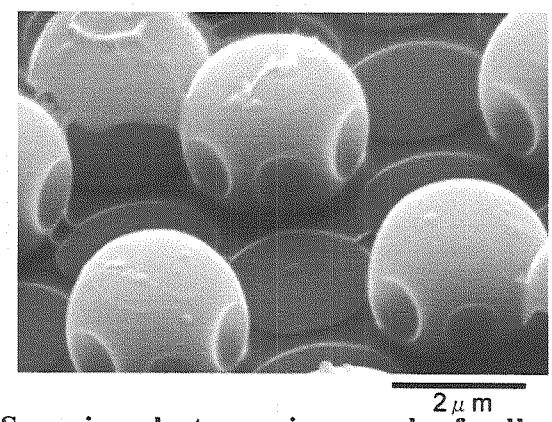

Figure 3-39. Scanning electron micrograph of collagen micro-spheres prepared in the honeycomb-pores.

The size and shape of the micro-spheres can be controlled by changing the size of the template honeycomb pores. The lengths of the long axis of the micro-spheres were changed from 5μm to 13μm by changing the pore diameter from 3.5μm to 10μm (Figure 3-29). The shape of the micro-spheres changed from spherical shape to straw bag shape by increase of the template pore diameters. These results indicate that the overlap of condensed water droplets, which was the templates of the honeycomb pores, extended by increasing of the solvent evaporation time.

The micro-spheres can be prepared from other materials. The collagen is one of the bio-compatible materials. The collagen was dissolved in water and casting onto the honeycomb-patterned film. After placing *in vacuo*, solvent water was gently evaporated under ambient condition. The collagen filled the honeycomb pores, and spherical negative mold was formed (Figure 3-30). The template honeycomb-patterned film was rinsed away by chloroform. And the micro-spheres from collagen were transferred onto carbon adhesive tape to observe by SEM. The micro-spheres with six-hold symmetrical dents were formed. These dents were formed on the connecting point between the each micro-sphere.

3.6.4. Preparation of positive mold and their properties

The positive image of the honeycomb-patterned films can be obtained by molding the negative mold. By using the PDMS negative molds as templates, the positive molds from polystyrene and water dispersed gold nano-particles were prepared. The prepared structures were varied by the preparation conditions, viscosity, and interaction between the template surfaces. In the case of polystyrene, chloroform solution of these materials casting onto the PDMS negative mold. According to the formulae 3-1, the high affinity of the solution enables the solution to penetrate the small pores by capillary force. Therefore the chloroform solution was adsorbed into the pores between the micro-spheres of the PDMS negative mold, the pillar

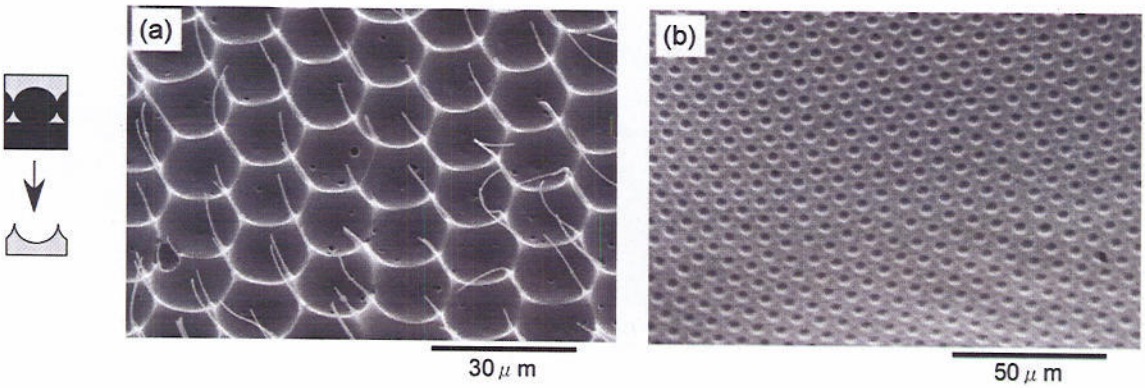

Figure 3-40. Scanning electron micrographs of positive molds. The polystyrene (a) and gold nano-particles (b) positive mold is shown.

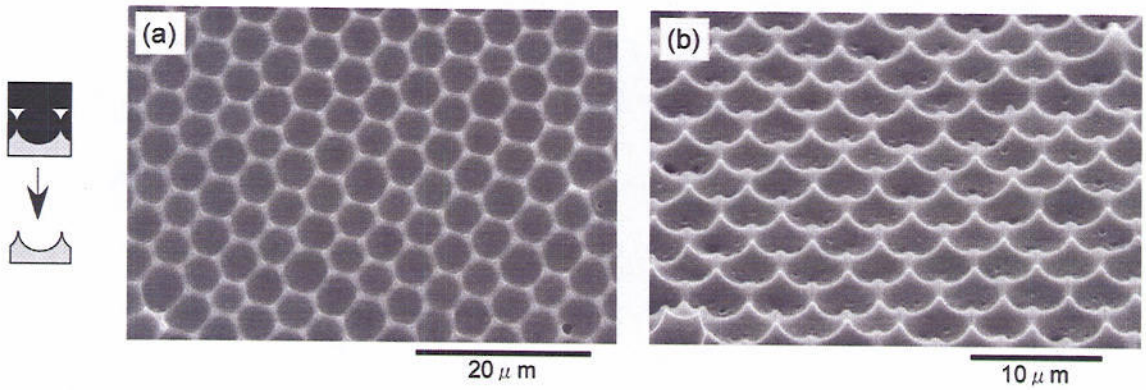

Figure 3-41. Scanning electron micrograph of the positive mold of fluorinated copolymer. The hexagonally arranged dents are observed (a). The bulges on the apex of hexagons are also observed by tilting the sample stage (b).

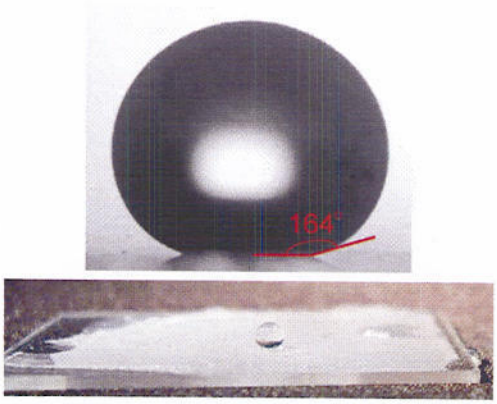

Figure 3-42. The water contact angles on the prepared positive mold from fluorinated copolymer.

structure was prepared (Figure 3-31(a)). On the other hand, water dispersion of gold nano-particles did not fill the pores. As the results, the hexagonally arranged dent structure was obtained (Figure 3-31(b)).

To prepare positive mold from polymer melt, the "heat stamping" method was applied. The fluorinated polymers did not dissolve in organic solvents except for fluorinated solvents. Therefore the pattern formation from polymer melts is effective. The powder of fluorinated copolymer was placed on the glass substrate and the PDMS negative mold was gently placed above the polymer powder. After the sample heating in a vacuum oven over Tm of fluorinated copolymer, the oven was vacuumed. The template negative mold was removed after cooling room temperature and ambient pressure. By scanning electron microscopy, the hexagonally arranged dent structure was observed (Figure 3-32) On the apex of the hexagon, the polymer bulged. The water contact angle of the flat film was c.a. 120°. However, the water contact angle on the prepared structure was over 164° (Figure 3-33). The surface structure enhances the hydrophobic properties of the fluorinated materials.

Reference

[3-1] J. D. Joannopoulos, R. D. Meade, J. N. Winn, *Photonic Crystals –Molding the Flow of Light*; Princeton University Press: New Jersey, (1995)

[3-2] E. Ostuni, C. S. Chen, D. E. Ingber, G. M. Whitesides, *Langmuir*, **17***(9)*, 2828 (2001)

[3-3] G. Widawski, M. Rawiso, B. François, *Nature*, **369**, 397, (1994)

[3-4] O. Pitois, B. François, *Eur. Phys. J. B*, **8**, 225 (1999)

[3-5] O. Pitois, B. François, *Colloid Polym. Sci.*, **277**, 574 (1999)

[3-6] M. Srinibasarao, D. Collings, A. Philips, S. Patel, *Science*, **292**, 79 (2001)

[3-7] L. V. Govor, I. A. Bashmakov, F. N. Kaputski, M. Pientka, J. Parisi, *Macromol. Chem. Phys.*, **201**, 2721 (2000)

[3-8] L. V. Govor, I. A. Bashmakov, R. Kiebooms, V. Dyakonov, J. Parisi, *Adv. Mater.*,**13**(8), 588 (2001)

[3-9] J. Nishida, K. Nishikawa, S. Nishimura, S. Wada, T. Karino, T. Nishikawa, K. Ijiro, M. Shimomura *Polym. J.*, **34**, 166-174 (2002)

[3-10] N. Kurono, R. Shimada, T. Ishihara, M. Shimomura *Mol. Cryst. Liq. Cryst.*, **377**,285-288 (2002)

[3-11] M. Shimomura, T. Sawadaishi *Current Opinion in Colloid & Interface Science*, **6**, No1. 11-16

(2001)

[3-12] M. Shimomura, Hierarchical Structuring of Nanostructured 2-Dimentional Polymer Assemblies. in *"Chemistry for the 21st Century - Organic Mesoscopic Chemistry"*, Ed. by H.Masuhara, F.C.DeSchryver, IUPAC monograph, Blackwell Science, 1999, 107-126

[3-13] O. Karthaus, N. Maruyama, X. Cieren, M. Shimomura, H. Hasegawa, T. Hashimoto, *Langmuir*, **16**(15), 6071 (2000)

[3-14] O. Karthaus, X. Cieren, N. Maruyama, M. Shimomura *Mater. Sci. Eng.*, C **10**, 103-106 (1999)

[3-15] T.; Nishikawa, J. Nishida, R. Ookura, S. Nishimura, S. Wada, T. Karino, M. Shimomura *Mater. Sci. Eng.*, C **8-9**, 485-500 (1999)

[3-16] N. Maruyama, O. Karthaus, K. Ijiro, M. Shimomura, T. Koito, S. Nishimura, T. Sawadaishi, N. Nishi, S. Tokura, *Supramol. Science.*, **5**, 331 (1998)

[3-17] M. H. Stenzel, *Aust. J. Chem.*, **55**, 239 (2002)

[3-18] B. de Boer, U. Stalmach, H. Nijland, G. Hadziioannou, *Adv. Mater.*, **12**, 1581 (2000)

[3-19] B. de Boer, U. Stalmach, P. F. van Huttern, C. Melzer, V. V. Krasnikov, G. Hadziioannou, *Polymer*, **42**, 9097-9109 (2001)

[3-20] T. Yonezawa, S. Onoue, N. Kimizuka, *Adv. Mater.*, **13**(2), 140 (2001)

[3-21] M. Kakimoto, M. Suzuki, T. Konishi, Y. Imai, M. Iwamoto, T. Hino, *Chem. Lett.*, 823, (1986)

[3-22] P. Ball, *Nature*, **400**, 507 (1999)

[3-23] (a) H. Tada, H. Nagayama, *Langmuir*, **11**(1), 136 (1995), (b)T. Nishino, M. Megro, K. Nakamae, M. Matsushita, Y. Ueda, *Langmuir*, **15**(13), 4321 (1999)

[3-24] W. Chen, A. F. Fadeev, M. C. Hsieh, D. Oner, J. Youngblood, T. J. McCarthy, *Langmuir*, **15**(10), 3395 (1999); J. Bico, C. Marzorin, D. Quere, *Europhys. Lett.* **47**(2): 220 (1999); D. Öner, T. J. McCarthy, *Langmuir*, **16**(20), 7777 (2000); Z. Yoshmitsu, A. Nakajima, T. Watanabe, K. Hashimoto, *Langmuir*, **18**(15), 5818 (2002); J. Kim, C. J. Kim, *IEEE*, 479 (2002)

[3-25] T. Onoda, N. Satoh, K. Tsujii, *Langmuir*, **12**(9), 2125 (1996)

[3-26] A. Hozumi, O. Takai, *Thin. Sol. Films.*, **303**, 222 (1997)

[3-27] A. Nakajima, A. Fujishima, K. Hashimoto, T. Watanabe, *Adv. Mater.*, **11**(16), 1365 (1999), M. Miwa, A. Nakajima, A. Fujishima, K. Hashimoto, T. Watanabe, *Langmuir*, **16**(13), 5754 (2000), ,

[3-28] A. Nakajima, K. H., T. Watanabe, *Monatshefte fur Chemie*, **132**, 31 (2001)

[3-29] H. Li, X. Wang, Y. Song, Y. Liu, Q. Li, L. Jiang, D. Zhu, *Angew. Chem. Int. Ed.*, **40**(9), 1743 (2003), S. Li, H. Li, X. Wang, Y. Song, Y. Liu, L. Jiang, D. Zhu, *J. Phys. Chem. B*, **106**, 9274 (2002), L. Feng, S. Li, Y. Li, H. Li, L. Zhang, J. Zhai, Y. Song, B. Liu, D. Zhu, *Adv. Mater.*, **14**(24), 1857 (2002)

[3-30] Z.-Z. Gu, H. Uetsuka, K. Takahashi, R. Nakajima, H. Onishi, A. Fujishima, O. Sato, *Angew. Chem. Int. Ed.*, **42**(8), 894 (2003)

[3-31] H. Y. Erbil, A. L. Demirel, Y. Avci, O. Mert, *Science*, **299**, 1277 (2003)

[3-32] A. B. D. Cassie, *Discuss Faraday Soc.*, **3**, 11 (1948)

[3-33] D. Beysens, C. M. Knobler, *Phys. Rev. Lett.*, **57**(12), 1433 (1986)

[3-34] D. Beysens, *Atmos. Res.*, **39**, 215

[3-35] A. V. Limaye, R. D. Narhe, A. M. Dhote, S. B. Ogale, *Phys. Rev. Lett.*, **76**(20), 3762 (1996)

[3-36] D. Fritter, C. M. Knobler, D. A. Beysens, *Phys. Rev. A*, **43**(6), 2858 (1991)

[3-37] A. Steyer, P. Guenoun, D. Beysens, *Phys. Rev. B*, **42**(1), 1086 (1990)

[3-38] A. Steyer, P. Guenoun, D. Beysens, *Phys. Rev. E*, **48**(1), 428 (1993)

[3-39] P. D. Aversana, G. P. Neizel, *Phys. Today.* **38** (1998)

[3-40] E. Yablonovitch, *Phys. Rev. Lett.*, **58**(20), 2059 (1987)

[3-41] S. Noda, A. Chutinan, M. Imada, *Nature*, **407**, 608 (2000)

[3-42] S. Hyuk, O. O. Park, *Langmuir*, **18**, 9642 (2002)

[3-43] A. Rugge, W. T. Ford, S. H. Tolbert, *Langmuir*, **19**, 7852 (2003)

[3-44] P. G. de Gennes, F. Brochard-Wyart, D. "Quéré, Gouttes, bulles, perles et ondes",

[3-45] P. Nussbaum, R. Völkel, H. P. Herzig, M. Eisner, S. Haselbeck, *Pure Appl. Opt.*, **6**. 617 (1997)

[3-46] P. Ruther, B. Gerlach, J. Göttert, M. Ilie, J. Mohr, A. Müller, C. Oβmann, *Pure Appl. Opt.*, **6**, 643 (1997)

[3-47] W. Däschner, P. Long, R. Stein, C. Wu, S. H. Lee, *J. Vac. Soc.Technol. B*, **14**(6), 3730 (1996)

[3-48] J. Bähr, K.-H. Brenner, *Appl. Opt.*, **35**(25), 5102 (1996)

[3-49] H. Chase, M. A. Handschy, M. J. O'Callaghan, F. W. Supon, *Opt. Lett.*, **20**(12), 1444 (1995)

[3-50] B. Messerschmidt, T. Possner, R. Goering, *Appl. Opt.*, **34**(34), 7825 (1995)

[3-51] M.-H. Wu, G. M. Whitesides, *Appl. Phys. Lett.*, **78**(16), 2273 (2001)

[3-52] Y. Lu, Y. Yin, Y. Xia, *Adv. Mater.* 13(1), 34 (2001)

Chapter 4

Preparation of Mesoscale Polymer Patterns by Dewetting

4.1. Introduction

Dewetting is a spatio-temporal phenomenon that a thin liquid film on a solid substrate ruptures into liquid droplets. Once dewetting occurs in a homogeneous liquid film, randomly formed liquid droplets are arranged to form irregular figures like Voronoi pattern [4-1]. Dewetting is an undesirable phenomenon for lubrication, lamination, and adhesion in the coating technology and industry. Therefore, dewetting phenomenon of polymer melts on solid substrates has been intensively investigated theoretically [1-4~4-3] and experimentally [4-4~4-6] to fabricate homogeneous polymer thin films. Recently, we have reported that regular polymer patterns are formed from casting a dilute polymer solution on a solid substrate. Dissipative structures formed in the evaporating polymer solution and subsequent dewetting of the polymer film on the substrate cooperatively induces the regular pattern formation. Dissipative structures, e.g. Rayliegh-Bénard convection [4-7], fingering instability [4-8], and other spatio-temporal structures [4-9], are formed in the evaporation process of the casting polymer solution. The fingering instability, so-called "Tears of Wine" phenomenon, caused by Marangoni convection induces periodic condensation of polymer at the casting solution edge. Then the periodic deposition and highly ordered dewetting of polymer are occurred to form regular mesoscale patterns, e.g. stripe, lattice and hexagonally arranged dots patterns, from polystyrene [4-10], electron conducting polymers [4-11], and liquid crystalline polymers [4-12] etc.

Though the dissipative structures are typical self-organization phenomena of complexity fluctuated by many physical and chemical conditions, it can be applicable to polymer patterning because of their physical generality. If the patterning process is carried under controlled casting condition, e.g. temperature, polymer concentration, solvent, and so on, we can prepare regular polymer patterns reproducibly and continuously. It is noticeable that the key events inducing pattern formation, the fingering instability and dewetting, are occurred at the evaporating solution edge. Controlled production and manufacturing of

patterned polymer films is prospective when the evaporating solution edge, especially the meniscus region on the casting substrate, is formed under the controlled casting process. In this report, we have fabricated a computer-controlled apparatus having two glass plates sliding precisely. A narrow and thin liquid film of the polymer solution with a receding meniscus is continuously supplied from a narrow gap between two glass plates and the patterned polymer film is formed from the evaporating solution edge successively on the sliding glass substrates. A fluorescence microscope equipped to the apparatus carries an *in situ* observation of the pattern formation at the moving solution edge continuously provided on the sliding glass plate. Several types of polymer patterns are reproducibly prepared by changing preparation conditions, e.g. sliding speed and concentration. More complicated patterns are prepared by the secondary processing of the patterned films.

4.2. Experimental

To control the pattern formation process, we fabricated a new apparatus composed of two moving substrate-holders and a microscope system (Figure 4-1(a)). A glass plate (76mm×26mm, MATSUNAMI, Japan) was fixed on a substrate-holder, which smoothly moved with controlled velocity by a computer controlled driving system. Another glass plate was set on the other substrate holder. Each glass plate was overlapped with 3~4cm wide and spaced out with a narrow gap of 200μm. Chloroform solutions of polystyrene (PS, Scientific Polymer Products Inc., Mw=2,316,000, Mn=2,276,000, Mw/Mn=1.02, concentration ranging from 0.1g/l to 4.0g/l) and poly (3-hexylthiophene) (PHT, Aldrich, U.S.A., 1.0g/l) were fleshly prepared before casting. Two hundred micro-litters of the polymer solution were supplied into the gap of two glass plates. Then the substrate-holder fixing the upper glass plate was moved straightly at its velocity from 10μm/s to 400μm/s. A thin liquid film of polymer solution and meniscus were continuously formed behind the moving edge of the upper glass plate during its sliding. After immediate evaporation of solvent at the meniscus polymer was deposited on the bottom glass plate continuously.

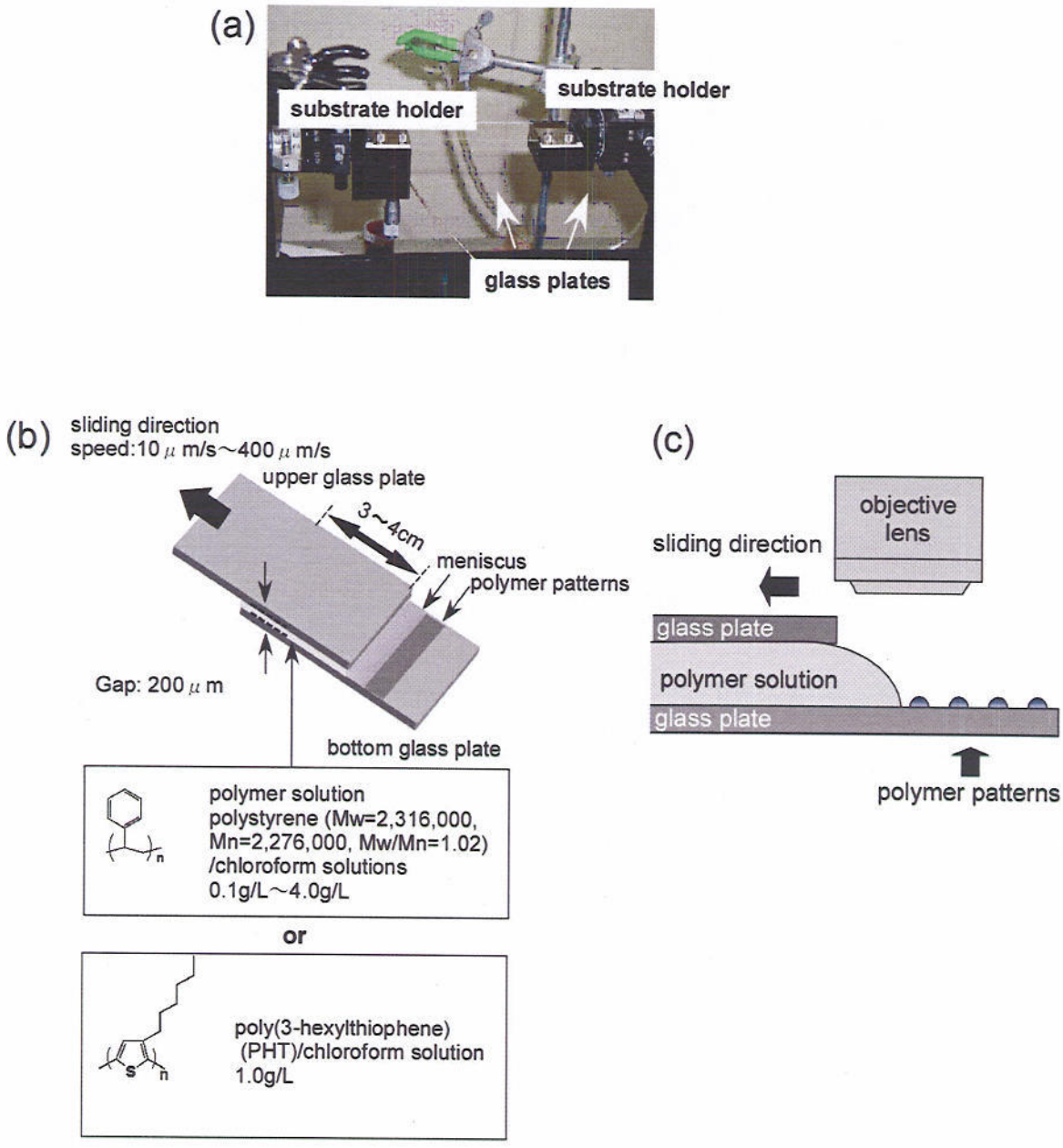

Figure 4-1. Schematic illustration of experimental set up

The fixed polymer pattern was observed by optical microscopy (BH-2, Olympus, Japan), atomic force microscopy (AFM, SPA-400, Seiko Instruments, Japan) and scanning electron microscopy (SEM, S-3500, Hitachi, Japan). The process of pattern formation was observed by *in situ* fluorescence microscopy with using polymer solution containing 0.05 weight percent of octadecyl rhodamine B (Molecular Probe, INC. U.S.A.) as a fluorescence probe (Figure 4-1(b)). Top and side views of the moving meniscus were observed by a movable objective lens around the glass plates. The pattern formation process along the evaporating solution edge and the side view of the receding meniscus were stored as digital video images in a video recorder (DV-CAM, SONY, Japan).

The electric current of the PHT pattern was measured by AFM. The patterned PHT film was fixed on the AFM sample stage with a conductive carbon tape (Nitto Denko, Japan). Five volts of bias voltage was applied between the PHT film and a gold-coated AFM tip (SN-AF-01-A, Seiko Instruments Inc., Japan). The topography and the current image were simultaneously obtained.

4.3. Dot, stripe and ladder structures.

Optical micrographs and AFM images of patterned polystyrene films are shown in Figure 4-2(a). Regular array of micron-sized polymer dot was formed when polystyrene solution of 0.1g/l was deposited at sliding speed of 50μm/s. The mean diameter of each micro-dot was 10μm. AFM measurement showed the height of the micro-dot ranged from 50nm to 100nm. Spacing between two dots were about 10μm along to the sliding direction and 2~5μm perpendicular to the sliding direction. In the case of higher concentration (0.5g/l), micron-sized periodic stripes were formed. The stripes perpendicularly oriented to the sliding direction. Atomic force microscopy revealed that the width and height of the micro-stripe were 10μm and 100nm, respectively, and line spacing was 10μm. Highly uniformed ladder like polymer patterns were formed when the 4.0g/l solution was supplied for casting. These

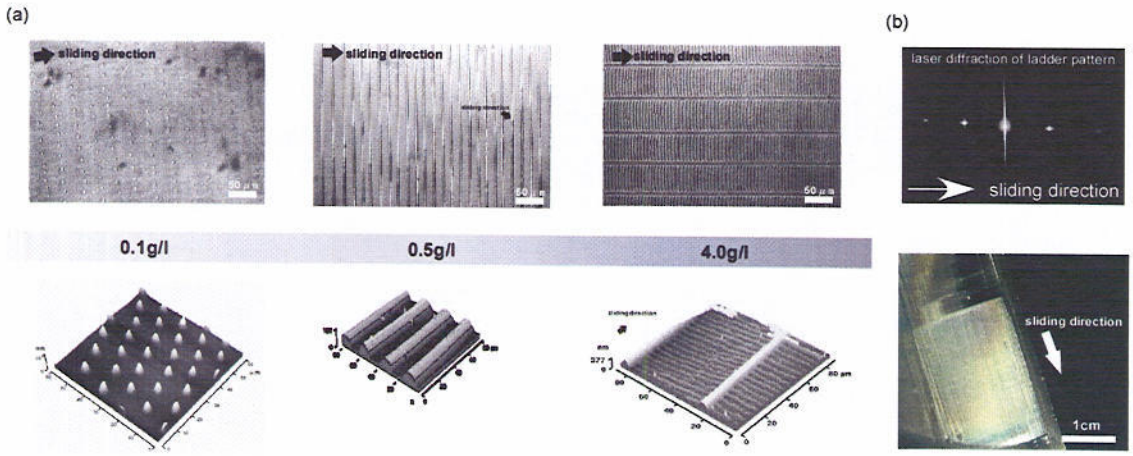

Fig. 4-2. Various patterns prepared by the novel method. (a) Optical (upper column) and atomic force (lower column) micrographs of polymer patterns prepared from polystyrene solutions. (b) The ladder pattern prepared on the glass plate and its laser diffraction.

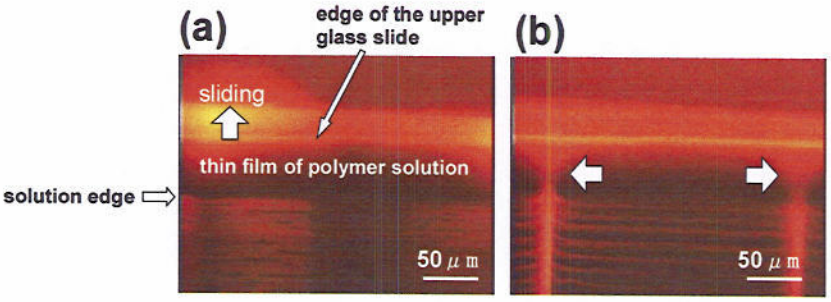

Figure 4-3. In situ fluorescence micrograph of pattern formation process. The sliding speed was 50 μ m/s and the solution concentration was (a) 0.5g/l and (b) 4.0g/l, respectively.

"ladder pattern" consisted of thick lines with 400nm height along to the sliding direction and thin lines with 100nm height perpendicular to the sliding direction.

Figure 4-2(a) clearly shows that the concentration of polymer solution is one of the important determining factors of pattern formation. The sequentially arrayed micro-dots perpendicular to the sliding direction converts to single continuous line with increasing the concentration. Further concentration yields new stripes parallel to the moving direction to form the ladder patterns. Under the sliding at 50μm/sec, 0.3g/l and 1.0g/l were the critical

concentrations of the stripe and the ladder formation because the coexistence of two patterns, dots and stripes, stripes and ladders, was found at these concentrations, respectively.

As shown in Figure 4-2(b) the glass plate coated by the patterned polymer film shows strong interference color originated from the microstructures, especially from the ladder pattern. Periodic diffraction spots of the laser beam (diode pumped solid state (DPSS) Nd:YVO_4 laser, λ=532nm.) from the ladder patterned polymer film are shown in Figure 4-2(b), too. Two periodic structures formed in the ladder pattern were reflected in two series of diffraction spots crossing each other. Diffraction spots arrayed on an equator run parallel to the sliding direction of the glass plate. These diffractions with long spacing reflect the regular arrangement of the stripes with short repeating period formed vertically to the sliding direction. Another series of the diffraction spots arrayed vertically to the former series has shorter spacing. They are diffracted from another stripe structure formed parallel to the sliding direction with long repeating distance. This result clearly indicates that the regularity of the micron scale lattices in the ladder pattern is high enough as a grating. Without conventional lithographic technique, highly ordered periodic structure can be easily prepared by our sliding apparatus. These micro-patterns can be applied for optical wave guide arrays, diffraction gratings and photonic band gap materials.

4.4. Formation mechanism of polymer patterns.

Pattern formation process was observed at the edge of the upper glass plate by *in situ* fluorescence microscopy. Figure 4-3 shows snap shots of the stripe and the ladder formation. A thin liquid film of polymer solution (dark) follows the moving edge (bright) of the upper glass plate, and polymer deposition occurs at the meniscus region of the solution edge (bright). Bright area indicates that solutes, polymer and fluorescence probe, are locally condensed. In the case of the 0.5g/l solution, polymer was deposited intermittently from the meniscus of the solution to form the periodical stripes perpendicular to the sliding direction

(Figure 3(a)). This type of the periodical deposition is caused by the "stick-slip motion", which is often observed in colloidal crystals (13) and well known as coffee stein phenomenon (14). Dew to evaporation of solvent at the meniscus, polymer was condensed at the edge of solution. Increasing local viscosity of polymer solution caused by polymer gelation, pinning of the solution edge was occurred at meniscus. After complete deposition of polymer onto the glass substrate, the pinning stress relaxed and the solution edge moved to the sliding direction like a receding tide until the next pinning. Repeating of the deposition and the receding cycle formed the regularly periodic stripes of the deposited polymer.

In the case of the 4.0g/l solution, a series of bright spots emerged along the glass slide edge (Figure 4-3(b), white arrows). The polymer was deposited from these spots on the substrate to form thick lines parallel to the sliding direction. The interval of these lines was uniform. The periodic condensation of polymer along the glass edge was caused by the convectional flow in the solution, so-called fingering instability [4-15]. The fingering instability is one of the typical dissipative structures known as the "Tears of Wine" phenomenon caused by Marangoni convection occurred by the balance of the surface and the interfacial tension. It is known that local condensation of polymer decreases the local surface tension of the solution. Therefore the solution spreads to the higher concentration region. The convectional flow caused by the local fluctuation of the surface tension is known as "solutal Marangoni effect" [4-16]. Then the local condensation of polymer forms "fingers". These fingers are fixed on the substrate due to their high viscosity, and then the regular lines are formed by the continuous polymer deposition from the fingers. If the stick-slip motion and the fingering instability occur simultaneously, the ladder pattern is formed.

The dot pattern only formed in diluted solution (e.g. 0.1g/l) was resulted by the dewetting of the stick-slip stripes. Hydrophobic polymer solution was spontaneously ruptured into droplets on the hydrophilic surface to minimize their surface free energy.

4.5.Regulation of patterns

Figure 4-4(a) shows the effect of the sliding speed on the spacing of the stick-slip stripe. With increasing the sliding speed the spacing of the stick-slip stripes decreases to the minimum value at the sliding speed of 75μm/s and then increases. Deposition frequency of polymer depends on the evaporation rate of the solvent. And the evaporation rate also depends on the surface area of the meniscus region where the evaporation events occur. To estimate the area of meniscus region and its effect on the deposition frequency, the side view of the receding meniscus was observed during the sliding of the glass plate by the *in situ* fluorescence microscopy. Figure 4-4(b) shows the cross sectional views of the receding meniscus and their schematic models at various sliding speeds. At the slow sliding (30μm/s), the receding contact angle of the polymer solution was about 31 degree and the meniscus spread about 200μm from the solution edge to the glass edge. With increasing the sliding speed to 50μm/s the receding contact angle decreased to 11 degree and the area of meniscus expanded to 800μm. Fluorescence microscopy clearly revealed that the meniscus was deformed and decreased its thickness with increasing the sliding speed. Enlarged surface area of the deformed meniscus sufficiently required shorter time for evaporation than the slower sliding, and then the deposition frequency was increased to decrease the spacing of the stick-slip stripes. Faster sliding over 75μm/s provided the continuous liquid thin film of the polymer solution and the meniscus. In the case of the 150μm/s sliding, the receding contact angle was larger than that of the 50μm/s sliding. The shear stress applied to the meniscus was relaxed and the surface area of the meniscus was decreased. Then the deposition frequency decreased again and the spacing of stick-slip stripe increased in proportion to the sliding speed.

The relation between the sliding distance and the fingering wavelength were plotted in Figure 4-4(c). The first stage of the sliding, the spacing of the finger was diverse. The spacing was decreased with the proceeding of the sliding. Cazabat et. al. investigated the

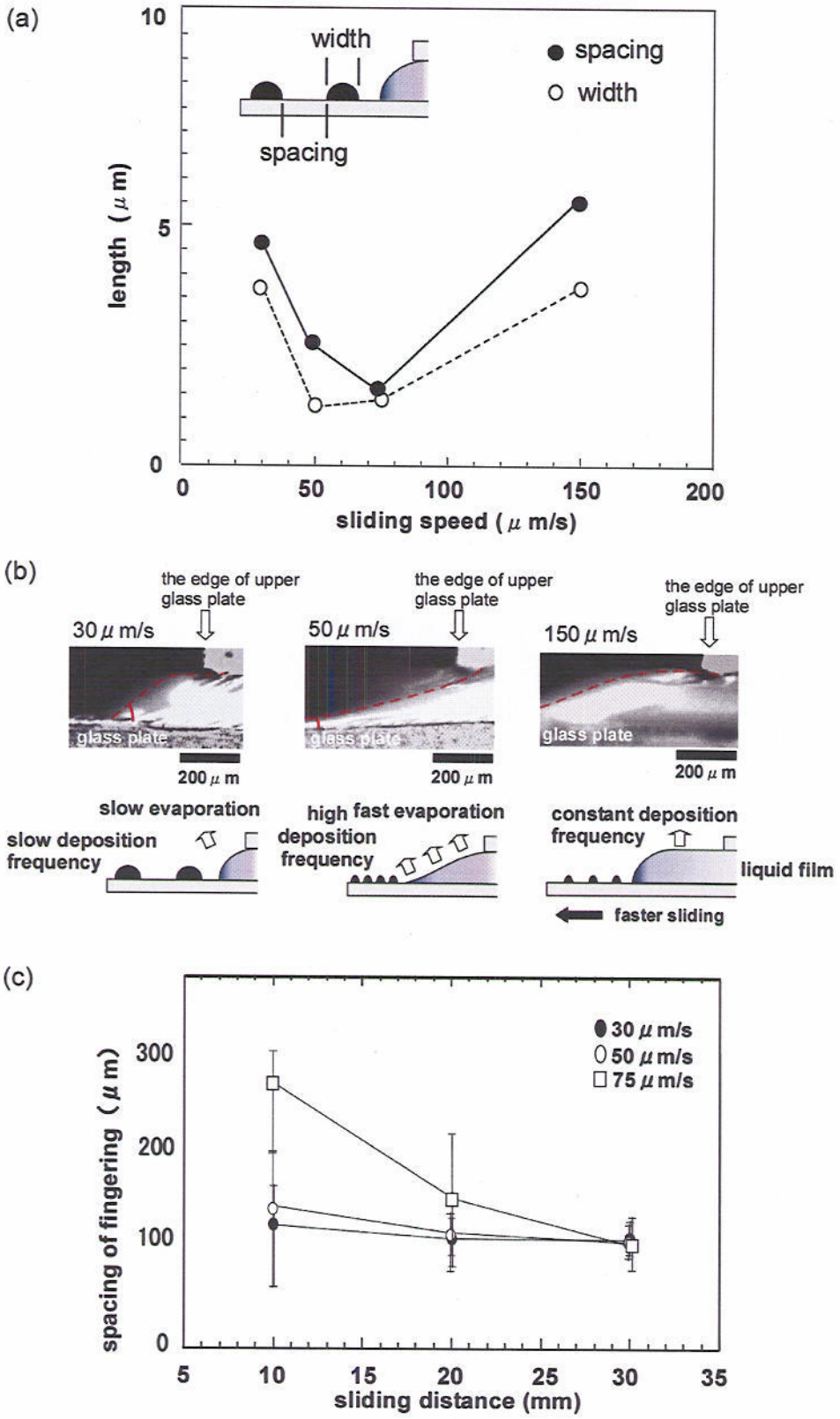

Figure 4-4. Effect of sliding speed and sliding distance. (a) Effect of the sliding speed on the spacing of the stick-slip stripe. (b) Side view of the receding solution edge at 30 μ m/s, 50 μ m/s, and 150 μ m/s, and their schematic illustrations. (c) Plots of distance and fingering spacing at sliding rates of 30 μ m/s, 50 μ m/s and 75 μ m/s, respectively

growth of the fingering instability in heptan/dodecane mixture system [4-17]. The instability grew up until a certain period, and then the system reached stationary state. In our case, after 400s~600s, the spacing of the fingers reached at 100μm in any sliding speed.

4.6..Preparation of poly(3-hexylthiophene) micro-patterns.

One of the advantages of this method is no restriction of polymer materials for micro patterning. Here, we show the micro patterning of conducting polymer, PHT. The chloroform solution of PHT was placed in the gap of the glass plates, and the one plate was slid at 50μm/s. The metallic and interference colored film was obtained (Figure 4-5. (a)). Optical microscopy revealed the stripe and the ladder pattern was formed (Figure 4-5. (b) and (c)).

Topography and current image simultaneously observed by AFM (Figure 4-5. (d) and (e)) reveals that micro-patterned film has electron-conductivity. The measured current corresponds to semi-conductor level (σ=1.3X10^{-4} S/cm), which is same conductivity as the bulk PHT [4-18]. This result also shows that the wide variety of materials can be patterned by using this method.

4.7.Secondary processing of the complicated structures and patterning on the curved surface.

The prepared patterns can be peeled off from the glass substrate in water. The floated patterned film was transferred onto another substrate or patterned film. Figure 4-6(a) shows a double mesh structure of polystyrene prepared by crossing and pilling up two ladder films. Furthermore, this method can be utilized for patterning onto curved surface. One glass tube with 0.60mm external diameter was inserted into another glass capillary with 0.70mm internal diameter. Chloroform solution of polystyrene (1.0g/l) was filled into the gap between two capillaries. After sliding the inner glass tube, polystyrene micro rings were prepared on the inner glass surface (Figure 4-6(b)). These rings are the stick-slip stripes. By the

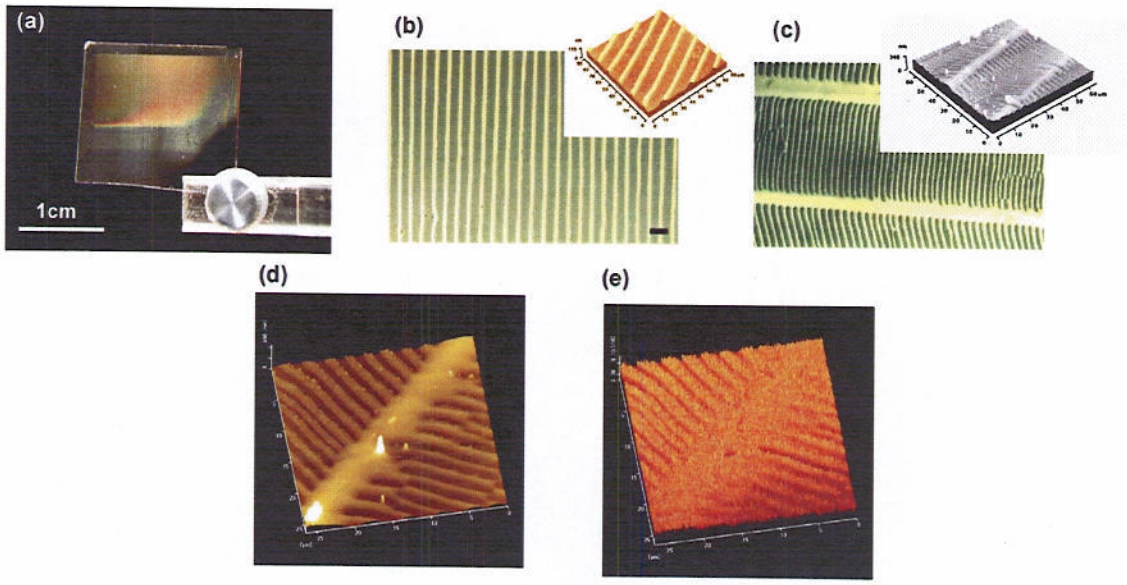

Figure 4-6. PHT pattern on the glass plate (a). The optical micrograph of stripe (b) and ladder (c) patterns, respectively. The insets are the AFM images. The topography (d) and current image (e) of PHT ladder pattern simultaneously observed at 5.00V/cm bias voltage.

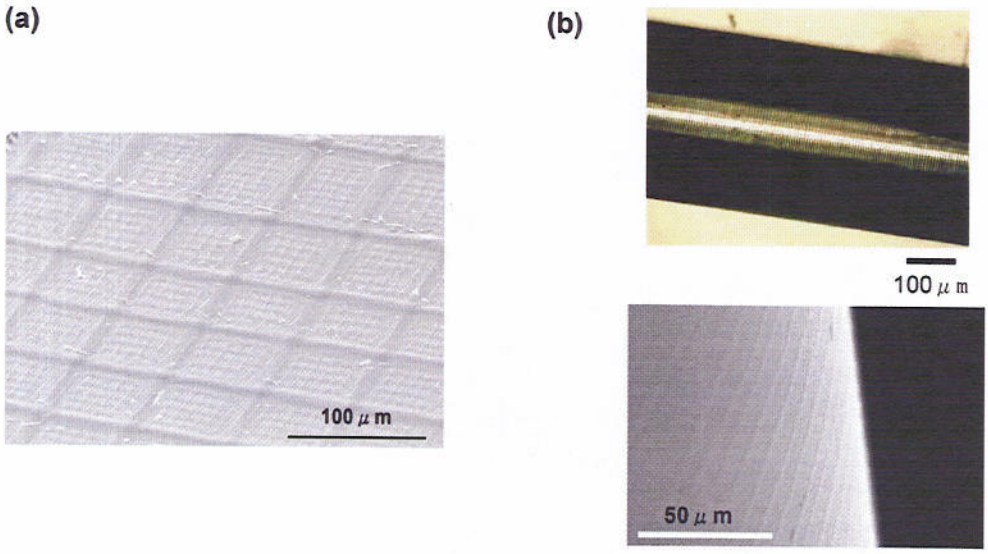

Figure 4-7. Scanning electron micrograph of a double mesh structure (a). Optical micrograph and scanning electron micrograph of ring pattern formed on a glass capillary (b).

conventional lithographic technique, patterning of the curved surface is difficult. Our method can be widely applicable fabrication method of polymer patterning on various substrates.

4.8. Conclusion

We developed a novel method and an instrument to control mesoscopic patterning from polymer solutions. The polymer solution kept the gap of two glass plates, and then the one glass plate was slid. The meniscus of the polymer solution followed the edge of the upper glass plate and the polymer patterns were formed on the bottom glass plate after solvent evaporation. Three different types of mechanisms, dewetting, stick-slip motion, and fingering instability, originate three types of patterns, micron-sized dot, stripe and ladder with controlled size, respectively. The polymer pattern can be prepared not only on a planner substrate but also on a curved surface. This method can be applicable for patterning of any kinds of polymer materials that have various functions because the dissipative phenomena and dewetting process are general physical phenomena of polymer materials in any scales from nanometer to micrometer. The patterned materials can be applied to photonics (19), electronics (20), biotechnologies (21) and building blocks for nanotechnologies (22).

Reference

[4-1] Stange, T. G., Evans, D. F., Hendrikson, W. A., Langmuir 1994, 10, 1566

[4-2] de Gennes, P. E., Rev. Mod. Phys. 1985, 57, 827 ()

[4-3] Khanna, R., Sharma, A., J. Colloid Interface Sci. 1997, 195, 42

[4-4] Sharma, A., Reiter, G., J. Colloid Interface Sci. 1999, 178, 383

[4-5] Reiter, G., Sharma, A., Casoli, A., David, M.-O., Khanna, R., Auroy, P., Langmuir1999, 15(7), 2551

[4-6] Yuan, C., Ouyang, M., Koberstein, J. T., Macromolecles 1999, 32(7), 2329

[4-7] Koschmieder, E. L., Adv. Chem. Phys. 1974, 26, 177

[4-8] Cazabat, A. M., Heslot, F., Troian, S. M., Carles, P., Nature 1990, 346, 824

[4-9] Nicolis, G., Prigogine, I., "Self-organization in nonequiliburim systems", John Wiley and Sons, 1977

[4-10] (a) Karthaus, O., Grasjo, L., Maruyama, N., Shimomura, M., Chaos 1999, 9(2), 1

[4-11] Karthaus, O., Koito, T., Shimomura, M., Mater. Sci. Eng. C 1999, 8-9, 523

[4-12] (a) Karthaus, O., Maruyama, N., Yabu, H. Koito, T., Akagi, K., Shimomura, M., Macromol. Symp. 2000, 160, 137 (b) Karthaus, O., Yabu, H., Akagi, K., Shimomura, M., Mol. Cryst. Liq. Cryst., 2001, 364, 395, (c) Karthaus, O. Yabu, H., Koito, T., Akagi, K., Shimomura, M., Mol. Cryst. Liq. Cryst. 2001, 370, 353

[4-13] Adachi, E., Dimitrov, A. S., Nagayama, K., Langmuir 1995, 11(4), 1057

[4-14] R. D. Deegan, O. Balajin, T. F. Dupont, G. Huber, S. R. Nagel, T. A. Witten, Nature, 1997, 389, 827

[4-15] Maruyama, N., Karthaus, O., Ijiro, K., Shimomura, M., Koito, T. Nishimura, S., Sawadaishi, T., Nishi, N., Tokura, S., Supramol. Sci. 1998, 5, 331

[4-16] (a) Vuilleumier, R., Ego, V., Neltner, L., Cazabat, A. M., Langmur 1995r, 11(10), 4117, (b) Cachile, M., Cazabat, A. M., Langmuir1999, 15(4), 1515

[4-17] Fanton, X., Cazabat, A. M., Langmuir 1998, 14(9), 2554

[4-18] Carter, F. L., Siatkowski, R. E., Wohltjen ed., "Molecular electronic devices", North-Holland, NY., 1988

[4-19] Joannopoulos, J. D., Meade, R. D., Winn, J. N., "Photonic Crystals –Molding the Flow of Light", Princeton University Press, 1995

[4-20] Jacobs, H. O., Whitesides, G. M., Science 2001, 291, 1763

[4-21] Ostuni, E., Chen, C. S., Ingber, D. E., Whitesides, G. M., Langmuir 2001, 17(9), 2828

[4-22] Shimomura, M., Sawadaishi, T., Curr. Opn. Colloid and Interface Sci. 2001, 6, 11

Chapter 5

Hybrid Structures

5-1.Introduction

In former chapters, preparation of nano- and micro-structures from zero dimension to three dimension by self-organization. In this chapter, the hybrid structures of these individual self-organized structures are shown. Titanium oxide (Titania) has high refractive index and photo-catalytic properties. It was reported that nano- or micro-porous honeycomb films were prepared from titania by sol-gel reaction of titan alkoxide sol with amphiplile [5-1]. To combine the micro-porous titania film and colloidal particles, it was expected that a novel type of organic/inorganic hybrid materials with photo-catalysts and photonic band gap (PBG) properties was prepared. We showed the preparation of highly ordered titania porous membranes. Furthermore, the composite formation of the titania films and polystyrene micro-particles by self-organization was reported. The arrangements of embedded particles were discussed.

5-2.Experimental

Honeycomb patterned films were prepared according to the literature [5-2]. By the analogy of honeycomb films from polymer materials [5-3~5-5], chloroform solution of 3.51M of titanium isopropoxide **5-1** and 0.246M of ditetradecyl-phosphate **5-2** (Figure 5-1.) was prepared. After casting of 20 μ l~500 μ l of the solution on horizontal glass substrate, solvent chloroform was evaporated by applying humid air. The relative humidity of applied air was controlled c.a. 60%. Evaporation heat allowed condensing water droplets on the reaction solution. The condensed water droplets were stabilized by amphiphile **5-2** and then regular arrays of water droplets were formed. After evaporation of solvent and water, the polymer film with hexagonal arranged pores was remained on the substrate.

Pyrolysis was performed under N_2 atmosphere by hot-stage at 400℃ (RINKAM-600, Japan-hitech, Japan). Polystyrene particles, diameter of 1.5 μ m and 3.2 μ m were obtained

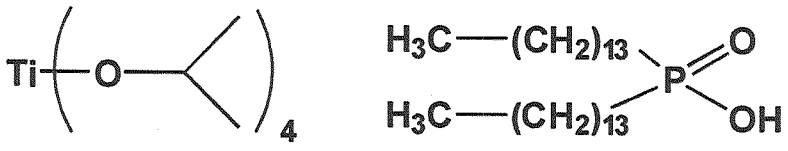

1 2

Figure 5-1. Chemical formulae of used compounds. 1 and 2 were purchased from TCI, Japan and Sogo Pharmaceuticals, Japan, respectively.

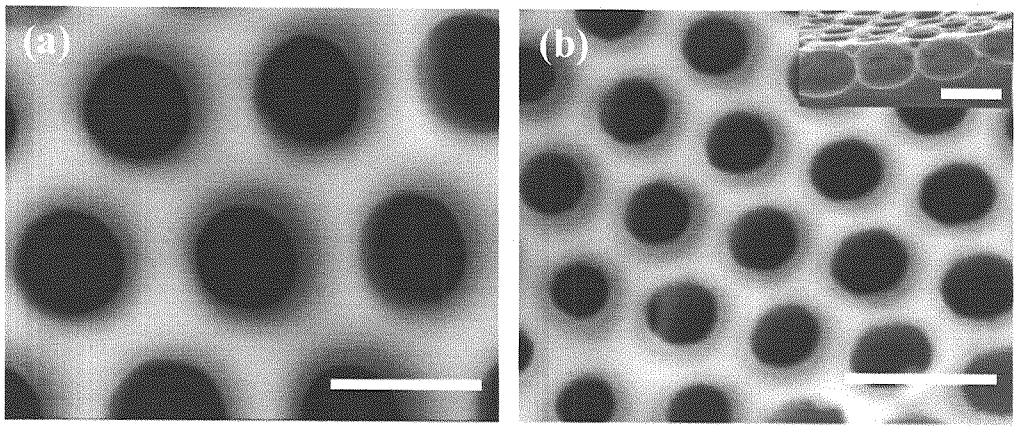

Figure 5-2. Scanning electron micrograph of titania honeycomb films. (a) Honeycomb film of titania before pyrolysis. (b) Honeycomb film of titania after pyrolysis. Inset micrograph shows cross section of the film. Each white bar indicates 1.0 μ m.

from Scientific Polymer Products, Inc., U. S. A. After pyrolysis, 20 μ l of 1.0g/l particle dispersions were casting on prepared honeycomb films and dried at room temperature. The prepared patterns were imaged by optical microscopy (Olympus BH-2), equipped with a CCD camera and a video recording system and by scanning electron microscopy (S-3500, Hitachi).

5-3.Results and Discussion

Metal alkoxides are known to form metal oxides in a sol-gel process when it contacts water. After completely solvent evaporation, titanium oxide films with hexagonally arranged pores were prepared. The pore size from 800nm to 5.0 μ m, was controlled by changing

casting volume[5]. Scanning electron micrograph of typical honeycomb structure was shown in Fig. 2 (a). The concentration of solution changed the thickness of the films. After pyrolysis at 400℃ for 3h, the film shrank and the average pore size changed from 800nm to 500nm. The white gel films turned to black because of thermal decomposition of amphiphile and other organic compounds. These grimes were washed away by chloroform and ethanol. The honeycomb structure was kept even after pyrolysis (Figure 5-2(b)). The cross-section of honeycomb structures showed that the pores kept original shape of template water droplets (Inset of Figure 5-2. (b)).

There are some approaches to combine micro-patterns and colloidal clusters. It was reported that the colloidal clusters usually fixed by electrostatic interactions between self-assembled monolayers (SAMs) and the surface charges on the colloids[6]. But here we show the procedure to form organic/inorganic hybrid materials without surface modification. An aqueous dispersion of polystyrene (PS) particles (1.0g/l, average diameter was c.a. 1.5 microns) was cast on the honeycomb films and water was evaporated under ambient condition. After completely evaporation of water, the films were observed by SEM. When the dispersion was cast on the honeycomb film having pores of 3.3 μ m diameter, three PS micro-particles were trapped in the honeycomb pores by the advection and capillary force (Figure 5-3. (a)). PS particles were arranged in a triangle in the pores. When the particles aggregate in a small dimension, lateral capillary force allowed PS particles to close packed arrangements. In case of the smaller pore honeycomb film (2.7 μ m diameter), only one particle was kept in each pores (Figure 5-3. (b)). Moreover, when larger PS particles (3.2 μ m) were cast on the same honeycomb film, particles were not trapped in the pores but some of them capped over the pores (Figure 5-3. (c)). These results show that the size of honeycomb pores and particles dominates the number of particles embedded in the pores.

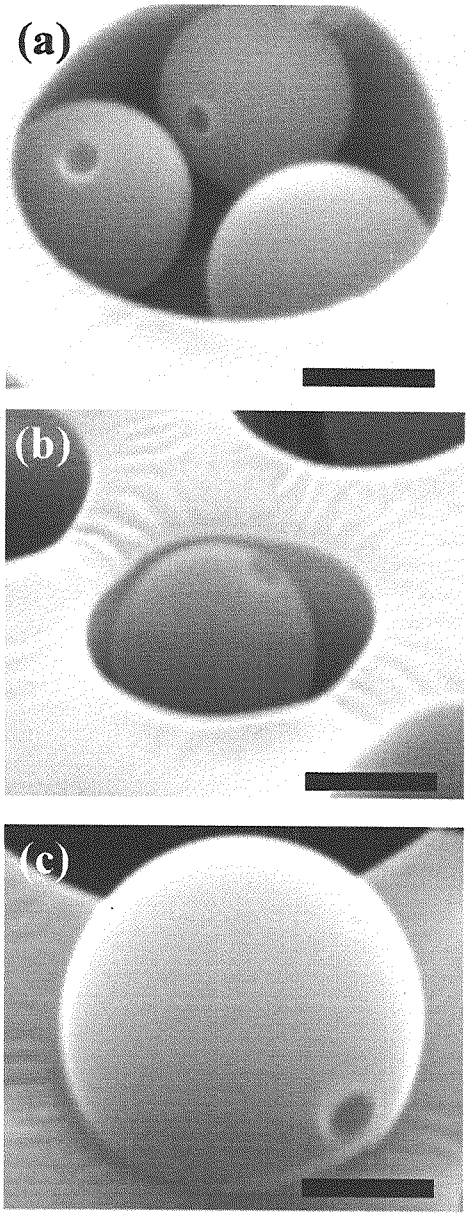

Figure 5-3. Scanning electron micrographs of combination of PS particles and titania honeycomb films. (a) 1.5 μ m PS particles in a 3.3 μ m honeycomb pore. (b) A single 1.5 μ m PS particle in a 2.7 μ m honeycomb pore. (c) A 3.2 μ m PS particles capped over a 2.7 μ m honeycomb pore. Each black bar indicates 1.0 μ m.

The preparation of composite of titania honeycomb films and PS particles by self-organization are shown. The pore sizes of titania honeycomb film were controlled from 500nm to 5 μ m. PS particles were embedded in the pores. Number and aggregation arrangements of particles were controlled by changing of the pore and particle size. The

organic/inorganic hybrid meso-structures can be utilized for novel type of photonic band gap materials and photo-catalysts.

References

[5-1]. O. Karthaus, X. Cieren, N. Maruyama, M. Shimomura, *Mater. Sci. Eng. C*, **10**, 103 (1999)

[5-2] O. Karthaus, N. Maruyama, X. Cieren, M. Shimomura, H. Hasegawa, T. Hashimoto, *Langmuir*, **16**(15), 6071 (2000), N. Maruyama, O. Karthaus, K. Ijiro, M. Shimomura, T. Koito, S. Nishimura, T. Sawadaishi, N. Nishi, S. Tokura, *Supramol. Science,* **5**, 331 (1998)

[5-3]. M. Shimomura, T. Sawadaishi, *Curr. Opn. Colloid and Interface Sci.*, **6**, 11 (2001)

[5-4] S. A. Jenekhe, X. L. Chen, *Science*, **283**, 372 (1999)

[5-5]. T. Nishikawa, R. Ookura, J. Nishida, K. Arai, J. Hayashi, N. Kurono, T. Sawadaishi, M. Hara, M. Shimomura, *Langmuir*, **18**(15), 5734 (2002)

[5-6]. I. Lee, H. Zheng, M. F. Rubner, P. T. Hammond, *Adv. Mater.*, **14**(8), 572 (2002)

Chapter 6

Conclusion

This research aimed to prepare building blocks to fabricate nano- and micro-scale architectures by using self-organization. Various types of structures ranging from tens nanometer to tens micro-meter were fabricated by using self-organization method, especially in the process of solvent evaporation from the polymer solutions. Four strategies building up mesoscopic architectures are shown in this thesis.

In chapter 2, the novel preparation method of nano-particles, which can applicable for wide variety of materials, were shown. Simple mixing of poor solvent into materials solution and following evaporation of good solvent forms nano-particles. Solvent component changes gradually by evaporation of good solvent, and then, the polymer precipitated as nuclei of particles. The nuclei grow up to consume whole polymer molecules in the solution. Various types of nano-particles containing dyes, biodegradable polymers, and polynucleic acid-amphiphile polyion complexes are prepared by using this method.

Another strategy is fabrication method of micro-pours polymer films by using condensed water droplets on the surface of polymer solution as templates (Chapter 3). The amphiphilic polymer stabilizes the water droplets and it localizes the micro-pore edge. By annealing treatment on the solid substrate, the amphiphilic polymer rings and dots can be transferred onto the substrate surface. Furthermore, the honeycomb-patterned films from super engineering plastics such as polyimide or fluorinated polymers can be fabricated by this method. The negative and positive molds also can be prepared by simple molding method. Micro lens arrays, super hydrophobic surface were prepared from these structures.

In chapter 4, the polymer micro-patterns prepared by using dewetting of dilute polymer solution. Dot, stripe and ladder patterns can be formed by using a novel fabricated apparatus, which provide continuous liquid membrane and meniscus on the evaporation edge. The patterns from electron conductive polymers, double mesh structures are also formed by this method. The ring pattern was prepared on the surface of glass capillary.

Finally, these micro-patterns are used for preparing hybrid structures. The honeycom-nano-particle hybrid structure was prepared by simple casting nano-particle dispersion onto the honeycomb-patterned film. The honeycomb template directed the aggregation of the nano-particles.

By using these strategies, the mesoscopic architectures ranging from tens nanometer to tens micrometer were easily formed. These are the fundamental result of micro-patterning and fabrication method of polymer materials by self-organization in the mesoscopic scale. Moreover, the structured polymer materials can be applied for electronics, photonic, and biotechnologies. It is believed that these self-organization methods are key strategies in the fields of nanotechnology and nanoscience, especially in nano-fabricastion field.

Acknowledgement

This work was performed under assistance of **Prof. Masatsugu Shimomura,** (*Nanotechnology Research Center (NRC), Research Institute for Electronic Science (RIES), Hokkaido University*) and **Prof. Kuniharu Ijiro** (*RIES, Hokkaido University*). I would like to express my gratitude to them for invaluable suggestion and encouragement throughout this work.

I am deeply grateful to **Prof. Kohei Uosaki** and **Prof. Noboru Kitamura** (*Graduate School of Science, Hokkaido University*) for significant suggestion to summarize this thesis.

I would like to thank **Dr. Masaru Tanaka** for helping DSC measurements and other thorough discussions. I would also like to thank **Dr. Olaf Karthaus** for helping TGA measurements.

I am sincerely grateful to the staffs and the students of *Molecular Devise Laboratory, RIES, Hokkaido University*, and *Nanomaterials Research Laboratory, NRC, RIES, Hokkaido University* for helping and encouraging me to summarize this thesis. The staffs of *Dissipative Hierarchic Structures Laboratory, Spatio-temporal Materials Research Group, Frontier Research System, RIKEN Institute* give me unrestrained comments concerning about this work.

I would like to have my parents, my brother and my sister to thank for mentally and financially supports throughout this work. And I would like to conclude this thesis by acknowledgement to my children and my wife.

June, 2004

Hiroshi Yabu

藪 浩